2021
September
No. 3
ISSN 1453-7303
ISSN-L 1453-7303

HIDRAULICA

HYDRAULICS-PNEUMATICS-TRIBOLOGY-ECOLOGY-SENSORICS-MECHATRONICS

CAD - CAE - CAM

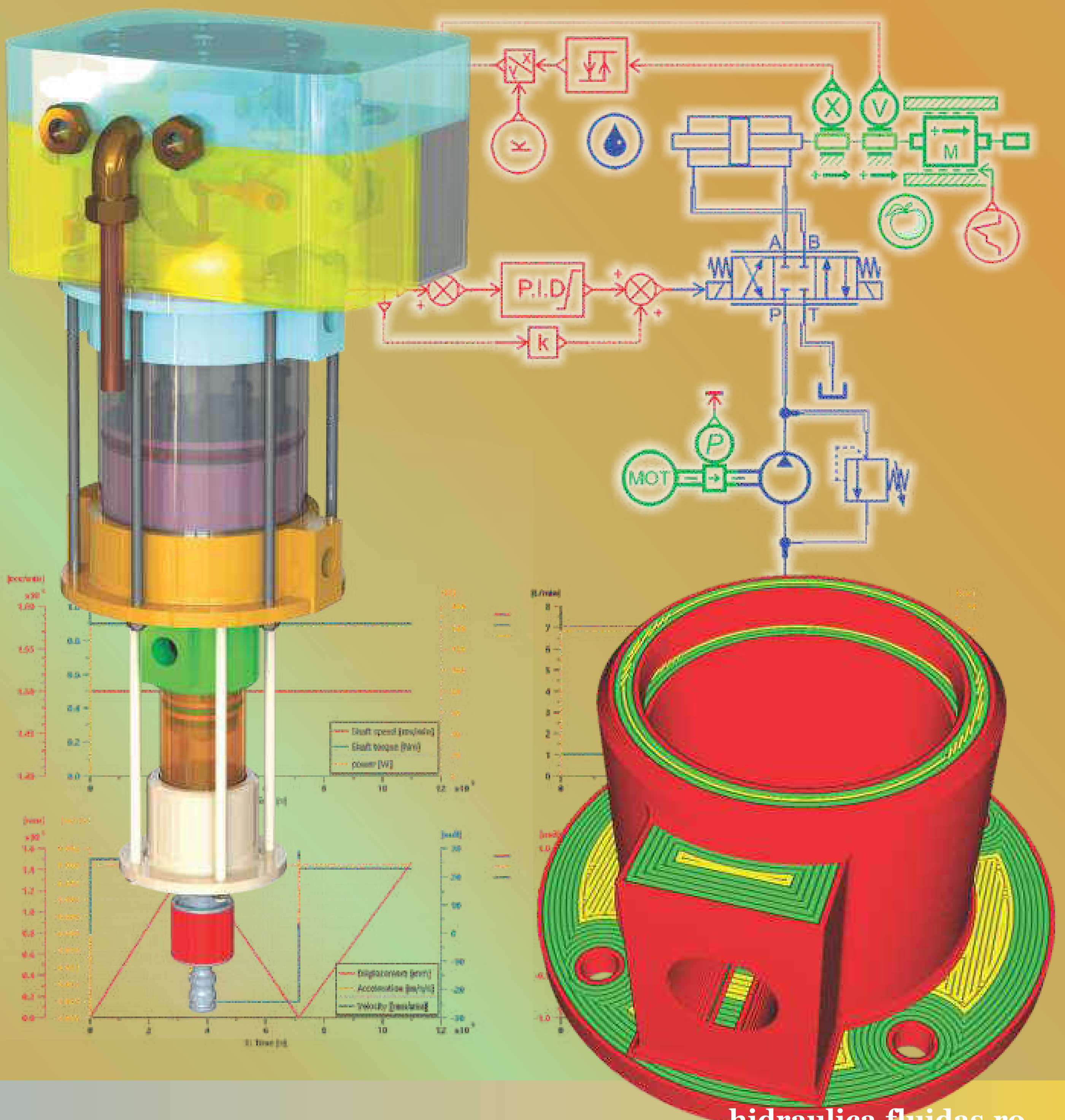

hidraulica.fluidas.ro

CONTENTS

Published by:
Hydraulics and Pneumatics Research Institute, Bucharest-Romania
Address: 14 Cuţitul de Argint, district 4, Bucharest, 040558, Romania
Phone: +40 21 336 39 91; Fax: +40 21 337 30 40; e-Mail: ihp@fluidas.ro; Web: www.ihp.ro
with support from:
National Professional Association of Hydraulics and Pneumatics in Romania - FLUIDAS
e-Mail: fluidas@fluidas.ro; Web: www.fluidas.ro

HIDRAULICA Magazine is indexed by international databases

ISSN 1453 – 7303; ISSN – L 1453 – 7303

EDITORIAL

Cercetare fără conținut?

Dr. Ing. Petrin DRUMEA
DIRECTOR PUBLICAȚIE

Este necesar sa fac precizarea că materialul se referă la cercetarea din domeniul tehnic, în principiu la cel mecanic, cu precădere la cel al Fluid Power.

Dacă despre cercetarea fundamentală nu pot face aprecieri bine susținute, despre cercetarea aplicată și cercetarea de dezvoltare pot face câteva aprecieri concrete. Nu voi discuta nici despre motivele și bazele diverselor împărțiri ale cercetării, nici despre cine se ocupă sau ar trebui să se ocupe de cercetarea de zi cu zi, nici de resursele financiare și nici măcar de beneficiarii acestei activități.

În acest editorial îmi pun câteva întrebări despre subiectele cercetării, despre metodologia cercetării și despre rezultatele așteptate.

Noi fiind o zona tipică a cercetarii aplicative, ar trebui să ne concentram pe rezolvarea practică a unor probleme care apar în activitatea economico-industrială, mai ales în modernizarea instalațiilor industriale. În aceste condiții, rezultatele așteptate sunt clare, sunt palpabile și nu își caută obiectivitatea în relații matematice care să ne dea o iluzie a corectitudinii. Sigur că trebuie căutată teoretic soluția optimă, dar trebuie să fim atenți să nu transformăm acest mijloc obiectiv de lucru în rezultatul final al cercetării.

În realitate, trebuie să discutam despre utilizarea aparatului de calcul ca despre o etapă necesară în procesul de dezvoltare a cercetării. În metodologia de desfășurare a cercetării trebuie incluse elementele care să precizeze pașii necesari îndeplinirii obiectivelor, probele de verificare și modalitățile de realizare a acestora, precum și datele concrete și corecte care se așteaptă de la instalația, stația pilot, tehnologia sau obiectul obținut în urma procesului de cercetare. Verificarea trebuie să dovedească totodată și faptul că cercetarea va obține rezultate asemănătoare dacă se repetă condițiile inițiale și metodologiile de lucru.

Sigur că în timpul unei cercetări vor fi publicate articole care se extrag din diverse faze sau etape, sigur că pot apărea invenții care nu se referă la toată cercetarea, ci doar la elemente singulare din diversele faze, etape sau subansamble ale produsului final, dar cercetarea de acest tip se va referi întotdeauna la o instalație, un obiect, o tehnologie sau o metodologie de lucru cu finalizare economico-industrială. Este evident că dacă rezultatele sunt destinate dosarelor și dulapurilor, cercetarea respectivă nu a avut obiective corecte și, practic, nu prea a fost cercetare științifică aplicativă.

În final, consider că nu poate exista o cercetare științifică fără un conținut adecvat.

EDITORIAL

Research with no content?

Ph.D.Eng. Petrin DRUMEA
MANAGING EDITOR

First, I should say that this material relates to the research in the technical field, basically - the mechanical field, especially - the field of Fluid Power.

While I cannot make well-grounded assessments on basic research, I can make some concrete assessments on applied research and development research. I will discuss neither the reasons and bases of the various categories of research, nor who is or should be involved in day-to-day research, nor the financial resources, and not even the beneficiaries of this activity.

In this editorial, I ask myself some questions about the research topics, about the research methodology and about the research expected results.

As we are a typical area of applied research, we should focus on finding practical solutions to some issues that (might) occur in the economical and industrial activity, especially related to upgrading of industrial facilities. Under these conditions, the expected results are clear, tangible, and do not seek objectivity in mathematical equations that would give us an illusion of correctness. Of course, the optimal solution must be sought theoretically, but we must be careful not to turn this objective means of work into the final result of the research.

In reality, we need to discuss the using of computation instrumentation as a necessary step in the research development process. The research conducting methodology must include the elements that specify the steps necessary to achieve the objectives, the verification tests and how to perform them, as well as the actual and correct data expected from the facility, pilot station, technology or object obtained from the research process. The verification must also prove that the research will obtain similar results if the initial conditions and working methodologies are replicated.

No doubt, while conducting a certain research, articles will be published that are extracted from various phases or stages of the research; no doubt, inventions might emerge that do not refer to all the research, but only to singular elements from the various phases, stages or subassemblies of the final product; still, research of this kind will always refer to a facility, an object, a technology or a working methodology with economic and industrial end-impact. It is obvious that if the results are intended for files and cabinets, that research did not have the right objectives and, actually, it has not really been applied scientific research.

To conclude, I believe that there can be no scientific research without proper content.

Overview of Human-Machine Interaction of Pneumatically Actuated Industrial Exoskeletons

Csaba HAJDU[1*], Dr. **Flóra HAJDU**[2], Dr. **Rajmund KUTI**[2]

[1] Vehicle Industry Research Center, Széchenyi István University, Győr, Hungary

[2] Department of Mechatronics and Machine Design, Széchenyi István University, Győr, Hungary

* hajdu.csaba@ga.sze.hu

Abstract: *Increasing human physical strength is a long researched area. Mainly military applications have been developed in order to increase the load-bearing capacity of the soldiers. However, in addition to military developments, healthcare and industrial applications are also gaining prominence. In this paper, the development directions of industrial exoskeletons with an emphasis on pneumatically operated devices are reviewed. An essential part of this paper is the analysis of the human-machine interaction. With our research results, we want to contribute to disseminating exoskeletons and facilitating adaptation to related areas.*

Keywords: *Exoskeleton, pneumatics, industrial application, human-machine interaction*

1. Introduction

The exoskeleton is an external frame attached to the user's human body. It senses the user's movement, and based on that, it multiplies the force exerted by the human, thus increasing the physical strength of the wearer. The equipment has been developed primarily for military applications [1] [2]. However, it can be stated that successful experiments have also been carried out in civilian applications. Full-body exoskeletons are used for most military applications, but only support devices have been developed to move or hold the given body part for some target tasks. Each exoskeleton must be optimized for a specific task to be performed. Therefore the materials used and the possible solutions are wide-ranging. In order to use human power optimally, more attention has been paid to the development of continuously operated exoskeletons in industrial applications. One type of these devices is the pneumatically operated exoskeleton, which can be operated indefinitely from a built-in industrial compressed air network. In this review paper, the development directions of civil exoskeletons are reviewed, and then the human-machine interaction in the case of pneumatically operated exoskeletons is examined in detail.

2. Development of non-military exoskeletons

The first exoskeletons were not developed for military purposes but to improve movement coordination in health care. The first 'exoskeleton' was developed and tested in 1969 at the Mihajlo Pupin Institute in Belgrade in the former Yugoslavia under the leadership of Miomir Vukobratović. With this device, the movement or motion of the patients was facilitated, thus supporting the work of the doctors and promoting the patients' rehabilitation. Based on practical experience, the device had continuously been developed, whereby it was achieved that the device could perform the same movement several times in succession, with a variable amount of force. With this, the researchers aimed to enable patients to perform individual rehabilitation exercises without less and less machine help, eventually using their muscle power [3]. Yugoslav researchers made further improvements, as the first device was only partially kinematically programmed, its propulsion was pneumatic, so it was unable to track every detail of human motion. Nevertheless, research continued so that by 1974, the first device using electric motors could be completed, which was successfully used in medical applications [3]. Based on the research, Vukobratović developed the theory of zero-momentum point [4] [5] and the theory of control of bipedal robots [6].

By the 1960s, research into the robotization of specific industrial processes was already underway, but there were processes where human activity was essential. Therefore, support equipment development to increase the force required for each work process has also begun [7]. In addition, recognizing the benefits of using exoskeletons in healthcare, industrial developments have also taken place. Besides full-body support devices, equipment that facilitates arm or hand movement and lifting were also developed in this area. The manufacturing and operating cost of these devices is significantly lower than for full-body exoskeletons, and has therefore been widely used in many industrial areas, particularly in the automotive industry [8] (Fig. 1).

Fig. 1. Industrial upper limb exoskeletons [9]

These exoskeletons primarily reduce the use of the user’s manual force by taking over part of the load, thus also reducing failure caused by fatigue. A possible grouping of upper-limb exoskeletons is depicted in Fig. 2 [10].

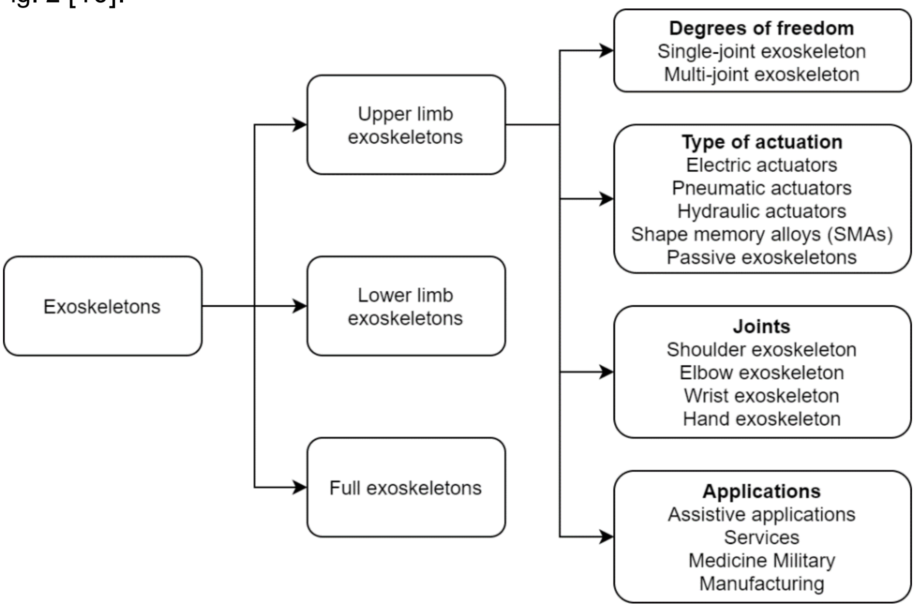

Fig. 2. Grouping of upper limb exoskeletons (based on 0)

In the following, the functional characteristics of industrial exoskeletons with pneumatic actuators are reviewed, focusing primarily on the human-machine interaction.

3. Functional characteristics of exoskeletons

During the operation of upper-limb exoskeletons, the force sensor built into the device measures the interaction force, then directly controls the motor current during signal processing and amplification, proportional to the torque exerted by the device. The man-exerted torque that rotates the exoskeleton element attached to the arm around the pivot point is added to the torque exerted by the device. The movement of the exoskeleton arm may not be exactly the same as the movement of the user. In this case, the control unit further changes the power of the motor until the movement of the exoskeleton arm and the user arm is approximately the same. The key to the proper functioning of the exoskeleton is the control device regardless of the application field. The control diagram is shown in Fig. 3.

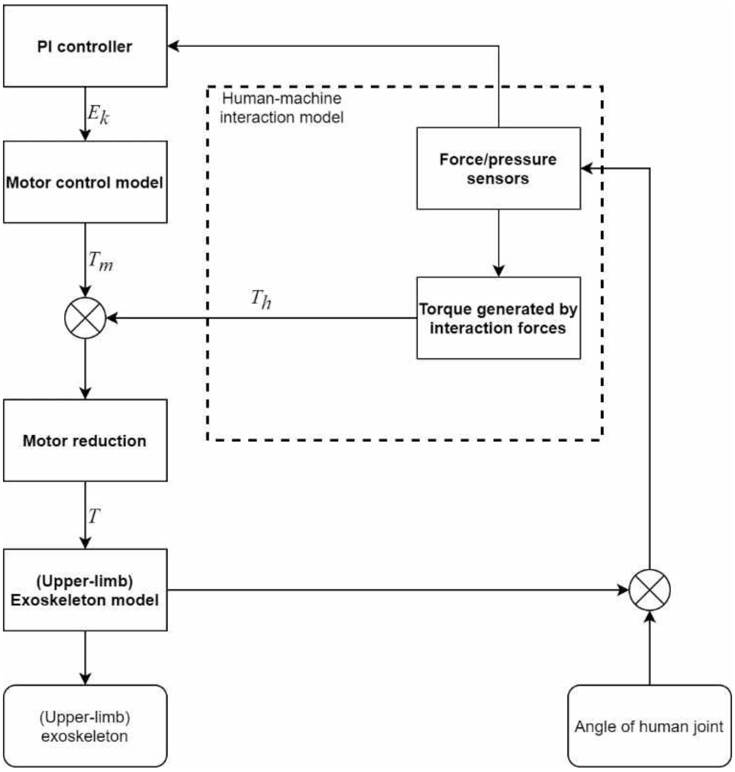

Fig. 3. The control diagram of exoskeletons

The elements (arms) of the exoskeleton can be identified as a nonlinear dynamic system, which is illustrated in Fig. 4.

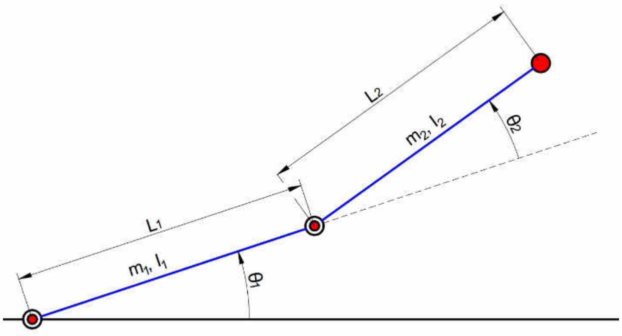

Fig. 4. Schematic of a nonlinear dynamic system

In the figure above (Figure 4), $L1$ and $L2$ are the lengths of the elements, m_1 and m_2 are their masses, I_1 and I_2 are their moments of inertia, and θ_1 and θ_2 are their rotations with respect to the horizontal. T_q is the torque vector of the actuators and $H(\theta)$ is the $N \times N$ inertia matrix of the system.

The mathematical model of this simple two-element system is derived by the Euler-Lagrange equation:

$$T_{q1} = H_{11}\ddot{\theta}_1 + H_{12}\ddot{\theta}_2 - h\dot{\theta}_2^2 - 2h\dot{\theta}_1\dot{\theta}_2 \tag{1}$$

$$T_{q2} = H_{22}\ddot{\theta}_2 + H_{21}\ddot{\theta}_1 - h\dot{\theta}_1^2 \tag{2}$$

where,

$$H_{11} = m_2L_1^2 + I_1 + m_2(L_1^2 + L_2^2 + 2L_1L_2cos\theta_2) + I_2 \tag{3}$$

$$H_{12} = H_{21} = m_2 L_1 L_2 cos\theta_2 + m_2 L_2^2 + I_2 \quad (4)$$

$$H_{22} = m_2 L_2^2 + I_2 \quad (5)$$

$$h = m_2 L_1 L_2 sin\theta_2 \quad (6)$$

3.1. Human-machine interactions

In the field of exoskeletons, the analysis of human-machine interaction is emphasized as an essential but complex task. The problem is particularly complicated when it comes to prostheses, as the task of the exoskeleton, in this case, is also to maintain weight while aiding movement. Although the paper's primary focus is on upper-body exoskeletons, the subsection also discusses interaction issues for lower-body exoskeletons, providing some inspiration for possible solutions to human-machine interaction and control engineering.

For the exoskeleton, the primary input is the measured interaction force and its magnitude. The device can change the motion states (e.g., standing position, movement). Some solutions are also used for working point linearization, but these solutions work primarily in simulations because robustness might be lost in the real environment. Another disadvantage is that force sensors of such accuracy are expensive and sensitive to the multidirectional force and torque present in human walking. Instead, the standard method for characterizing reaction force is to capture motion, which is used in general to study human motion. Some authors have further refined modeling of reaction forces, such as Kalman filters: for example, in [11], the gait and speed of the walker are estimated. In [12] the force load of the ground expressed on the ankle was studied using the lower-limb model using nonlinear Kalman Filtering Methods.

In another approach, the exoskeleton is implemented as a brain-machine interface. In this case the signals induced by the motor cortex of the brain can be used directly to control the device in addition to or in place of the force sensors. Interaction based on EEG signal processing is still widespread (e.g., [13]). Recently the method of electromyography (EMG) has been used to control exoskeletons (e.g., C. Fleischer [14]). In this case, muscle activation is measured by electrodes. The human-machine interaction based on electromyography is illustrated in Fig. 5.

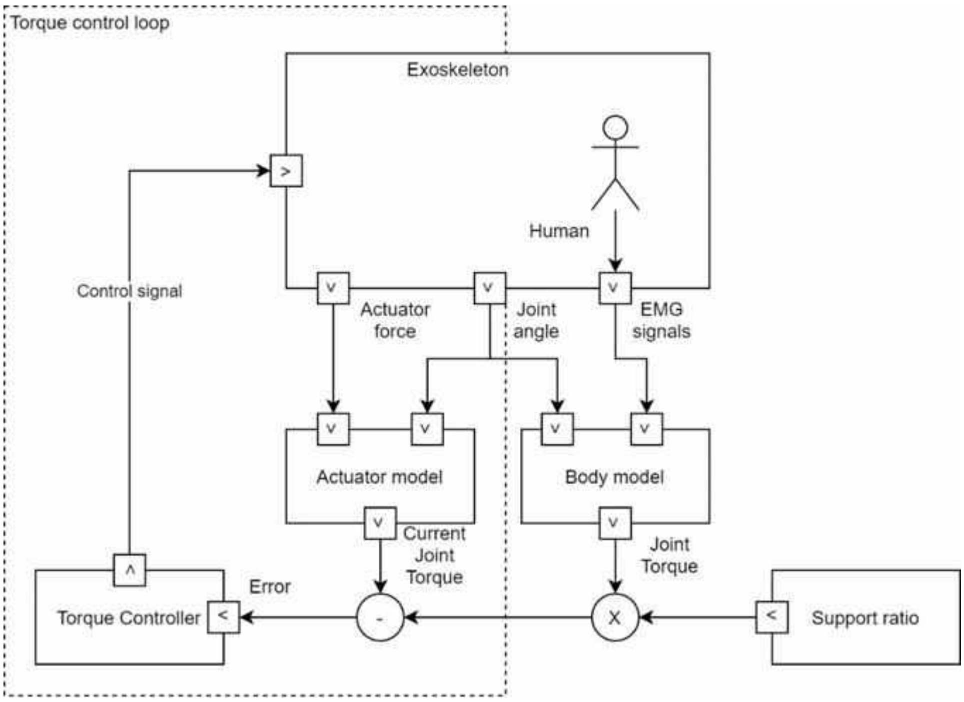

Fig. 5. Human-machine interaction in the case of exoskeletons

It is a challenge that human from a control point of view is a nondeterministic actor whose movement can only be estimated, therefore modeling the expected interaction is also complicated. In order to be able to model the interaction and the ergonomic aspects, it is advisable to review the latest breakthroughs. A common robust control method in case of humanoid robots is the Lyapunov Control Function (CLF) method and its complementation by quadratic programming (CLF-QP) [14]. In the case of exoskeletons, CLF is most easily applied by studying phase variables, therefore the trajectory of human motion is modulated. In this case, however, the control model considers only basic human dynamics based on biomechanical research [16]. For this reason, this model cannot be used, for example, in the case of prosthesis control. Extending CLF-QP, model-independent control or model-dependent control can be used [17]: More accurate and robust trajectory tracking can be achieved with the latter. In some cases, predefined (offline) trajectories can also be traced. In many cases, the most critical components are the knee and ankle joints, which are typically controlled by robust-passivity (RP) or robust sliding mode (RS) controllers with predetermined excitation-response model-dependent control.

Many authors test complex control (and in many cases, an initial estimate of tuning) using simulations. In case of simulations, the big challenge is to model the human motion system properly. However, simulation is also necessary in other use cases so that it can be considered as an actively verified area (OpenSIM) [18]. Another exciting question is how a haptic interface, even in virtual reality environments, may be suitable on the exoskeleton. In this case, the interaction interface covers not only the tracking and estimation of human movement, but also the perception of touch [19].

In other research, human motion is modelled by an analytical mathematical model, whose starting point is the creation of a limb model. In one example, S. Jatsun et al. [20] replace the foot with simple elements, equipped with a 2DOF gauge on each joint. The measurements were also verified by a numerical simulation based on a cascade control based on the inverse kinematics of the foot. Specifically for upper limb models, different model representations had appeared [21]. In one particularly interesting approach used the theory of screws to model the upper limb of the human [22].

The operation of the exoskeleton requires adequate torque, which can be generated by electric motors, hydraulic / pneumatic or linear actuators. The selection of the proper actuator is already critical during the design phase, as they affect the weight of the equipment and the applicability of the exoskeleton. It is advisable to choose an actuator that has a high power-to-mass ratio and can exert high torque and precise movement. Each actuator has its advantages and disadvantages. In the present study, we focus on pneumatic actuators.

3.2. Pneumatic exoskeletons

The advantage of pneumatic actuators is lower impedance and lower weight compared to electric actuators. They require low maintenance, are suitable for continuous operation and can be shut down under load without endangering the user. Compared to hydraulic and electric exoskeletons, pneumatics provide fast and flexible operation. Their biggest disadvantage, however, is their lower accuracy, which limits their field of application. Because they require a pneumatic power supply to operate, they are generally suitable for stationary tasks. In the case of a compressed air network, which is often available in industrial plants, the area of use can be increased by creating several connection points 0.

Pneumatic exoskeletons consist of pneumatic cylinders, which are operated by compressed air at a suitable pressure and solenoid valves 0-0. The functional diagram of the pneumatic exoskeleton is shown in Fig. 6.

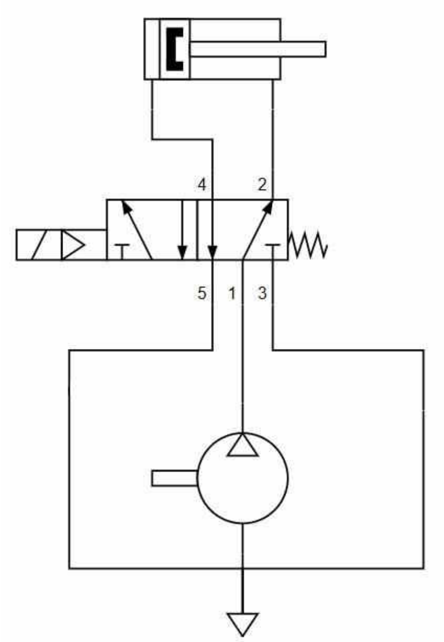

Fig. 6. Functional diagram of a pneumatic exoskeleton

There are also full-body pneumatic exoskeletons as described in 0. Recyclable, lightweight materials have been used with safety and environmental considerations taken into account. The structure works with pneumatic cylinders that are suited to human anatomy. The structure helps the movement of different muscle groups (biceps, triceps, legs and deltoid muscles). In addition to physiotherapy applications, these exoskeletons can also be used in industry, for example for lifting heavy objects or for work that requires constant hand support. The parts of the device are pneumatic cylinders, solenoid valves, compressed air pipes and transducers. The upper limb part is designed to be easily resizable. Two cylinders are mounted to the frame, they are the same size but operate in opposite directions. Examples of pneumatic exoskeletons for industrial use are shown in Fig. 7.

Fig. 7. Pneumatic exoskeletons for industrial use 0, 0

4. Summary

This article provided an overview of pneumatic exoskeletons for industrial use. The focus was on upper-limb exoskeletons with a particular emphasis on the interaction capabilities with humans. Throughout this article, the control- and interaction-model of full- and lower-limb exoskeletons have been discussed. The purpose of this article is to point out the possible dimensions of optimization of the exoskeleton applications for a specific task.

This article pointed out, that the control model is vital for proper interaction with humans. There are numerous approaches for modelling, some based on analytical methods and empirical studies based on biometrical studies. More recent methods are based on robust control methods (robust-sliding, robust passive) based on Lyapunov control methods. Besides the overview of computational methods of control, the interaction platform have been also discussed (force sensors, EEG, electromyography).

Acknowledgments

This article was supported by the ÚNKP-20-03. New National Excellence Program of the Ministry for Innovation and Technology from the source of the National Research, Development and Innovation Fund.

References

[1] Baechle, D. M. "A Mobile Arm Exoskeleton for Firearm Aim Stabilization." MSc Thesis, University of Delaware, 2013.
[2] Horváth, P., Á. Ballagi, A. Nagy, and R. Kuti. "Military applications of exoskeletons" / "Az exoskeletonok katonai alkalmazási lehetőségei." *Műszaki Katonai Közlöny*, no. 2 (2018): 35-43.
[3] Vukobratovic, M. K. "When were active exoskeletons actually born?. "*International Journal of Humanoid Robotics* 4, no. 3. (2007): 459-486.
[4] Vukobratovic M., and D. Juricic. "Contribution to the Synthesis of Biped Gait." *IEEE Transactions on Biomedical Engineering* BME-16, no. 1 (1969): 1-6.
[5] Vukobratovic M., and B. Borovac. "Zero-Moment Point - Thirty Five Years of its Life." *I. J. Humanoid Robotics* 1 (2004): 157-173.
[6] Vukobratovic M. *Biped Locomotion*. Berlin, Heidelberg, Springer-Verlag, 1990.
[7] Önen, Ü., F. M. Botsalı, M. Kalyoncu, M. Tınkır, N. Yılmaz, and Y. Sahin. "Design and Actuator Selection of a Lower Extremity Exoskeleton." *IEEE/ASME Transactions on mechatronics* 19, no. 2 (2014): 615-623.
[8] Wolff, B. "The Promise of Powered Industrial Exoskeletons: Reducing Occupational Injuries One "Lift" at a Time." *Exoskeleton Report*, 2018. Accessed May 16, 2019. https://exoskeletonreport.com/2018/04/the-promise-of-powered-industrial-exoskeletons-reducing-occupational-injuries-one-lift-at-a-time/.
[9] Carlos, G. "Manufacturing Workers Become More than Human with Exoskeletons." *Machine Design*, 2017. Accessed Juny 30, 2021. https://www.machinedesign.com/mechanical-motion-systems/article/21836235/manufacturing-workers-become-more-than-human-with-exoskeletons.
[10] Gull, M.A., S. Bai, and T. Bak. "A Review on Design of Upper Limb Exoskeletons." *Robotics* 9, no. 16 (2020): 16. https://doi.org/10.3390/robotics9010016.
[11] Karulkar, R. M., and P. M. Wensing. "Application of Interacting Models to Estimate the Gait Speed of an Exoskeleton User." Paper presented at the 2020 IEEE/RSJ International Conference on Intelligent Robots and Systems (IROS), Las Vegas, USA, October 25-29, 2020.
[12] Fakoorian, S., V. Azimi, M. Moosavi, H. Richter, and D. Simon. "Ground Reaction Force Estimation in Prosthetic Legs With Nonlinear Kalman Filtering Methods." *Journal of Dynamic Systems Measurement and Control* 139, no. 11 (Nov. 2017): 111004 (11 pages). https://doi.org/10.1115/1.4036546.
[13] Schnieders, T. M., and R. T. Stone. "Current Work in the Human-Machine Interface for Ergonomic Intervention with Exoskeletons." *International Journal of Robotics Applications and Technologies* 5, no.1 (January-June 2017): 1-19. https://doi.org/10.4018/IJRAT.2017010101.
[14] Fleischer, C., and G. Hommel. "A Human-Exoskeleton Interface Utilizing Electromyography." *IEEE Transactions on Robotics* 24, no. 4. (2008): 872 – 882.
[15] Gehlhar, R., Y. Chen, and A. D. Ames. "Data-driven Characterization of Human Interaction for Model-based Control of Powered Prostheses." Paper presented at the 2020 IEEE/RSJ International Conference on Intelligent Robots and Systems (IROS), Las Vegas, USA, October 25-29, 2020.
[16] Wehner, T., L. Claes, and L. U. Simon. "Internal loads in the human tibia during gait." *Clinical Biomechanics* 24, no. 3. (2019): 299-302.
[17] Azimi, V., T. Shu, H. Zhao, E. Ambrose, A. D. Ames, and D. Simon. "Robust control of a powered transfemoral prosthesis device with experimental verification." Paper presented at the 2017 American Control Conference (ACC), Seattle, WA, USA, May 24-26, 2017.
[18] Seth, A., J.L. Hicks, T.K. Uchida, A. Habib, C.L. Dembia, J.J. Dunne, C.F. Ong, M.S. DeMers, A. Rajagopal, M. Millard, S.R. Hamner, E.M. Arnold, J.R. Yong, S.K. Lakshmikanth, M.A. Shermann, and S.L. Delp. "OpenSim: Simulating Musculoskeletal Dynamics and Neuromuscular Control to Study Human and Animal Movement." *Plos Computational Biology* 14, no. 7. (July 2018): e1006223. https://doi.org/10.1371/journal.pcbi.1006223.

[19] Bergamasco, M., A. Frisoli, and C. A. Avizzano. "Exoskeletons as Man-Machine Interface Systems for Teleoperation and Interaction in Virtual Environments." *Advances in Telerobotics. Springer Tracts in Advanced Robotics* 31. (2007): 61-76. https://doi.org/10.1007/978-3-540-71364-7_5.
[20] Jatsun, S., A. Malchikov, O. Loktionova, and A. Yatsun. "Modeling of Human-Machine Interaction in an Industrial Exoskeleton Control System." ICR 2020: Interactive Collaborative Robotics, 5th International Conference, St Petersburg, Russia, October 7-9, 2020, Proceedings (2020): 116-125.
[21] Krishnan, R., N. Björsell, E. M. Gutierrez-Farewik, and C. Smith. "A survey of human shoulder functional kinematic representations." *Medical & Biological Engineering & Computing* 57 (2019): 339–367.
[22] Ziai, A. "Kinematic & Dynamic Analysis of the Human Upper Limb Using the Theory of Screws." *ArXiv* abs/1906.02458 (2019). Accessed Juny 30, 2021. https://arxiv.org/abs/1906.02458.
[23] Shinde, N. P., Daji S. Shinde, Kirtisen R. Gaikwad, and A. V. Naik. "Exo-Skeleton Arm Using Pneumatic Cylinder." *Journal of Mechanical Robotics* 4, no. 2. (2019): 22-25.
[24] Kumara, P. B., K. A. Pais, R. M. Pereira, M. A. Sahil, and V. S. Mallya. "Design and fabrication of Pneumatic Exoskeleton." *Journal of Mechanical Engineering and Automation* 7, no. 3 (2017): 85-88.
[25] Krishna, G., P. Hosmutt, B. M. Nyamagoud, M. V. Patil, and O. Hunnur. "Design and Fabrication of Pneumatic Powered Exoskeleton Suit for Arms." *International Research Journal of Engineering and Technology (IRJET)* 5, no. 4. (2018): 4415-4419.
[26] Pavithrana, A., E. Skariaa, R. Rajana, and J. Joseb. "Design and Fabrication of Pneumatic Exoskeleton." *International Journal of Advanced Research Trends in Engineering and Technology (IJARTET)* 4, no. 15 (2017): 36-42.
[27] Radoi, R., M. Blejan, I. Dutu, G. Sovaiala, and I. Pavel. "Determining the Step Response for a Pneumatic Cylinder Positioning System." *Hidraulica*, no. 2 (June 2014): 25-31.

Heat Treatment Influence of Alloy 5083 on Cavitational Erosion Resistance

PhD.Eng. **Dionisie ISTRATE[1],** Lecturer PhD.Eng. **Cristian GHERA[2],**
Univ. assist.PhD.Eng. **Laura SĂLCIANU[3],** Prof.PhD.Eng**. Ilare BORDEAȘU[4],**
Prof.PhD.Eng**. Brândușa GHIBAN[5],** PhD.Eng. **Dumitru Viorel BĂZĂVAN[6],**
Assoc. prof. PhD.Eng. **Lavinia Mădălina MICU[7],** Lecturer PhD.Eng. **Daniel-Cătălin STROIȚĂ[8],**
Assoc. prof. PhD.Eng**. Daniel OSTOIA[9]**

[1] Politehnica University of Bucharest, dionisieistrate@yahoo.com

[2] Politehnica University of Timisoara, cghera2000@yahoo.com

[3] Politehnica University of Timisoara, salcianu.laura@yahoo.com

[4] Politehnica University of Timisoara, ilarica59@gmail.com

[5] Politehnica University of Bucharest, ghibanbrandusa@yahoo.com

[6] Politehnica University of Timisoara, bazavanvio303@yahoo.com

[7] University of Agricultural Sciences and Veterinary Medicine of Banat "King Mihai I of Romania", lavimicu@yahoo.com

[8] Politehnica University of Timisoara, daniel.stroita@upt.ro

[9] Politehnica University of Timisoara, dostoia@yahoo.com

Abstract: *Aluminum based alloy type 5083 have a large applicability in the area of automobile and naval constructions (such as: Shipbuilding, Rail cars, Vehicle corps, Type truck body, Mine skips and cages, Pressure vessel). The components of these parts are sometimes required for high aggressiveness factors. Thus, during operation, both the pump rotors and the propellers are subjected to hydrodynamic stresses of the cavity, which, by erosion, leads to their removing, completely or until repair. At the same time, to increase the service life, chemical corrosion of the liquid environment, these others contain various alloying elements, which change the structure and improve the chemical, physical and mechanical properties. In order to increase the resistance to erosion and mechanical stresses of the cavitational current, heat treatments are applied which also modify the microstructure and the values of the mechanical properties. The study presents the results of research on its vibrating cavity of another 5083 cast, subjected to the heat treatment of the solution at 350°C followed by artificial aging at 180°C with different maintenance times (one hour, 12 hours, 24 hours). The analysis of the results, based on the specific curves used in the Cavitation Erosion Research Laboratory in Timișoara, recommended by ASTM G32-2016, as well as macro images of eroded surfaces for 165 minutes, shows the dependence of cavitation erosion resistance of the microstructure type results from heat treatment and not of durable value, respectively of resilience, properties with great influence on the resistance to cavitation stresses, as happens, most often, in the case of steels.*

Keywords: *Alloy 5083 aluminum, erosion of cavitation, mass loss, erosion rate, microstructure, tearing, hardness, resilience*

1. Introduction

The use of aluminum-based alloys is known for its thermal and electrical properties, but its use in the shipbuilding industry, automobiles, aviation, etc. is due to the advantage offered, in particular, by its low specific mass [1-4]. Depending on the application and the operating conditions, the choice of the alloy is made according to the chemical composition, structure and mechanical properties. Some of these components, such as the warhead and wings of aircraft, the propellers of motorboats and boats and the water cooling pumps of motor vehicles are subjected to mechanical, destructive stresses, through the hydrodynamic mechanism of the cavity [5 - 10]. The parts affected by these stresses have pitting erosion surfaces, sometimes with very large caverns, which require the operation to be stopped and the eroded surface to be repaired, or even the part to be replaced. To increase the resistance to these stresses, researchers use various technologies

and methods to increase the resistance of surfaces exposed to impact by micro-jets and shock waves, produced by the hydrodynamic mechanism of the cavitation. They aim to change the structure and mechanical properties such as hardness, mechanical strength, yield strength, resilience, which, according to extensive experimental studies, over 100 years, made of various metals, such as those made in the Erosion Research Laboratory by Cavitation of the Politechnica University of Timișoara [6-10], by Hobbs, Garcia and Hammitt [9], Franc and collaborators [8], Steller [11], Xiao-ya Li a.o. [12], contribute to increasing the resistance to erosion caused by cavitation.
The paper presents the research results concerning the vibrating cavity of the cast 5083 alloy, subjected to the heat treatment hardening solution at 350°C followed by artificial aging at 180°C with different maintenance times (one hour, 12 hours, 24 hours). The most used techniques are the volumetric heat treatments that also ensure mechanical resistance to vibrations during operation (in the case of aircraft wings, boat propeller blades). As aluminum alloys, through heat treatments, undergo some changes that do not align with the mechanisms of transformation suffered by steels, the results of the paper show substantial differences between the destruction of the structure of surfaces attacked by cavitation, resulting after heat treatments, despite mechanical properties known to be favorable for increasing the resistance of the structure to cavity erosion.

2. The researched material. Experimental procedure

For the research, initially, a piece of material was taken from a boat propeller that sailed on the Danube in the area of Romania, Figure 1, whose chemical composition, presented in Table 1, was determined in the specialized laboratory of the Politechnica University of Timișoara.

Table 1: Chemical composition of the experimental propeller alloy

Alloy	Chemical composition, [%] mass									
	Si	Fe	Cu	Mn	Mg	Cr	Zn	Ti	Other	Al
Experimental propeller	0.389	0.378	0.102	0.83	4.71	0.19	0.246	0.141	-	Rest
5083	0.4	0.4	0.15	0.4-1.0	4-4.9	0.05-0.25	0.25	0.15	0.05	Rest

Fig. 1. Boat propeller that sailed on the Danube
(purchased from the Drobeta Turnu-Severin Shipyard)

Compared with the data provided by the literature [4], it was found that the material is other aluminum 5083, cast state (see the standard chemical composition in Table 1), obtained by continuous casting, most often in the form of plates, characterized by: semi-hardness, very good corrosion resistance (especially in the marine environment), very good behavior at low temperatures, very good machinability, good and uniform mechanical properties in the mass of others, low internal stress, homogeneous microstructure, Figure 2.

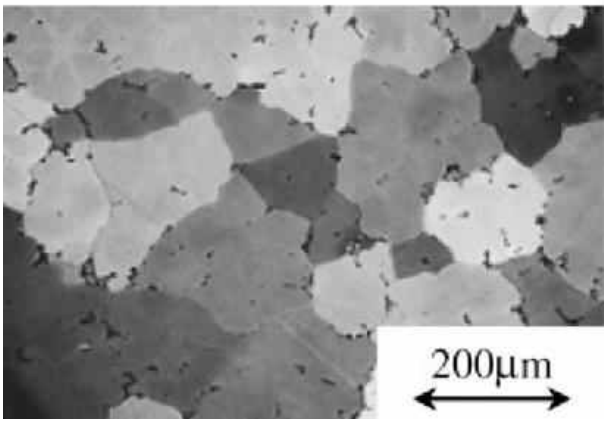

Fig. 2. Microstructure of cast 5083 alloy [4]

The used applications of this alloy are [1-3]: for airplanes, automobiles, pressure vessels, sailboats, dinghies and boats.
Because it was not possible to cut pieces from the propeller to allow the specimens to be made to the dimensions necessary to perform cavitation tests, the Special Materials Expertise Center of the Politechnica University of Bucharest was used, which provided a set of 12 cubes with a side of 30 mm, 5083 aluminum alloy, taken from a cast plate, purchased from Color Metal.
Table 2 gives the main mechanical properties, according to [4] and those determined in the Laboratory.

Table 2: Physical-mechanical properties of experimental alloy type 5083

Alloy	R_m [MPa]	$R_{p0..2}$ [MPa]	HB [daN/mm^2]	A_5 [%]	KCU J/cm^2	E [GPa]	ρ [kg/dm^3]
Experimental	260	117	72,8	11	25,2	70	2.66
Standard [4]	230-290	110-130	68-75	10-15	-	70	2.66

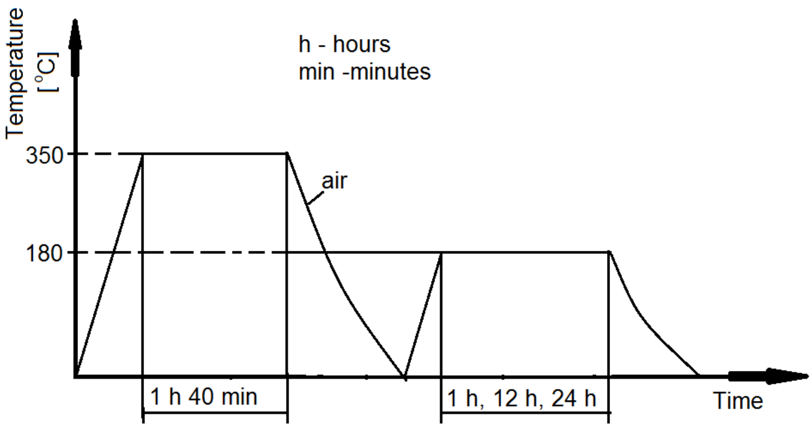

Fig. 3. Cyclorama of heat treatment

Of the 12 specimens, 9 were heat treated in the Laboratory of Metallic Materials Science, Physical Metallurgy within the Politechnica University of Bucharest. All 9 specimens were subjected to heat treatment at 350°C, with air cooling. The heat treatments were performed in a Nabertherm type oven. Then sets of three were subjected to artificial aging at 180°C, with different durations of maintenance, according to the cyclogram in Figure 3.

Table 3 shows the average values of hardness measured at 5 points on each heat-treated sample and resilience measured on three other specimens. In addition, these measurements were performed in the Laboratory of the Special Materials Research Center of the Politehnica University of Bucharest.

To simplify identification and ease of analysis, the specimens / heat treatments were symbolized as follows:

I - without heat treatment;

II - heating at 350 ℃ (holding time 1 hour and 40 min, cooling in air) followed by artificial aging at 180 ℃ (holding time 1 hour);

III - heating at 350 ℃ (holding time 1 hour and 40 min, cooling in air) followed by artificial aging at 180 ℃ (holding time 12 hours);

IV - heating at 350 ℃ (holding time 1 hour and 40 min, cooling in air) followed by artificial aging at 180 ℃ (holding time 24 hours).

Table 3: Values of mechanical properties of experimental 5083 alloy after application of various heat treatments

Property	Type of treatment		
	II	III	IV
HB, [MPa]	79	77.9	71.8
KCU, [%]	25.8	31.7	16.4

The values in Table 4 show that, by increasing the holding time, the hardness values decrease and the resilience values are not influenced by this duration. This aspect leads us to the opinion that a clear conclusion cannot be formulated regarding the influence of the maintenance duration at the artificial aging temperature, on the two mechanical properties, which according to Bordeașu's studies [5, 7, 13, 14], Franc [8], Gracia & Hammitt [9], Anton [10], influence the resistance to cavitation erosion.

As will be presented below, the resistance and cavitation behavior of the alloy in different structural states is influenced by the structure resulting from the volume heat treatment and it is difficult to highlight the dependence on hardness or resilience.

The experiment took place in the Cavitation Erosion Research Laboratory of the Polytechnic University of Timișoara, on the vibrating device with standard piezoceramic crystals, using cylindrical vibrating samples, with a diameter of 15.8 mm and 16 mm long [7]. The research conditions ,, on the total duration (165min), the intermediate periods (one of 5 and 10 minutes each and 10 of 15 minutes) on the liquid medium, the processing and interpretation of the recorded data are in accordance with the laboratory custom [5, 7, 13, 14] and those prescribed in the international standard ASTM G32-2016 [15].

Throughout the research, the functional parameters of the vibrating device, on which depends the intensity of the hydrodynamics of the vibrating cavity, respectively that of erosion, due to the automated control by a special software, were maintained at standard values [7, 15]: double vibration amplitude 50 μm, vibration frequency 20 ± 0.2 kHz, electronic ultrasonic generator power 500 W, distilled water temperature 22 ± 1°C.

3. Experimental results. Discussions

The evaluation of the behavior and resistance of the structure of the surfaces exposed to cavitation was made based on the variations of the mass of expelled material (Figure 5, 7, 9, 11, 13) and of the rate of material losses - erosion rate - (fig.6, 8, 10, 12, 14) with the duration of exposure to cavitation, as well as on the macro images of the eroded surface at significant times for the evolution of erosion as area and depth, Table 4.

For the analysis, the experimental values of the cumulated mass loss and of the erosion rates were approximated by curves constructed with the analytical relations, below, established by Bordeasu and collaborators [7, 16]:

$$m(t) = A \cdot t \cdot (1-e^{-B \cdot t}) \text{ – for cumulative mass losses } M_i \tag{1}$$

$$v(t) = A \cdot (1-e^{-B \cdot t}) + A \cdot B \cdot t \cdot e^{-B \cdot t} \quad \text{- for erosion speed (speed of mass loss)}$$

where:

A - is the scale parameter, statistically established for the construction of the approximation curve, provided that the deviations of the experimental points from this curve are minimal

B - is the shape parameter of the curve

The experimental values, approximated by the two curves described by relations (1), are calculated on the basis of the mass losses Δmi, recorded at the end of each intermediate test period, "i", according to the relations below.

$$M_i = \sum_{i=1}^{12} \Delta m_i$$

$$v_i = \frac{\Delta m_i}{\Delta t_i} \tag{2}$$

Δti – duration of cavitation corresponding to periods “i” (5 minutes, 10 minutes or 15 minutes)

Table 4 and Figure 4 shows macro images of the eroded cavitation surface obtained by shooting with the Canon Power Shot A 480.

From these images, one can easily observe the differences in behavior and resistance to cyclic stresses of cavitation micro-jets. Thus, in samples III, surface erosion begins relatively quickly (within 15-30 minutes of cavitation) and, by the end of the experiment (165 minutes), the pits turn into large caverns, which give the shape of the detachment of metal chips. In the rest of the samples, the erosion of the cavitation is manifested by pinches, which develop completely differently from sample III, they increase in number and depth with the duration of the cavitation, in the form of caves.

Table 4: Macro images, photographed with the Canon Power Shot A 480 camera

Cavity attack duration [min]	**I**	**II**	**III**	**IV**
5				
30				

60				
90				
120				

Sample I

Sample II

Sample III

Sample IV

Fig. 4. Appearance of the eroded surface after 165 minutes of cavitation

It should be noted that all samples follow the mechanical mechanism of erosion initiation [5, 7], in the form of pinches on a peripheral ring, which then develops on the area exposed to cavitation microjets, caused by the collapse of cavitation bubbles generated by ultrasonic vibration. As can be seen, especially on the enlarged surfaces, from 165 minutes, Figure 4, of the 3 treatments, the best behavior, respectively resistance to cavitation erosion are obtained for the duration of 24 hours of maintenance of the artificial aging treatment at 180℃.
According to the aspect of the degree of erosion (cave sizes and shapes, but also the porosity created by the large number of pits), correlated with the hardness values (table 3), the impression is created that by decreasing HB hardness and KCU resilience the resistance to cavity erosion tends to increase (see sample IV characterized by the lowest values of HB = 71.8 daN / cm^2, KCU = 16.4 J / cm^2). False appearance, because the hardness negatively influences the resistance to cavitation, only when the surface becomes brittle [5, 8], and this is not the case.
The diagrams in Figure 5-12, through the experimental values and the approximation curves show the behavior of the surfaces at the cavitation demands, and those in Figures 13 and 14 serve to compare the resistance conferred by the three treatments, but also to the initial state of delivery (without treatment).
The areas marked by dark, red curves include the experimental values that express the yield of the surface material to the impact with the cavitation microjet which, in a significant duration of the cavitation (depending on the duration of maintenance to the artificial aging treatment) degrades by expanding the caverns in area and depth. At the same time, it is noticed, in all the samples, that after about 120 minutes of cavitation, until the completion (165 minutes), the mass losses and the erosion rates are approximately constant. From the experiences of the laboratory [5, 7, 13, 14] and other authors [8, 9, 11], we consider that this behavior, towards the end of the experiment, is caused by the air entering the caverns during the surface vibration, which dampens the pressure / the impact shock between the surface exposed with the shock wave and the micro-jets produced at the implosion of the cavitation bubbles, respectively.
Following the areas marked by curves and the macro images in Table 4 it can be seen that the corresponding periods correspond to those in which the surface erodes deeply.

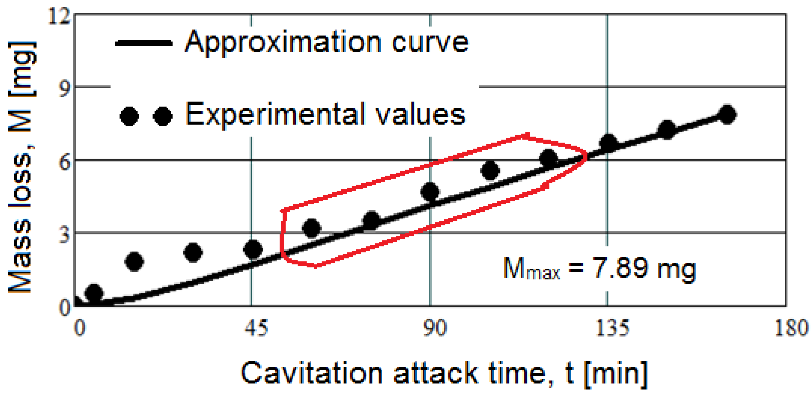

Fig. 5. Variation of eroded mass with cavitation duration (control sample)

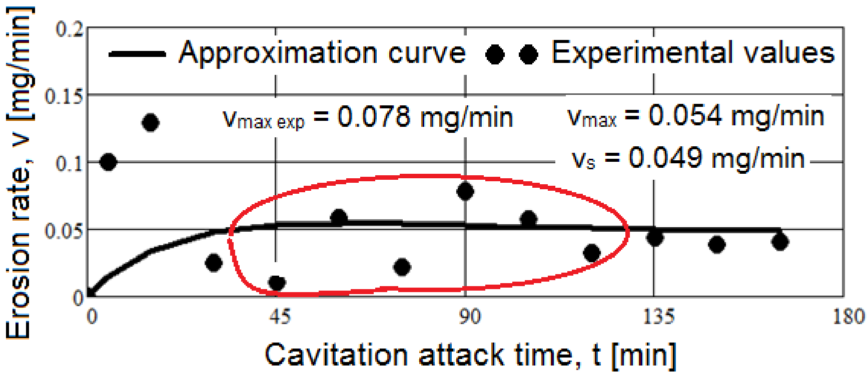

Fig. 6. Variation of erosion rate with cavitation duration (control sample)

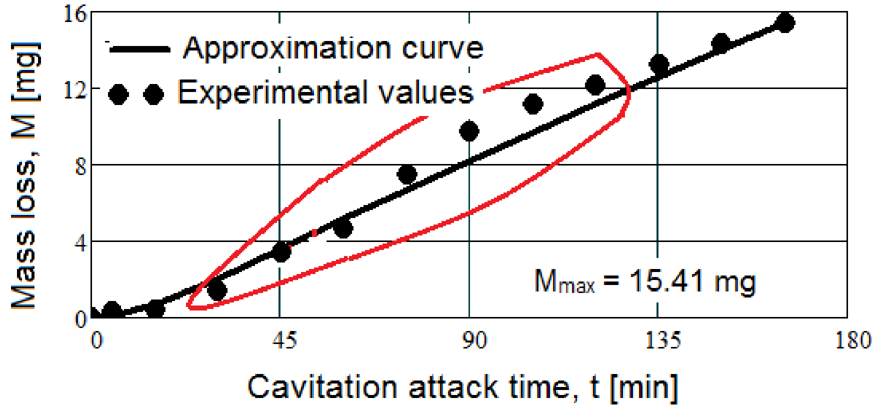

Fig. 7. Variation of eroded mass with cavitation duration (heat treatment duration 1 hour)

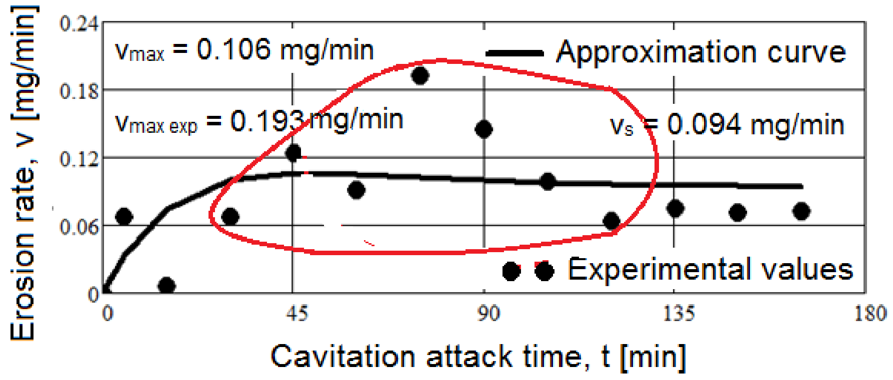

Fig. 8. Variation of erosion rate with cavitation duration (heat treatment duration 1 hour)

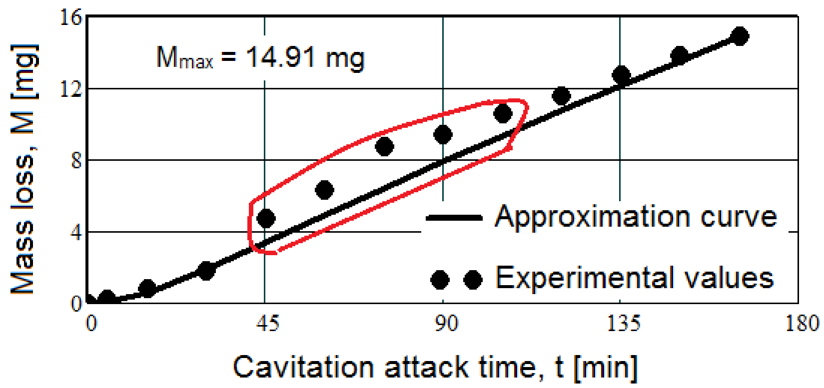

Fig. 9. Variation of eroded mass with cavitation duration (heat treatment duration 12 hours)

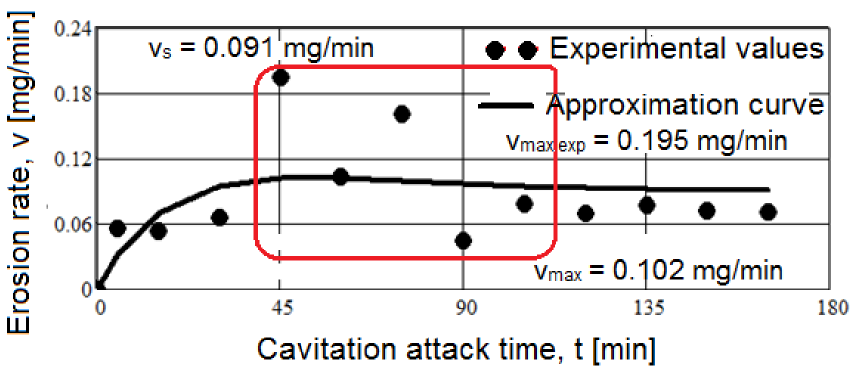

Fig. 10. Variation of erosion rate with cavitation duration (heat treatment duration 12 hours)

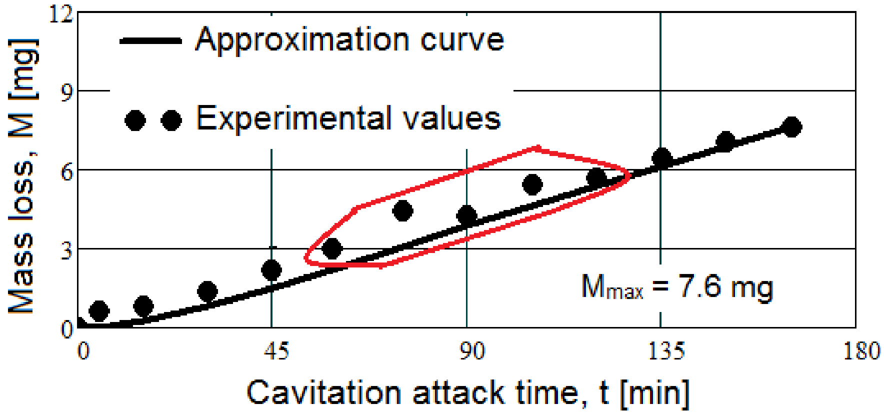

Fig. 11. Variation of eroded mass with cavitation duration (heat treatment duration 24 hours)

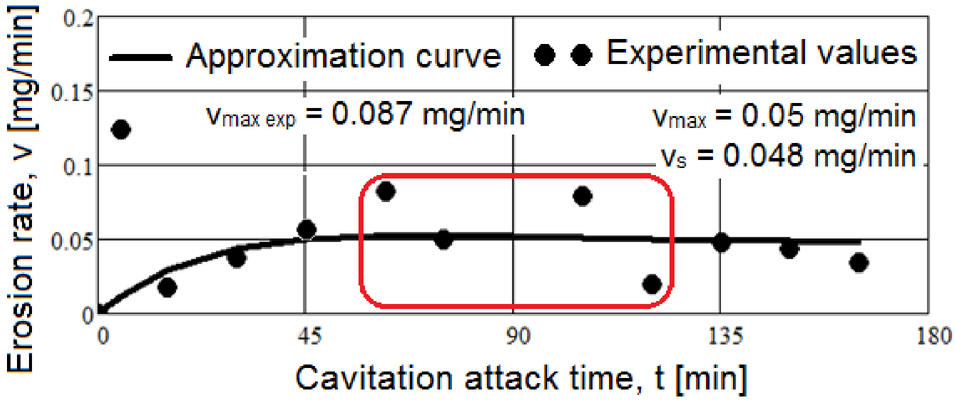

Fig. 12. Variation of erosion rate with cavitation duration (heat treatment duration 24 hours)

The comparison based on the curves of mass loss (Figure 13) and erosion rate (Figure 14) is in accordance with the appearance of the eroded surfaces, from Figure 4 and shows:
• behaviors and resistances approximately identical of the samples without treatment (I) with those of the samples with a maintenance duration of 24 hours at the temperature of artificial aging (180 °C), although they have significant differences in the mode of destruction;
• approximately identical behaviors and resistances of the samples with maintenance times of 1 hour (II) and 12 hours (III) at the temperature of artificial aging.
• Significant differences between hardness and resilience values (see Table 3) suggest that for this cast 5083 alloy not the mechanical properties have a significant influence on the resistance to cavity erosion but the microstructure resulting from the volume heat treatment.
The almost identical evolutions of the mediation curves and the differences shown by the appearance of the erosions produced in the exposed surfaces (see the images in Figure 4 and Table 4), are the proof of the complicated mechanism of destruction by cavitation, caused by the structures resulting from thermal treatments, or by retention periods (in this case). Therefore, in this aluminum alloy the evaluation/estimation of the behavior and resistance to cavity erosion, according to the values of hardness or resilience, obtained by the mentioned heat treatments, and does not align with those concluded in steels, where the duration of maintenance at the same temperature is very well reflected in the values of mechanical properties and in response to the cyclic stresses of the cavity [5, 7, 9, 10, 13, 14].

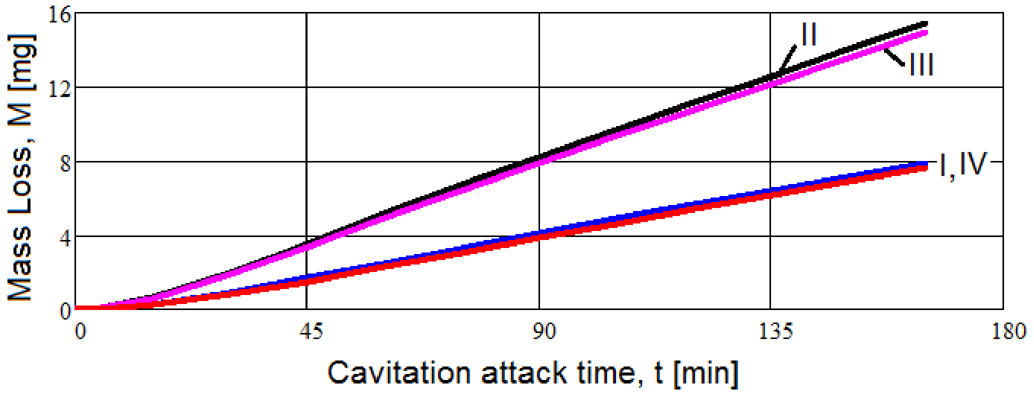

Fig. 13. Comparison of cumulative mass losses

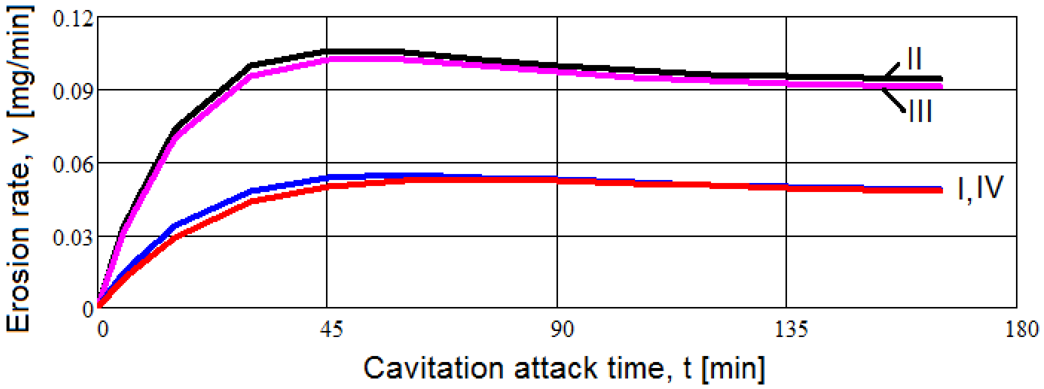

Fig. 14. Comparison of erosion speeds

4. Conclusions

1. The behavior and strength of cast 5083 aluminum alloy is strongly dependent on the microstructure resulting from the heat treatment of heating at 350 °C, followed by artificial aging at 180°C, with different maintenance times.
2. By artificial aging at 180°C / 24 hours the state of cavitation resistance is similar to the condition of non-aging test specimens, while after artificial aging at 180°C / 1 hour, or 12 hours the state of cavitation resistance is much deteriorated. A possible cause of this behavior may be due to the formation of the Guinier Preston’s Zones, which by consistent precipitation achieves a decrease in mechanical properties at these intermediate heat treatments (i.e. maintenance time of one hour and 12 hours). This can be demonstrated by conducting future structural investigations.
3. No clear conclusions can be drawn about the influence of cavitation strength by hardness and resilience, as is possible on steels, due to the complicated mechanism of destruction and surface response to cyclic stresses of micro-jets and shock waves, developed by implosion cavitation bubbles,
4. It is necessary to continue the study based on analyzes by electron or optical microscopy, of very high resolution, to explain the different way of breaking the structure (chip or pinch shape).

References

[1] http://www.placi-aluminiu.ro/en-aw-5083-almg45mn07].
[2] http://old.color-metal.ro/ro/aluminiu-turnat.
[3] https://fdocumente.com/document/aluminiu-catalog.html.
[4] https://gleich.de/en/wp-content/uploads/sites/4/2016/10/en_en_aw_5083.pdf.
[5] Bordeaşu, Ilare. *Cavitation erosion on the materials used in the construction of hydraulic machines and naval propellers. Scale effects / Eroziunea cavitațională asupra materialelor utilizate în construcția mașinilor hidraulice și elicelor navale. Efecte de scară*. Doctoral Thesis. Timişoara, 1997.

[6] Caplescu, Cristiana, Liviu Marsavina, Ilare Bordeasu, and Ramona M. Sechei. “The Fracture of Polyurethane Materials in the Presence of Stress Concentrators.” *Materiale Plastice* 47, no. 3 (September 2010): 379-382.
[7] Bordeasu, Ilare. *Monografia Laboratorului de cercetare a eroziunii prin cavitaţie al Universităţii Politehnica Timişoara: (1960-2020) / Monograph of the Cavitation Erosion Research Laboratory of Politehnica University of Timisoara (1960-2020)*. Timisoara, POLITEHNICA Publishing House, 2020.
[8] Franc, Jean-Pierre, François Avellan, Brahim Belahadji, Jean-Yves Billard, Laurence Briançon-Marjollet, Didier Fréchou, Daniel-H. Fruman, Ayat Karimi, Jean-Louis Kueny, and Jean-Marie Michel. *The Cavitation. Physical Mechanisms and Industrial Aspects. / La cavitation. Physical mechanisms and industrial aspects*. Grenoble, Press Universitaires de Grenoble, 1995.
[9] Garcia, R., Frederick G. Hammitt, and R.E. Nystrom. “Correlation of cavitation damage with other material and fluid properties”, *Erosion by Cavitation or Impingement*. ASTM - STP 408, Atlantic City, 1960.
[10] Anton, Ioan. *The Cavitation / Cavitatia.* Vol I. Bucharest, RSR Academy Publishing House, 1984.
[11] Steller, Kazimir, R. Bugola, and Janus Steller. “Cavitation Roads and their erosive effects.” 2 - emes, Journees Cavitation, Paris, France, March 1992.
[12] Li, Xiao-ya, Yong-gui Yan, Zhen-ming Xu, and Jian-guo Li. “Cavitation erosion behavior of nickel-aluminum bronze weldment.” *Transactions of Nonferrous Metals Society of China* 13, no. 6 (December 2003): 1317-1324.
[13] Bordeasu, Ilare, Ion Mitelea, Laura Salcianu, and Corneliu Marius Craciunescu. “Cavitation Erosion Mechanisms of Solution Treated X5CrNi18-10 Stainless Steels.” *Journal of Tribology* 138, no. 3 (2016): 031102.
[14] Bordeasu, Ilare, and Ion Mitelea. “Cavitation Erosion Behavior of Stainless Steels with Constant Nickel and Variable Chromium Content.” *Materials Testing* 54, no.1 (2012): 53-58.
[15] ASTM International. *Standard Test Method for Cavitation Erosion Using Vibratory Apparatus*. ASTM G32-16, 2016.
[16] Micu, Lavinia Madalina, Ilare Bordeasu, and Mircea Octavian Popoviciu. “A New Model for the Equation Describing the Cavitation Mean Depth Erosion Rate Curve.” *Revista de Chimie* 68, no. 4 (April 2017): 894-898.

Impact of Yttria Reinforced Nanolubricants onto the Tribological Properties

PhD Stud. Eng. **Álmos Dávid TÓTH*[1]**, PhD Stud. Eng. **Ádám István SZABÓ**[1],
Dr. Eng. **Jan ROHDE-BRANDENBURGER**[1], Full Prof. Dr. **Rajmund KUTI[2]**

[1] Széchenyi István University, Department of Internal Combustion Engines and Propulsion Technology

[2] Széchenyi István University, Faculty of Mechanical Engineering, Informatics and Electrical Engineering

*toth.almos@sze.hu

Abstract: *The continuous improvement of the tribological properties of lubricants is a vital task for engineers, not only in the case of internal combustion engine applications. The researchers are working on investigating different materials to find the possible lubricant additives of the future. One of the possibilities can be the different nanoparticles. Their spherical geometry with nanoscale can provide excellent tribological properties but they must be thoroughly investigated before using them in real machines. This paper introduces the experimental results with spherical yttria nanoparticles as tribological additives in different lubricant types. Ball-on-disc tribometer measurements were carried out to define their frictional behavior and the arisen wear scars were analyzed via high-magnitude scanning electron microscope completed with EDX element analysis. The yttria reinforced nanolubricants have provided astonishing antiwear properties and the SEM images have revealed marks that refer to the mending as their main working mechanism.*

Keywords: *Tribology, yttrium oxide, yttria, nano-ceramic, lubricant, additive, engine*

1. Introduction

Because of the strict emission and fuel consumption regulations all around the world, engine developers have to face huge challenges. To fulfill these regulations the whole vehicle including the combustion powertrain must be further developed to reduce the emission of harmful exhaust gas components, such as CO, NO_x, soot, or unburned fuel particles. The applied lubricants in the internal combustion engines play a crucial role in the tribological processes inside the engine, which also influences the emission and fuel efficiency of the engine. The current lubricants used inside the engines are very complex liquids and they contain different additives to influence the tribological effects of the lubricants and so of the engines as well.

Several research fields are existing to increase the tribological performance of the lubricants and so increase the efficiency of the engines. Low-viscosity lubricants were developed (e.g., SAE 0W-20 viscosity class) to lessen the internal friction of the liquid. Further research activities are running all around the world to find the possible lubricant additives of the future as well. The ionic liquid is a very hopeful field to replace the currently used materials of the engine oils.

Another promising field is the nano-scale particles used as tribological lubricant additives. These materials are scientifically researched in the past 10 years deeply by numerous scientists and they have reported significant improvements used different materials as nano-scale additives. These nanoparticles can be made from metal-oxides (e.g., TiO_2, CuO, Fe_3O_4, ZnO, Co_3O_4, Al_2O_3, etc.), metal-sulfides (MoS_2, WS_2, FeS, etc.), nanocomposites (Cu/CeO_2, Al_2O_3/SiO_2, ZrO_2/SiO_2, etc.) or rare-earth metal compounds ($CeVO_4$, Y_2O_3, $La(OH)_3$, LaF_3, etc.) [1]. The geometry of these nanoparticles can also be different: spherical, granulate, lamina, nanotube, or multilayer [1]. The size of the particles also plays a critical load in the measurable tribological properties of nanoparticles: Peña-Parás et al. have proved in their research that only those particles can provide positive effects whose average particle size is lower than the average roughness (Ra) of the contacting surfaces [2].

Different working mechanisms were reported by Zhang et al. to explain how these nanoparticles can provide such promising tribological properties: rolling (ball bearing), mending, polishing, and protective film mechanism [3]. However, each nanoparticle compound can act differently because of its particle size and hardness, which requires analyzing them with simplified methods before they could be used in a real operating machine.

The tribological properties of nanoscale yttrium oxide (yttria) particles were experimentally analyzed via ball-on-disc simplified tribological measurement method. Nanoscale yttria particles (CAS number: 1314-36-9) were used for these investigation activities with an average particle diameter of less than 50 nm. This paper contains the results and discussion of these experiments.

2. Yttrium oxide nanoparticles

Yttrium oxide (yttria, Y_2O_3) is an air-stable, white, solid crystalline oxide of yttrium transition metal. Yttria closely resembles lanthanide oxides in most of their properties. Generally, yttria is produced by the calcination of yttrium containing compounds and ores like samarskite-(Y) and yttrobetafite-(Y). The other industrial producing possibility is the solvent extraction from ores that also contain the heavier lanthanides. Yttria occurs naturally in its mineral, known as yttrialite-(Y). Naturally, yttria appears with a cubic centered crystalline structure but the structure depends on the temperature. Its body-centered cubic structure (Figure 1.) changes phase to a hexagonal form above 2640 K temperature [4].

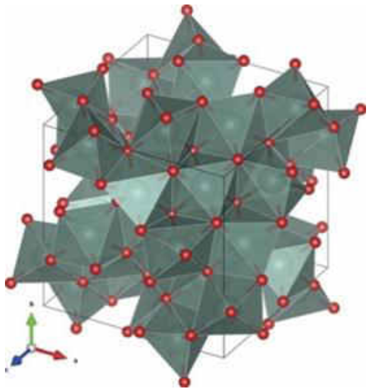

Fig. 1. Body-centered cubic crystal structure of Y_2O_3 [5]

Yttria is mainly characterized by its high thermal stability, and it is suitable for extreme operating conditions. The material engineering applications are based on this property. Due to its rarity, yttrium oxide is rarely used alone, usually as an additive in combination with other substances. Y_2O_3 is used in various applications: stabilizing zirconia against its phase transformation on elevated temperatures; as a sintering aid for silicon nitride and SiAlON ceramics, strengthening nickel alloys, LED components, producing high-temperature resistant transparent ceramics, basis material for solid-state lasers, the raw material for high-temperature superconductors and microwave filters [5].

The density of yttria is around 4.8-5.07 kg/m^3 and its plane strain fracture toughness varies between 1.2 and 3.27 GPa, depending on its production process. Cubic yttria has higher hardness (~2200-2800 HV) compared to steels. The bending strength of yttria (15-140 MPa) varies on a wide scale depending on its temperature, while Young's modulus of yttria (146-168 GPa) is lower than the common steel types [6]. Yttrium oxide is very similar in its properties to lanthanide oxides, which are excellent lapping agents [5]. Due to its physical properties, yttrium oxide can show a lapping-polishing mechanism of action when used as an additive in a tribological system.

Only a limited number of research papers are dealing with the characterization of net yttria ceramic material. Positive oxidation decreasing properties were reported by Wukusick when it was used as an alloying material [7]. In a research paper by Liu et al., the yttria was used as a lubricant additive and they investigated its corrosion preventing properties on the surfaces of specimens from 6061 Al alloy and 304 stainless steel materials with a pin-on-disc tribometer [8]. He et al. investigated sheet-like 2D yttria nanoparticles as liquid additives and they have reported a significant improvement in the mechanical and flow phenomena of various fluids [9].

3. Investigation methods

One of the key elements of the characterization of nanoparticles in liquids is the mixing procedure to homogenize them. No universal homogenization procedure can be found in the literature, so a self-developed mixing procedure were used for this purpose. For the tribological experiments both neat Group III base oil and engine oil with SAE 0W-20 viscosity class were used. The liquids were provided by MOL-LUB Ltd. The yttria particles were doped in the liquids and these mixtures were homogenized with magnetic stirrer for 3 minutes at 100 rpm and with ultrasonic homogenizer for 30 minutes and 50°C. After the ultrasonic homogenization the lubricant samples were further stirred magnetically until the lubrication pipes inside the tribometer were filled up with them.

For the tribological measurements the ball-on-disc system of an SRV®5 type tribometer were used. The specification of the specimens was correlated to the ISO 19291:2016 [10] standard. To simulate the circumstances of the lubricants inside the engine as precise as possible, a method with a self-developed setup parameters were used [11]. This method contains a supplementary oil circuit with a peristaltic pump which realize a continuous oil flow of 225 ml/h to the testing specimens and leads the used lubricant to the pump again. An oscillation movement were realized between the ball and disc specimens with 1 mm stroke, 50 Hz frequency. Both the specimens and the used lubricants were heated up to 100°C temperature separately. A 50 N preload was applied to the ball specimen for 30 seconds to avoid high damages in the specimen surfaces during the run-in phase and a further 2 hours of test with higher normal forces (100 N in case oil base oil, 200 and 300 N in case of formulated engine oil) was carried out to investigate the friction and wear behavior of the lubricant samples. The used testing machine with the realized oil circuit is presented in Fig 2.

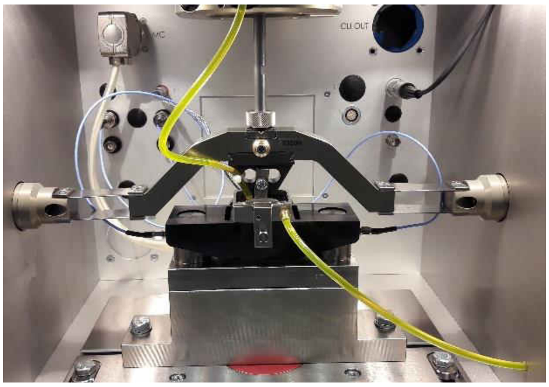

Fig. 2. The used Optimol SRV®5 tribometer with the installed pipes of the oil circuit

For the evaluation of the results, two different friction coefficient values were used, which were recorded with 1-second recording frequency:

- COF (coefficient of friction) value: the maximum friction coefficient value during one stroke, which arises usually from the dead centers of the oscillation movement, representing the property of the system under boundary lubrication conditions.
- FAI (friction absolute integral) value: an average value calculated from the area under the friction coefficient values recorded with high frequency, representing the property of the system under mixed and hydrodynamic lubrication regimes.

The produced wear scars on the ball and disc specimens were analyzed via digital (Keyence VHX-1000) and scanning electron microscope (Hirox SEM 4000M). The main goal of the microscopic investigation is to investigate the wear behavior of the yttria-doped lubricant samples. The wear scar diameter (WSD) on the ball specimens was measured in the direction of parallel and perpendicular and their average value was used for further evaluation. High-resolution SEM images were taken to analyze the possible yttria distribution on the worn surfaces and to define the major wear patterns on the surfaces.

4. Experimental results and discussion

The characterization of the yttria nanoparticles should have started with the investigation of dispersant necessity for the nanoparticles. As a dispersant, we used Triton X-100, because its chemical properties are the best to provide homogeneous nanoparticle distribution. Four different lubricant samples were prepared: neat Group III base oil as the reference, Gr III doped with 0.5% yttria nanoparticles, Gr III with 1 wt% of TX100, and Gr III doped with both 1 wt% TX100 and 0.5 wt% Y_2O_3. The results of the tribometer measurements are illustrated in Fig. 3. The bar chart clearly illustrates the trend, that the yttria-doped lubricant without dispersant provides no positive tribological properties, but in the case of the triton-doped samples, the positive effect of the yttria nanoparticles is significant. According to these results, only TX100-doped lubricant samples were used for further investigations.

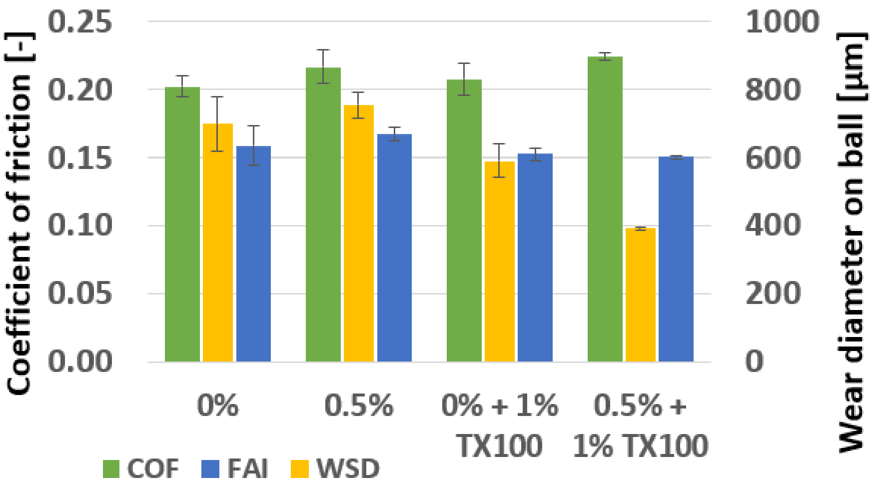

Fig. 3. Comparison of the tribological results with triton-doped and non-triton doped oil samples

To investigate the optimal yttria concentration in the lubricants, samples with 6 different concentrations were prepared (between 0.1 and 0.6 wt%). The tribological properties of these samples were tested with the same tribometer method and the results were presented in Fig. 4. It can be clearly seen that an optimum can be observed at 0.5 wt%: the measured wear scar diameter has significantly reduced with only a small amount of friction increase. The 0.4 wt% concentration has also shown an interesting tendency: the friction coefficient was reduced slightly, but the WSD on the ball specimen has increased and the measurable deviation has been also raised.

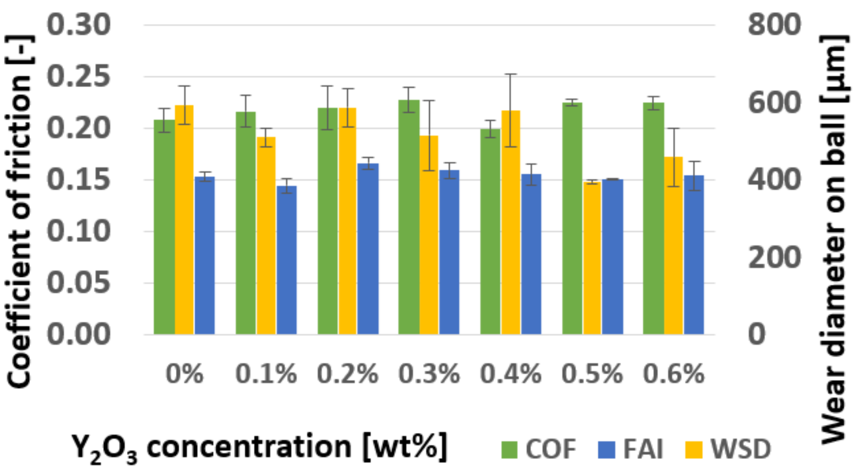

Fig. 4. Comparison of the experimental results of analyzed Gr III-based lubricant samples with various nanoparticle concentration

Similar yttria concentrations were also prepared based on the 0W-20 engine oils including 1 wt% of TX100. The tribological measurements with the same evaluations were carried out under two normal load values, 200 N and 300 N. The evaluation of the tribological results is presented in Fig. 5. The bar charts clearly illustrate the optimum concentration of yttria nanoparticles: 0.1 wt% yttria under 200 N and 0.2 wt% of yttria under 300 N load. Under both normal forces, the friction coefficient and the wear scar diameter were also reduced significantly.

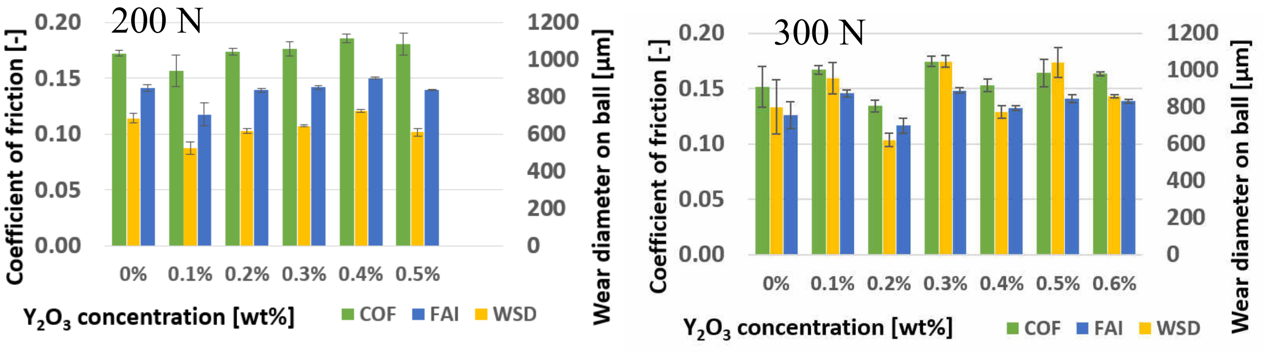

Fig. 5. Comparison of the experimental results of analyzed 0W-20-based lubricant samples with various nanoparticle concentration under 200 N (left) and 300 N (right) load

The digital microscopic analysis of the ball specimens has revealed an astonishing wear reduction property of the yttria nanoparticles. The wear scars on the disc specimens were also analyzed to understand how the wear was produced. The digital microscope images can be observed in Fig. 6. It can be stated that in the case of 100 N and 200 N loads the wear depth is enough low to see the valleys of the surface roughness. Besides, a significant positive effect of the yttria particles can be defined according to the images.

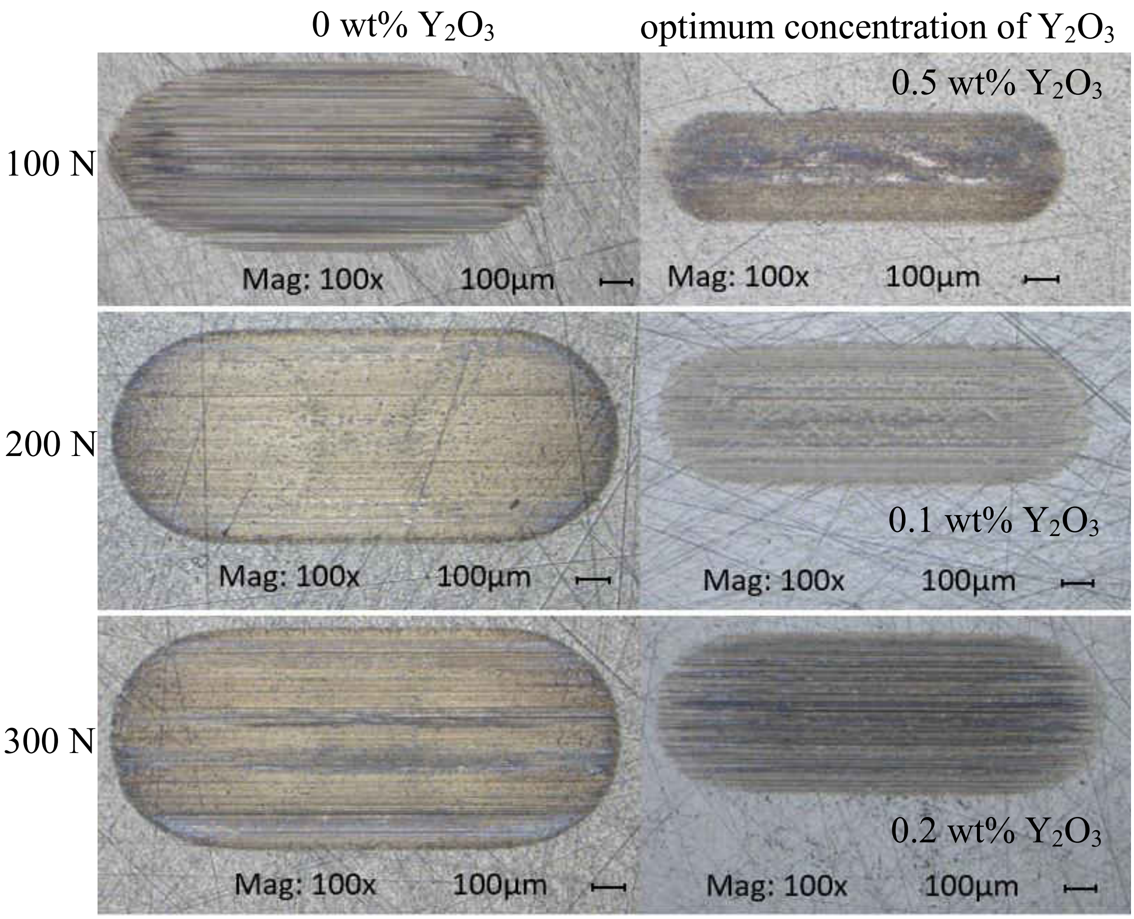

Fig. 6. Comparison of the wear scars on the disc specimen using digital microscopic images

Further scanning electron microscopic analysis was also carried out to define the wear mechanisms and the existence of yttria nanoparticles on the worn surface. Fig. 7. illustrates the SEM-images mage on the worn surface of the disc specimens with 0.5 wt% Y_2O_3 and 1 wt% TX100-doped Gr III base oil. The wear scars on the images can barely see and the grooves of the original surfaces are also seeable which proves the excellent antiwear properties of the investigated yttria nanoparticles. The EDX-analysis reveals that the yttria nanoparticles are collected in the grooves and on the top layer of the surface too. These SEM results are proof that the yttria nanoparticles are working by the mending mechanism.

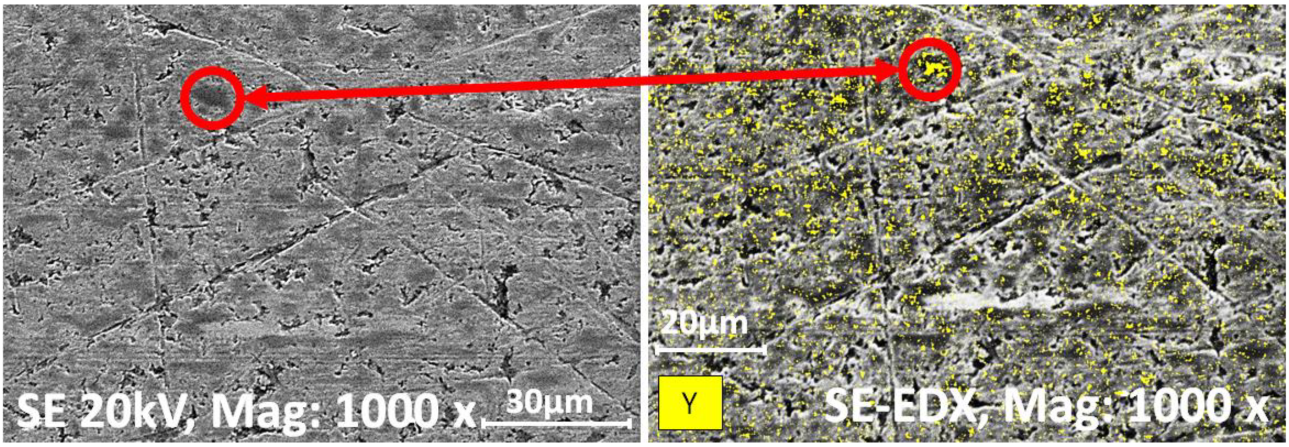

Fig. 7. SE-Scanning Electron Microscope image and EDX mapping picture about the surface of disc specimen with 0.5 wt% Y_2O_3 doped Gr III base oil

The element distribution on the worn surface was also investigated with the EDX sensor or the used scanning electron microscope. The worn surfaces with both the reference oil sample (Gr III base oil + 1 wt% TX100) and the optimum sample (Gr III base oil + 1 wt% TX100 + 0.5 wt% Y_2O_3) were quantitatively analyzed to understand how the tribosystem has changed with the addition of yttria nanoparticles. The measured data can be observed in Table 1. The results show a significant increase of yttrium, oxygen, and carbon elements on the worn surface with yttria-doped samples. The increased amount of carbon element can be explained by the increased amount of base oil molecules attached to the worn surface, compared with the yttria-free sample. The reference sample showed a high amount of wear which has reduced the amount of adhered base oil molecules to the surface, and this process did not appear in the case of yttria-doped samples. The significant increase of yttrium represents the number of yttria nanoparticles on the surface. The oxygen increase can indicate two effects: the presence of yttria nanoparticles on the surface and a small amount of oxidation of the metal substrate. For the SEM images, the specimens were thoroughly cleaned in an ultrasonic cleaner with brake cleaner liquid and at a temperature of 50°C multiple times, and the nanoscale yttria particles could be observed even after his cleaning procedure. The particles in this scale level can adhere to the surfaces via van-der-Waals forces, which can explain how the yttria nanoparticles worked on the surface and how they could realize their astonishing antiwear properties.

Table 1: Quantitative element analysis (wt%) on the worn surface of the disc specimen with 0.5 wt% Y_2O_3 lubricant sample and comparison with the reference results

Element	Gr III + 1% TX100	Gr III + 1% TX100 + 0.5% Y_2O_3
Fe	95.92%	77.43%
Cr	1.34%	1.24%
Si	0.11%	1.9%
O	1.52%	9.54%
C	1.11%	8.11%
Y	0%	1.78%

Compared to the previous results with the same investigation methods with Group III-based oil samples [12, 13], the yttria nanoparticles have provided astonishing antiwear properties and the measurable friction coefficient values could be reduced in case of the engine oil investigations too. The yttria nanoparticles could also fill up the surface roughness valleys and wear grooves, similar to the previously investigated zirconia nano additives [12]. However, the purchase costs of the yttria nanoparticles are significantly higher compared to the zirconia ones. The tribological investigation of the so-called yttria-stabilized-zirconia (YZS) [14] can be interesting, which could provide the excellent antiwear properties of the yttria nanoparticles cost-effectively.

5. Conclusions

This paper presents the results of the experiments with spherical yttria nanoparticles homogenized into a neat Group II base oil and a fully formulated engine oil with the viscosity class of SAE 0W-20. For the investigations, a ball-on-disc tribosystem completed with a wide microscopic analysis was carried out.

As the result, the following statements can be formulated:

- To achieve the maximum potential inside the yttria nanoparticles, an extra dispersant additive (Triton X-100) had to be mixed into the yttria-doped lubricant samples.

- The yttria nanoparticles have provided excellent antiwear properties for the used lubricants. The reduction of the wear scar diameter on the ball specimens was measured as 33% in Group III oil, 23% in engine oil under 200 N, and 22% under 300 N. In most of the cases, the measured friction coefficient values were also reduced.

- Different optimum concentrations could be defined, and their value was highly dependent on the used basis liquid. 0.5 wt%, 0.1 wt%, and 0.2 wt% values were determined in the case of neat Group III base oil, engine oil under 200 N, and engine oil under 300 N, respectively.

- The working mechanism of the yttria nanoparticles was examined with a scanning electron microscope completed with an EDX element analysis. According to the observed SEM-images it can be stated that the yttria nanoparticles could attach to the contacting surfaces via van-der-Waals forces, fill up the wear grooves and roughness valleys resulting in a smoother contact surface. This mechanism explains the excellent antiwear properties of the yttria nanolubricant.

The yttria-doped nanolubricant samples have provided astonishing antiwear properties to the investigated ball-on-disc tribosystem in both neat base oil and fully formulated engine oil. The purchase costs of the yttria nanoparticles lessen its potential to use in the engines of passenger cars in the future as well. To reduce the costs, tribological analysis of additional nanoparticles is recommended (e.g., yttria-stabilized-zirconia). Further investigation methods are also recommended to analyze the impact of nano additives for the engines like fuel- and oil consumption or exhaust gas emission.

Acknowledgments

The authors would like to thank Ms. Dóra Olimpia Csepreghy and Ms. Boglárka Nagy for their general support.

References

[1] Uflyand, Igor E., Vladimir A. Zhinzhilo, and Victoria E. Burkalova. "Metal-containing nanomaterials as lubricant additives: State of the art and future development." *Friction* 7, no. 2 (March 2019): 93-116.
[2] Peña-Parás, Laura, Hongyu Gao, Demófilo Maldonado, Azhar Vellore, Patricio García-Pineda, Oscar E. Montemayor, Karen Lorena Nava, and Ashlie Martini. "Effects of substrate roughness and nano/micro particle additive size on friction and wear in lubricated sliding." *Tribology International* 119 (September 2017): 88-98.
[3] Zhang, Zhenyu J., Dorin Simionesie, and Carl Schaschke. "Graphite and hybrid nanomaterials as lubricant additives." *Lubricants* 2, no. 2 (April 2014): 44-65.
[4] Götsch, Thomas, Wolfgang Wallisch, Michael Stöger-Pollach, Bernhard Klötzer, and Simon Penner. „From zirconia to yttria: Sampling the YSZ phase diagram using sputter-deposited thin films." *AIP Advances* 6, no. 2 (February 2016): 025119.
[5] Brook, R.J. *Concise Encyclopedia of Advanced Ceramic Materials*. Oxford, Elsevier Ltd., 1991.
[6] Quesada, Dolores Eliche. *Ceramic Materials – Synthesis, Characterization, Applications and Recycling*. London, IntechOpen Ltd., 2019.
[7] Wukusick, C.S., and J.F. Collins. "An iron-chromium-aluminum alloy containing yttrium." *Material Research and Standards* 4 (1964): 637-646.
[8] Liu, Rong, and D.Y. Li. "Protective effect of yttrium additive in lubricants on corrosive wear." *Wear* 225-229 (April 1999): 968-974.
[9] He, Xingliang, Huaping Xiao, Jonathan P. Kyle, Elon J. Terrell, and Hong Liang. "Two-dimensional nanostructured Y_2O_3 particles for viscosity modification." *Applied Physics Letters* 104, no. 16 (April 2014): 163107.
[10] ISO 19291:2016(E). Lubricants – Determination of tribological quantities for oils and greases – Tribological test in the translator oscillation apparatus, 2016.
[11] Tóth, Álmos Dávid, László Paulovics, Barna Hanula, Jan Knaup, and Andre Kopp. "Development of testing methodology for tribological characterisation of different engine lubricants / Methodenentwicklung zur Einstufung von Motorölen anhand tribologischer Eigenschaften." Paper presented at the 58th German Tribology Conference 2017, Göttingen, Germany, September 27-29, 2017.
[12] Tóth, Álmos Dávid, Ádám István Szabó, and Rajmund Kuti. „Tribological Properties of Nano-Sized ZrO_2 Ceramic Particles in Automotive Lubricants." *FME Transactions* 49, no. 1 (September 2020): 36-43.
[13] Tóth, Álmos Dávid, Ádám István Szabó, Rajmund Kuti, and Jan Rohde-Brandenburger. „Tribological Investigation of Applicability of Nano-Sized Cupric Oxide (CuO) Ceramic Material in Automotive Vehicles." *FME Transactions* 49, no. 2 (February 2021): 335-343.
[14] Ganapathy Pandian, Sakthinathan. „Tribological Characteristics of Yttria Stabilized Zirconia Nanolubricants." *SAE Technical Paper*, 2014-01-2790 (October 2014): 1-7.

Study of Electro-Pneumatic Circuits with Magnetic Proximity Switches

Prof. Dr. eng. **Mariana PANAITESCU**[1], Dipl. Eng. **Remus COJOCARU**[2],
Dr. eng. **Tiberiu AXINTE**[3*], Dipl. Eng. **Cătălin FRĂȚILĂ**[3], Dipl. Eng. **Roxana DAMIAN**[3],
Dipl. Eng. **Mihai DIACONU**[3]

[1]Constanta Maritime University, Romania

[2]Princess Cruises, USA

[3]Research Center for Navy, Romania

*tibi_axinte@yahoo.com

Abstract: *In this paper, we study electro-pneumatic systems with magnetic proximity switches. Besides, magnetic proximity switches are sensors compatible with T-Slot. These sensors with LED Indicator have the following characteristics: supply voltage 24 V dc, minimum operating is -40⁰C and maximum operating temperature is +85⁰C. The study of pneumatic and electro-pneumatic circuits is performed using the software FluidSim from Festo. In the first part, we make simple pneumatic circuits with one cylinder or two pneumatic cylinders. We continue with simple and complex electro-pneumatic schemes that have magnetic proximity switches.*

Keywords: *FluidSim, pneumatic, electrical, scheme, circuit, magnetic, proximity, switch*

1. Introduction

The pneumatic cylinder is an important device in the pneumatic circuit. Pneumatic cylinders are composed of several types, [1]:

- Rod cylinders, Fig. 1.
- Rodless cylinders.
- Tandem cylinders, high force cylinders and multi-position.
- Clamping cylinder.
- Stop and separator cylinder.
- Guided cylinder.

Fig. 1. Rod cylinder

The following relation defines the equilibrium of forces within the cylinder:

$$P_1 \cdot S_1 - P_2 \cdot S_2 = m \cdot a + F_E + F_F + F_S + F_W \quad (1)$$

Where:

- P_0 – excess pressure at connection 0;
- P_1 – excess pressure at connection 1;

- S_0 – effective piston area at the side of connection 0;
- S_1 – effective piston area at the side of connection 1;
- m – moving cylinder mass;
- a – acceleration of the moving cylinder mass;
- F_E – the user defined force;
- F_F – friction for the user defined force;
- F_S – the spring force of cylinders with spring return;
- F_W – the counteracting force of gravity during the extension.

As the atmospheric pressure remains the same for the complete cylinder, [2], the pressures are specified as excess pressures, Fig. 2.

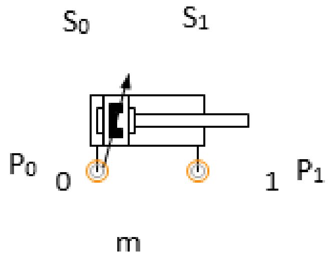

Fig. 2. Scheme of pneumatic cylinder

The simple pneumatic circuit of this paper consists of five devices, Fig. 3.
These pneumatic devices are:
1) Compressed air supply;
2) 3/2 – way valve with pushbutton (normally open);
3) Throttle check valve;
4) Pressure gauge;
5) Single acting cylinder.

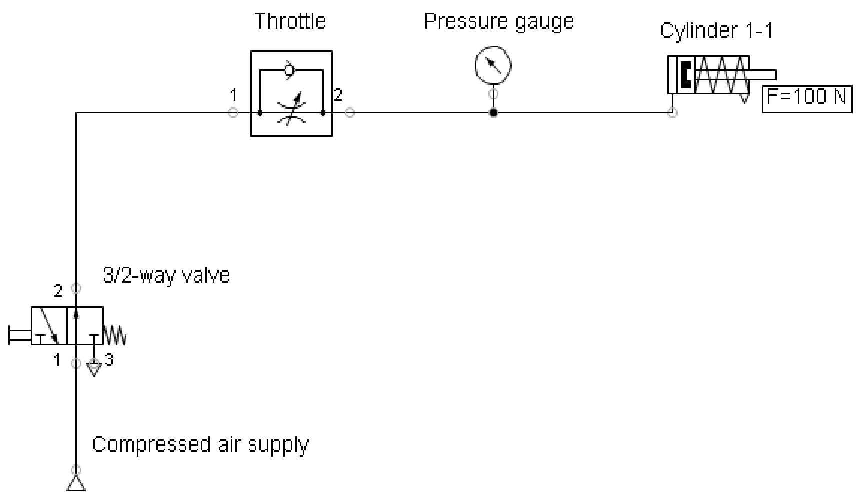

Fig. 3. Pneumatic circuit with cylinder

If force F_E = 100 N, when the piston is to middle distance, the pressure is P = 0.574 MPa, Fig. 4.

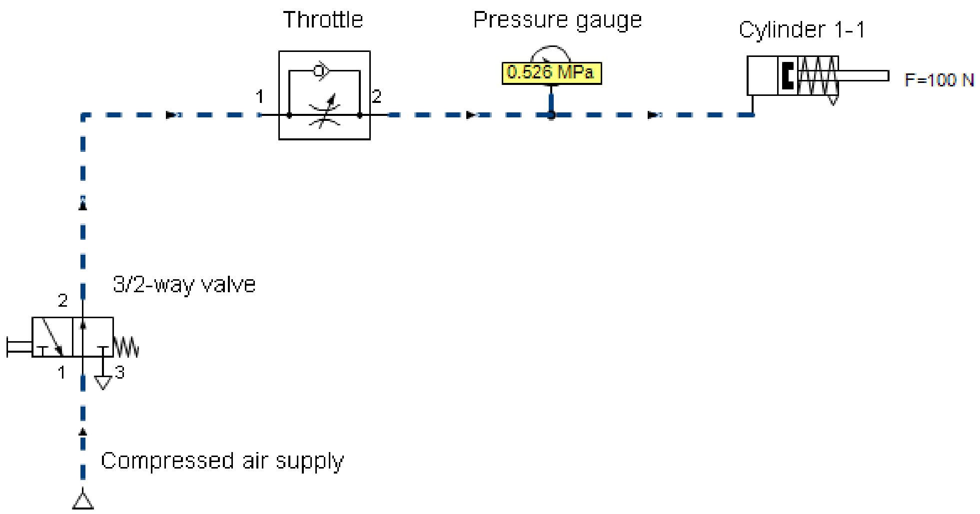

Fig. 4. Open pneumatic circuit with cylinder

Second pneumatic circuit is made of two cylinders that have in common air service unit and compressed air supply, Fig. 5.
The cylinder 2-1 is single acting and the cylinder 2-2 is double acting, Fig. 5.
The following devices are in cylinder 2-1, [3]:

- Throttle – one piece;
- 3/2 way valve – one piece.

The following devices are in cylinder 2-2:

- Throttle – two pieces;
- 5/n way valve – one piece.

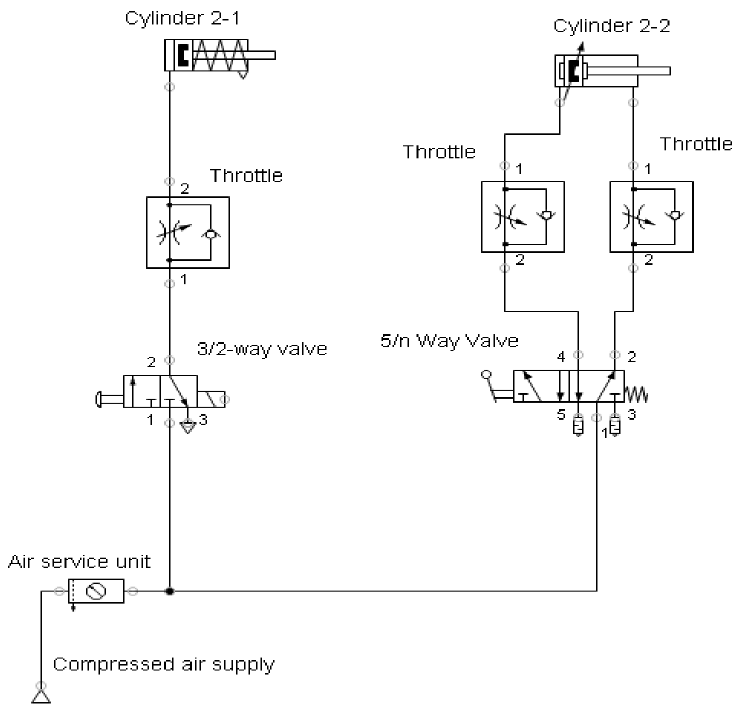

Fig. 5. Pneumatic installation with two cylinders

When we press the button from 3/2 way valve, then only the cylinder 2-1 opens. However, if we push the lever from the 5/n way valve, only cylinder 2-2 opens, Fig. 6.

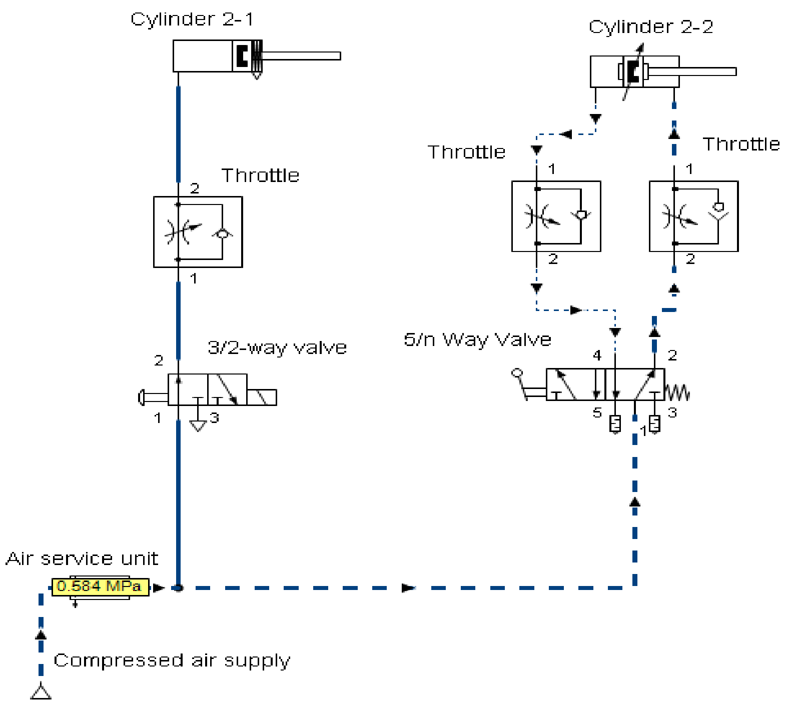

Fig. 6. Open pneumatic installation with two cylinders

2. Magnetic proximity switch

Proximity sensors are used for binary feedback of the piston position of pneumatic actuators. These sensors are used in electro-pneumatic circuits.
The main types of proximity sensors switch are: magnetic, capacitive, optical and inductive, [4].
In this paper, we study only electro-pneumatic circuits with magnetic proximity switches, Fig 7.

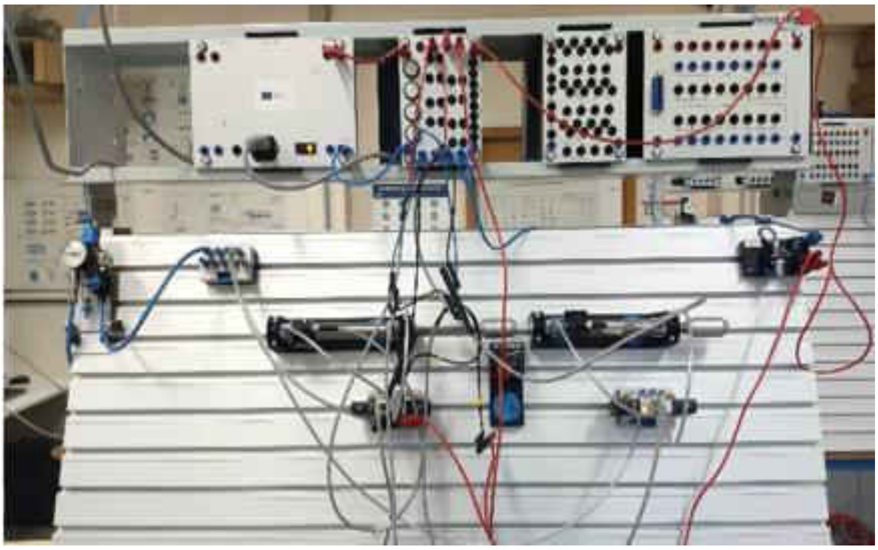

Fig. 7. Electro-pneumatic circuit with magnetic proximity switch

Magnetic proximity switches are sensors that detect the magnetic field of the piston magnet field or reed contact, Fig. 8.

Fig. 8. Magnetic proximity switch

In magnetic proximity switch, there exists Faraday's law. The equation for Faraday's law is:

$$\epsilon = -\frac{\Delta\Phi_M}{\Delta t} N \qquad (2)$$

Where:

- ε - induced voltage;
- $\Delta\Phi_N$ – change in magnetic flux;
- Δt – change in time;
- N – number of loops.

Description	Symbol
Magnetic proximity switches are mounted at the desired switching positon in the T-slot or circumferential slot of the cylinder and output a standardized 24 V switching signal when the piston magnetic field is detected.	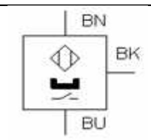

In the electric part of the circuit, the magnetic proximity switch is connected with relay, Fig. 9.

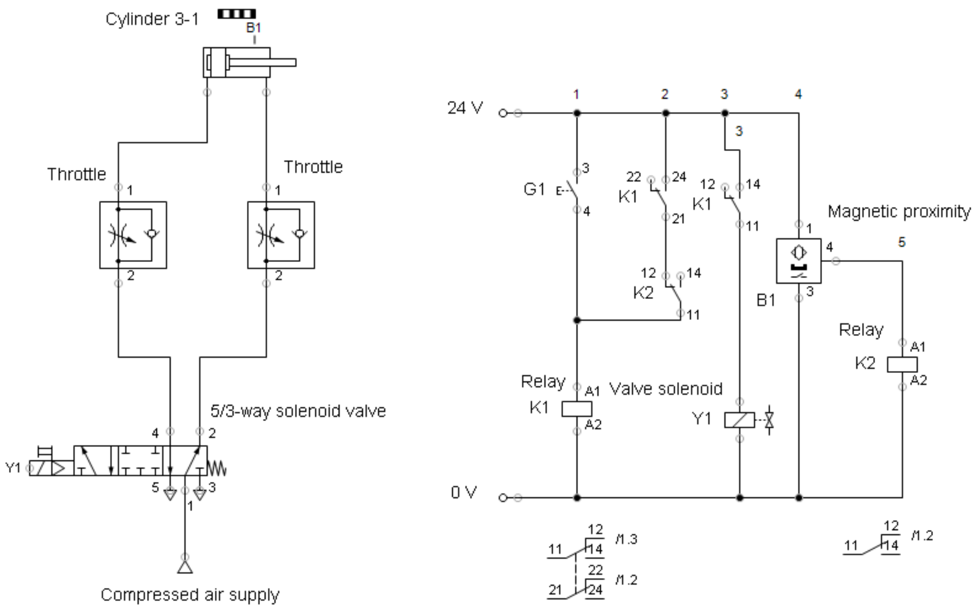

Fig. 9. Electro-pneumatic circuit with magnetic proximity switch

We must press the G1 button to open the electro-pneumatic circuit, Fig. 10.

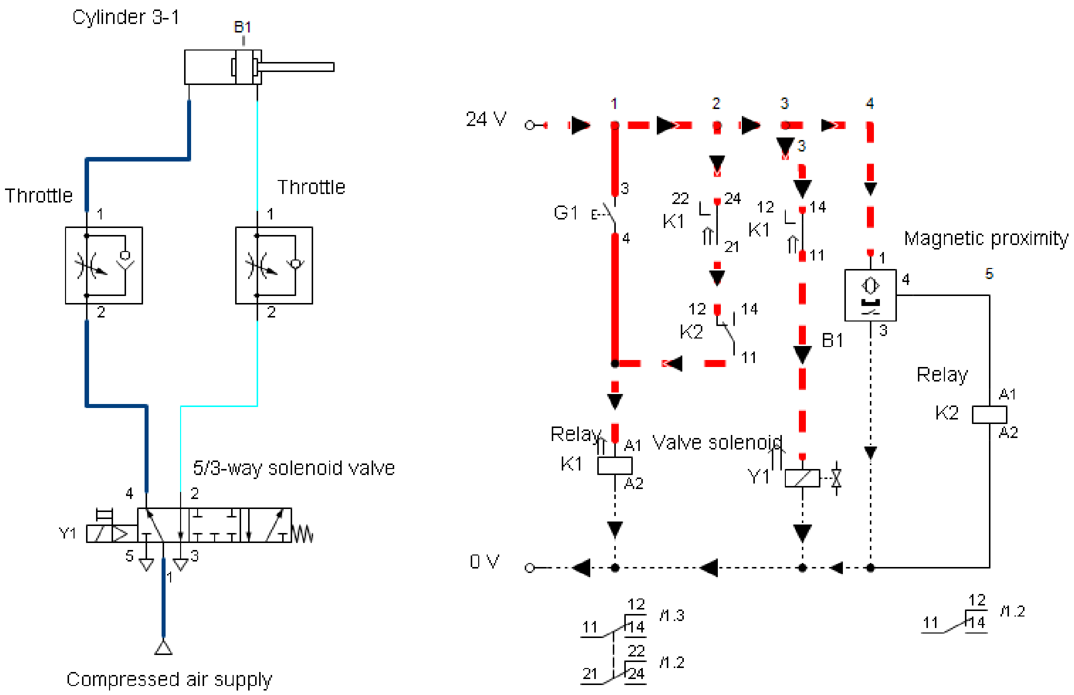

Fig. 10. Open electro-pneumatic circuit with magnetic proximity switch

We add a lamp to the electro-pneumatic installation, [5].
When we open the circuit, the light comes on, Fig. 11.

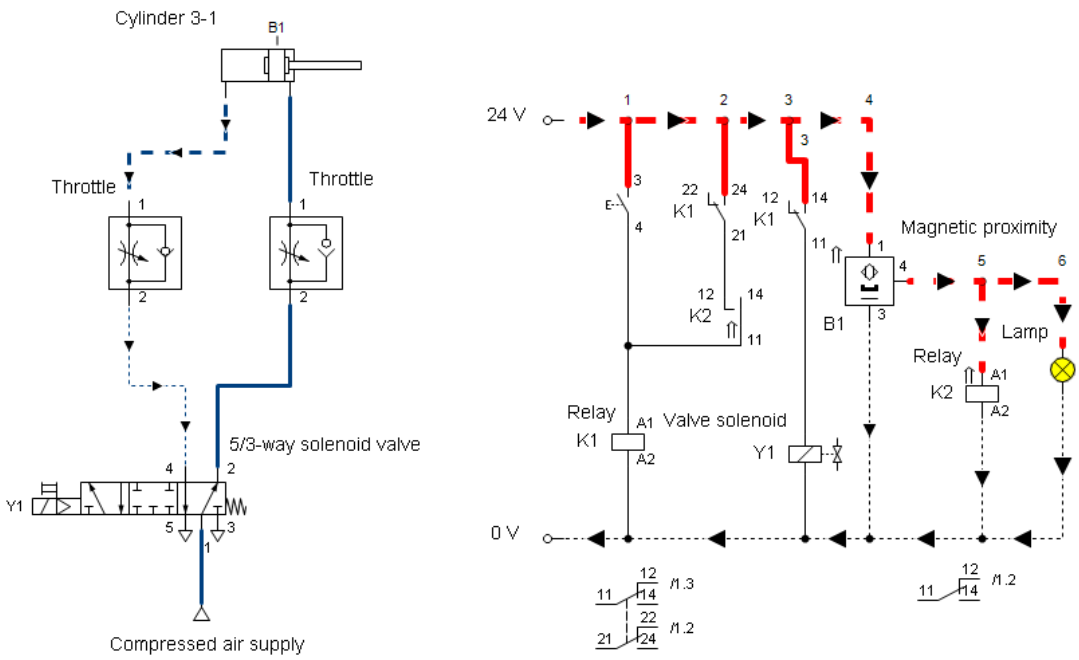

Fig. 11. Electro-pneumatic circuit with lamp

The penultimate electro-pneumatic circuit has three way valves, of which one is 5/n way valve and two are 3/n way valves, Fig. 12.

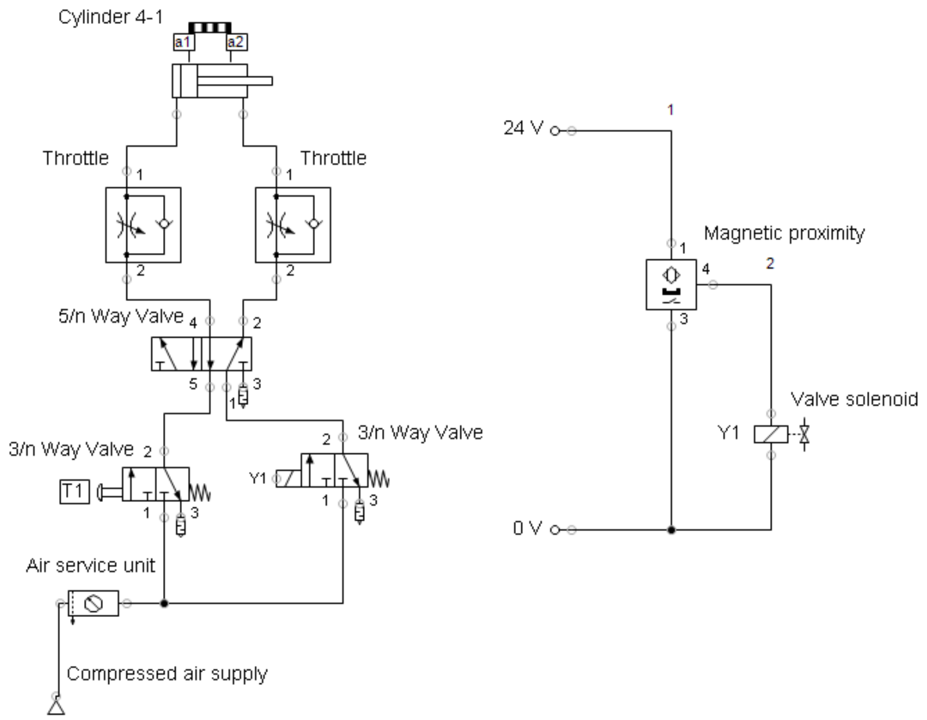

Fig. 12. Electro-pneumatic circuit with three way valves

The electrical circuit is made only of magnetic proximity switch and a solenoid valve, Fig. 12.

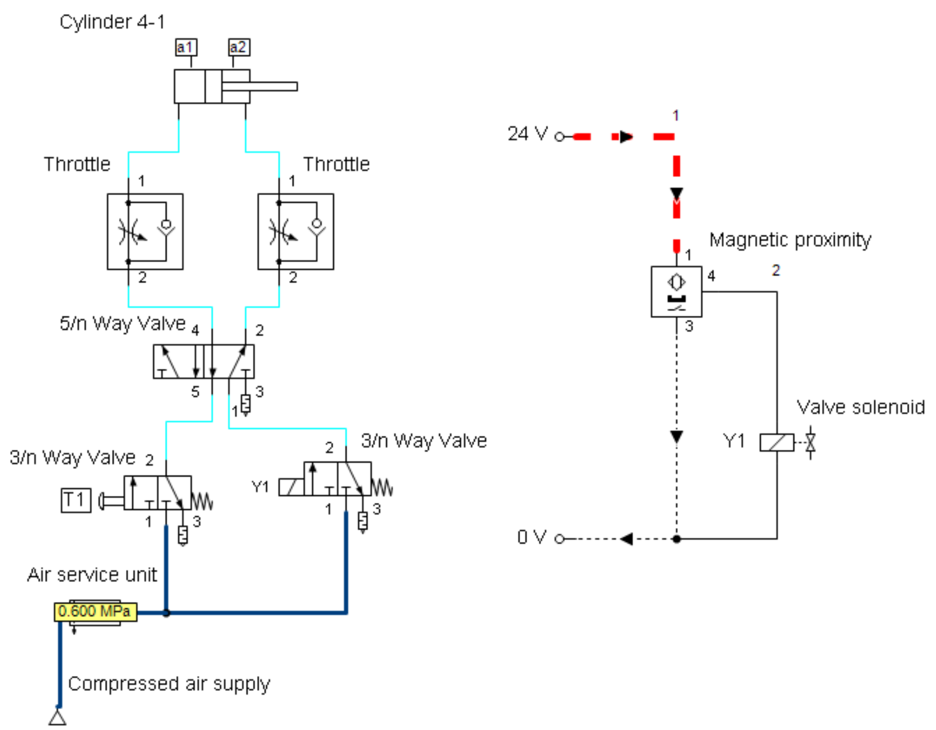

Fig. 13. Open electro-pneumatic circuit with three way valves

The electro-pneumatic installation opens if the T1 button on the 3/n way valve is pressed, Fig. 13. Thus, the piston of the cylinder 4-1 moves from point a1 to point a2. Then the piston returns to point a1, Fig. 13.

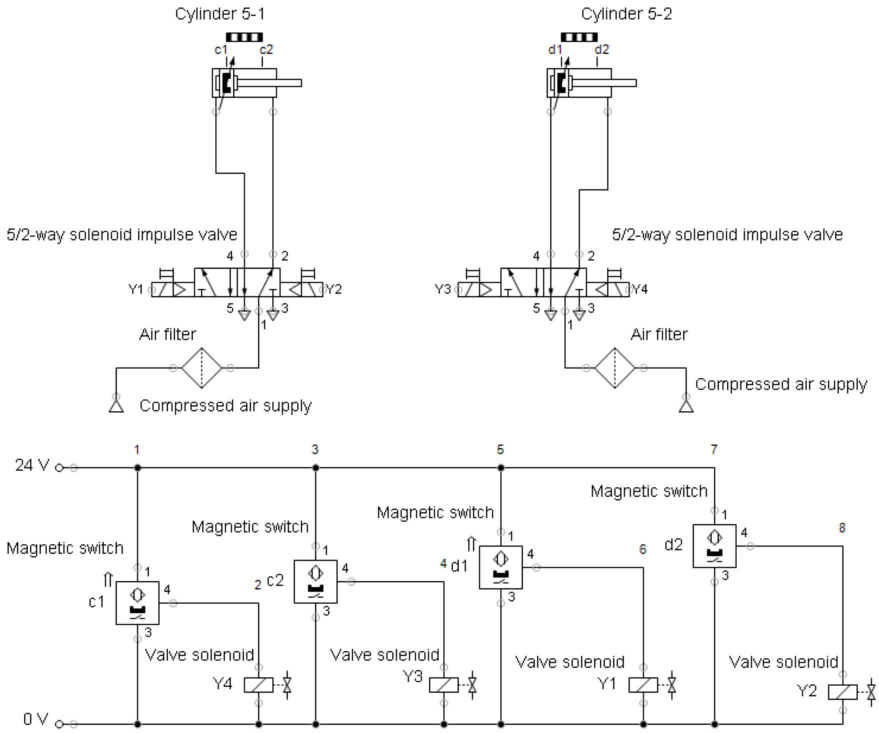

Fig. 14. Electro-pneumatic circuit with four magnetic proximity switches

In order to make an electro-pneumatic installation from two double acting cylinders, we must use four magnetic switches, Fig. 14.

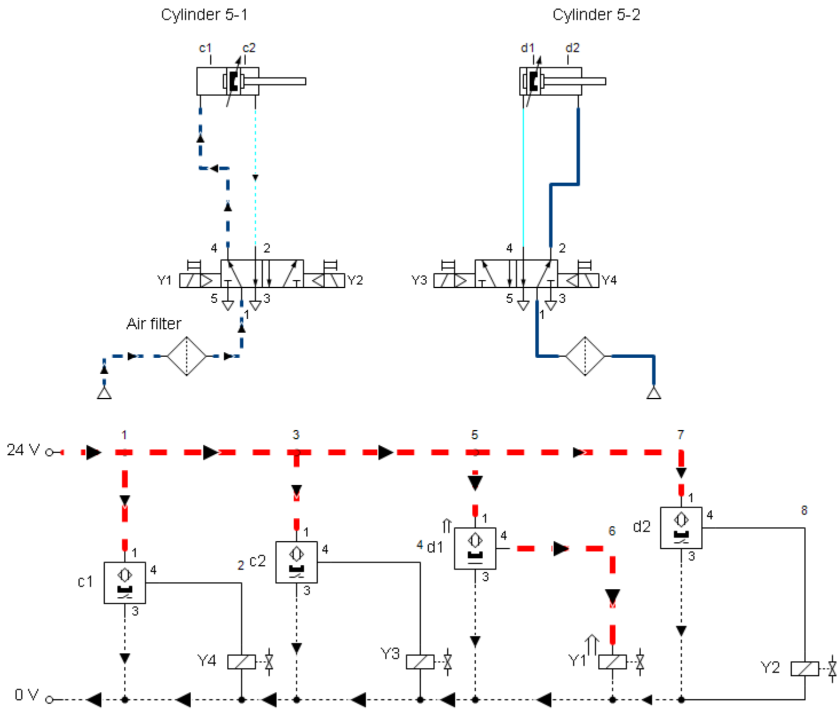

Fig. 15. Open electro-pneumatic circuit with four magnetic proximity switches

The pistons are moved automatically from the two cylinders. Thus, there are four steps for the pistons to reach the starting, Fig. 15.

These steps are:

I. From the cylinder 5-1 the piston moves from point c1 to point c2, [6].

II. After the piston in cylinder 5-1 reaches point c2, immediately starts the piston in cylinder 5-2 from point d1 to point d2.

III. When the piston from cylinder 5-2 reaches point d2, the piston from cylinder 5-1 returns from c2 to point c1.

IV. Finally, when the piston from cylinder 5-1 reaches point c1, the piston from cylinder 5-2 returns and reaches point d1, [7].

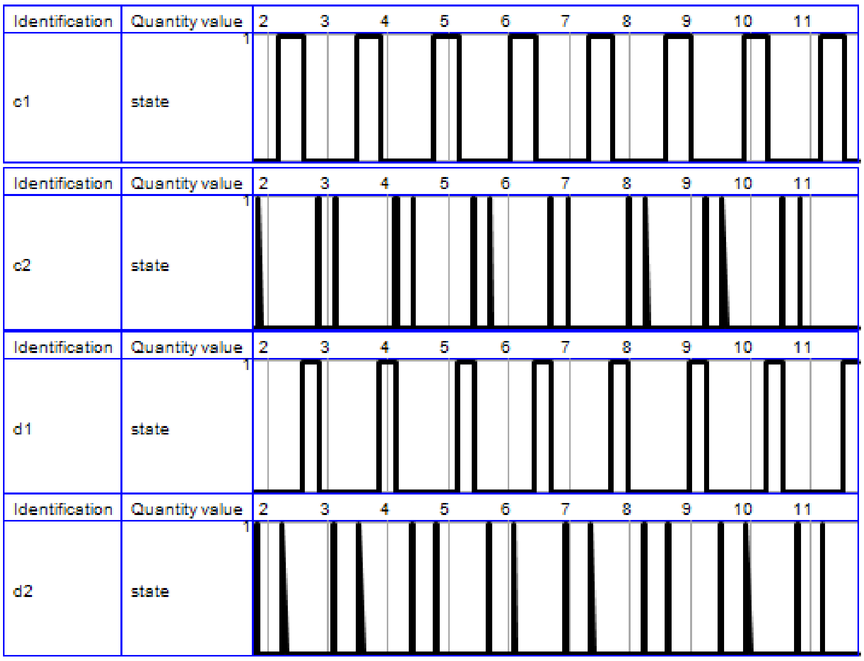

Fig. 16. Diagrams of magnetic proximity switches

3. Conclusions

If magnetic proximity switches are introduced in the electro-pneumatic installations, a lower energy consumption is achieved. The magnetic proximity switches are devices that are easily mounted and changed in electrical circuits.
Pneumatic cylinders are connected to magnetic proximity switches. In this case, the pneumatic cylinders are harder to wear.
For complex electro-pneumatic installations, it is recommended to install magnetic proximity switches together with relay or solenoid valve.

References

[1] www.festo.com.

[2] Panaitescu, M., G. Dumitrescu, and A. Scupi. "Sustainable pneumatic transport systems of cereals." Paper presented at EEEAD 2013: The 2013 International Conference on Environment, Energy, Ecosystems and Development, Venice, Italy, September 28-30, 2013, Proceeding: 128-134.

[3] Radoi, R., M. Blejan, I. Dutu, Gh. Sovaiala, and I. Pavel. "Determining the step response for a pneumatic cylinder positioning system." *Hidraulica Magazine*, no. 2 (June 2014): 25-31.

[4] Dumitrache, C., I. Calimanescu, and C. Comandar. "Naval standard safety valve design using CAD solutions." *Applied Mechanics and Materials* 658 (October 2014): 65-70.

[5] Belev, B., and S. Daskalov. "Computer technologies in shipping and a new tendency in ship's officers' education and training." *IOP Conference series: Materials Science and Engineering* 618 (2019) 012034.

[6] Cojocaru, R., P. Bocanete, D. Deleanu, C. Fratila, T. Axinte, and M. Diaconu. "Analysis of pneumatic circuits with FluidSim." *Hidraulica Magazine*, no. 2 (June 2021): 70-75.

[7] Deleanu, D., and C.L. Dumitrache. "Numerical study of a container ship model for the uncoupled parametric rolling." *IOP Conference Series: Materials Science and Engineering* 519 (2019): 012106.

ISSN 1453 – 7303 **"HIDRAULICA" (No. 3/2021)**
Magazine *of Hydraulics, Pneumatics, Tribology, Ecology, Sensorics, Mechatronics*

Defining the Main Parameters of a Darrieus Type Wind Turbine with a Power of 1 kW

Prof.PhD.Dr.Sc. **Valeriu DULGHERU[1]**, PhD **Cătălin DUMITRESCU[2,*]**,
Prof.PhD **Edmond MAICAN[3]**, PhD **Oleg CIOBANU[1]**, PhD **Radu RĂDOI[2]**

[1] Technical University of Moldova, Republic of Moldova

[2] Hydraulics and Pneumatics Research Institute INOE 2000-IHP, Bucharest, Romania

[3] Politehnica University of Bucharest, Romania

* dumitrescu.ihp@fluidas.ro

Abstract: *Utilizing huge amounts of cheap wind requires efficient, predictable, environmentally friendly conversion systems. Vertical-axis wind turbines are an area of less investigated wind energy conversion systems. Thanks to advantages over horizontal-axis wind turbines, vertical-axis wind turbines are becoming convenient for certain distinct regions, especially in urban and suburban areas. The article presents the argumentation of the geometric parameters of the blade with aerodynamic profile through numerical simulations, the development of a vertical-axis wind turbine and the investigation of its basic parameters.*

Keywords: *Wind turbine, vertical axis, aerodynamic profile*

1. Introduction

Wind energy has been used by humans for thousands of years. For over 3000 years, windmills have been used for grinding and pumping water. Even today, in the century of computer science, nuclear energy and electricity, thousands of windmills on various continents are used for pumping water and oil, for irrigation, for production of mechanical energy in order to operate low-power mechanisms.

Nowadays, the phrase "use of wind energy" means, first of all, non-polluting electricity produced on a significant scale by modern "*windmills*" called *wind turbines*, a term used to try to emphasize the similarity with steam or gas turbines, which are used to produce electricity, and at the same time to distinguish between their old and new destination.

The first attempts to obtain electricity from the wind date back more than a hundred years, starting with the end of the 19th century. But a real flourishing of this technology is attested only after the oil crisis of 1973. The sharp rise in oil prices has forced the governments of developed countries to allocate substantial financial resources for research, development and demonstration programmes. Over the course of 20 years, a new technology, a new industry and, de facto, a new market - the Wind Energy Conversion Systems (WECS) market - have been created worldwide.

If in 1973 the main incentive for the development of the WECS was the high price of oil, today a second one has been added - the tendency of mankind to produce "clean" or "green" electricity with no or with low carbon monoxide emissions. Of the EU's total greenhouse gas emissions, 79% come from the use of fossil fuels for energy production [1]. The year 1993 was marked as the beginning of a wind boom, which is characterized by an annual increase of over 20% of installed capacity. Thus, in 2000 the cumulative world capacity reached 650 GW. In the last 25 years, energy efficiency has doubled, with the cost of one kWh produced falling from 0.70 euros to about 0.32 euros today [2].

The world leader in installed capacity is the European Union, with a share of 65%, followed by China, the USA and India. No other sector of the world industry knows such a spectacular development. EU Energy Commissioner A. Piebalgs said at the launch of the European Wind Energy Technology Platform [1]: „*Wind energy is certainly one of the fastest growing technologies and it plays an important role in helping create a sustainable and competitive energy policy in Europe*".

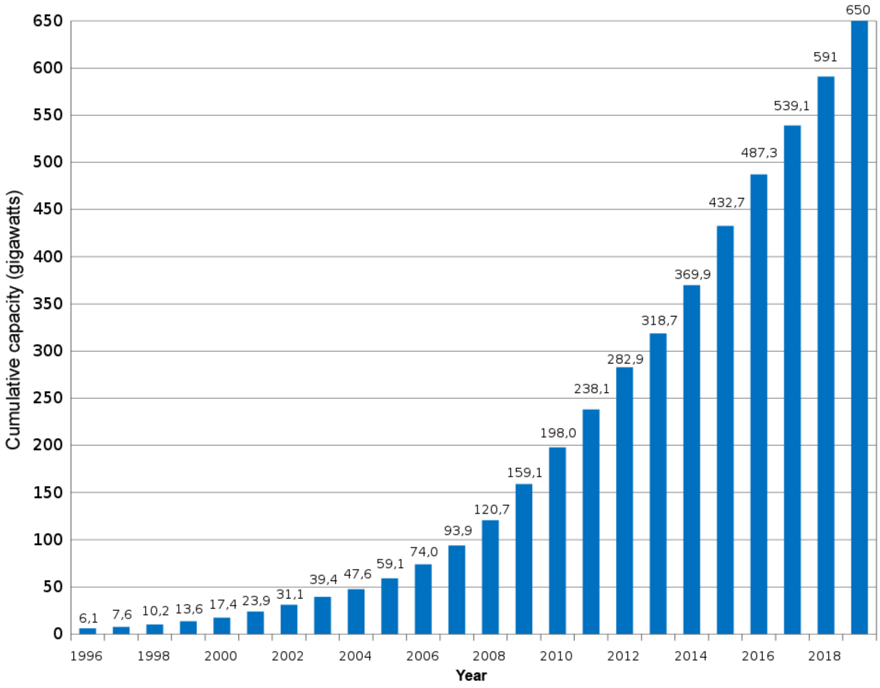

Fig. 1. Wind power: world installed capacity 1996 - 2020

To understand fully the technology of converting wind energy into electricity, knowledge is needed in various fields, including meteorology, aerodynamics, electrical engineering, mechanical engineering and civil engineering.
Depending on the orientation of the rotor axis, wind turbines are divided into horizontal-axis (HAWT) and vertical-axis wind turbines (VAWT). The latter are, in turn, divided into two basic types: the Darrieus turbine, invented by the French engineer George Darrieus; and the Savonius turbine, invented in 1920 by the Finnish engineer Sigurd J. Savonius [3].
Even though horizontal-axis wind turbines (HAWT) are much more widespread, vertical-axis wind turbines (VAWT) still have some advantages [4]: simpler construction; do not require the orientation of the rotor in the wind direction; a recent analysis, using an evolutionary algorithm, showed that the Betz limit, equal to 59.3% for HAWT, is approx. 6% higher at VAWT, because the principle of energy conversion of a VAWT turbine is different from that of a HAWT turbine; in an urban or suburban environment VAWTs are more competitive compared to HAWTs.

2. Parameters of the designed vertical-axis wind turbine

The vertical axis wind turbine was developed based on the technical solution, which was in the patenting stage [5]. The CAD model of the rotor (figure 2, a) was developed with SolidWorks software, and later imported into ANSYS simulation software. To reduce the degree of unevenness of the rotational movement, a rotor with helical blades was developed. The helical angle (of inclination of the blades) has the value of 30°, fact that ensures the coverage of a segment of approx. 60° (for each blade) on the circumference of the rotor projection on the plane. In the cross section of the blade, the Wortmann FX 63-137 aerodynamic profile was adopted with a maximum thickness of 30.9% of the rope length and a maximum curvature of up to 53.5% of the chord length, recommended for vertical-axis wind turbine rotors. The angle between ***AC*** (profile chord) and ***DE*** (axis of the blade fixing arm with the rotor) is 92° (fig. 2, b). The angle between ***AB*** (the axis joining the end points of the profile A and B) and ***DE*** is 93° (fig. 2, c). The length of the chord is 350 mm.
The estimated calculation of the power and geometric parameters of the elaborated vertical-axis wind turbine was performed in the MathCAD application.
Estimated power for yield $c_p = 0.33$:

$$Ar := H_t \cdot D_t = 3.78\ \text{m}^2. \tag{1}$$

$$P := \frac{\rho_{aer}\,Ar}{2} \cdot cp \cdot V_{ind}^{3} = 1016\ \text{W}. \tag{2}$$

Tangential speed: $V_t := \lambda \cdot V_{ind} = 3.5 \times 11 = 38.5$ m/s. (3)

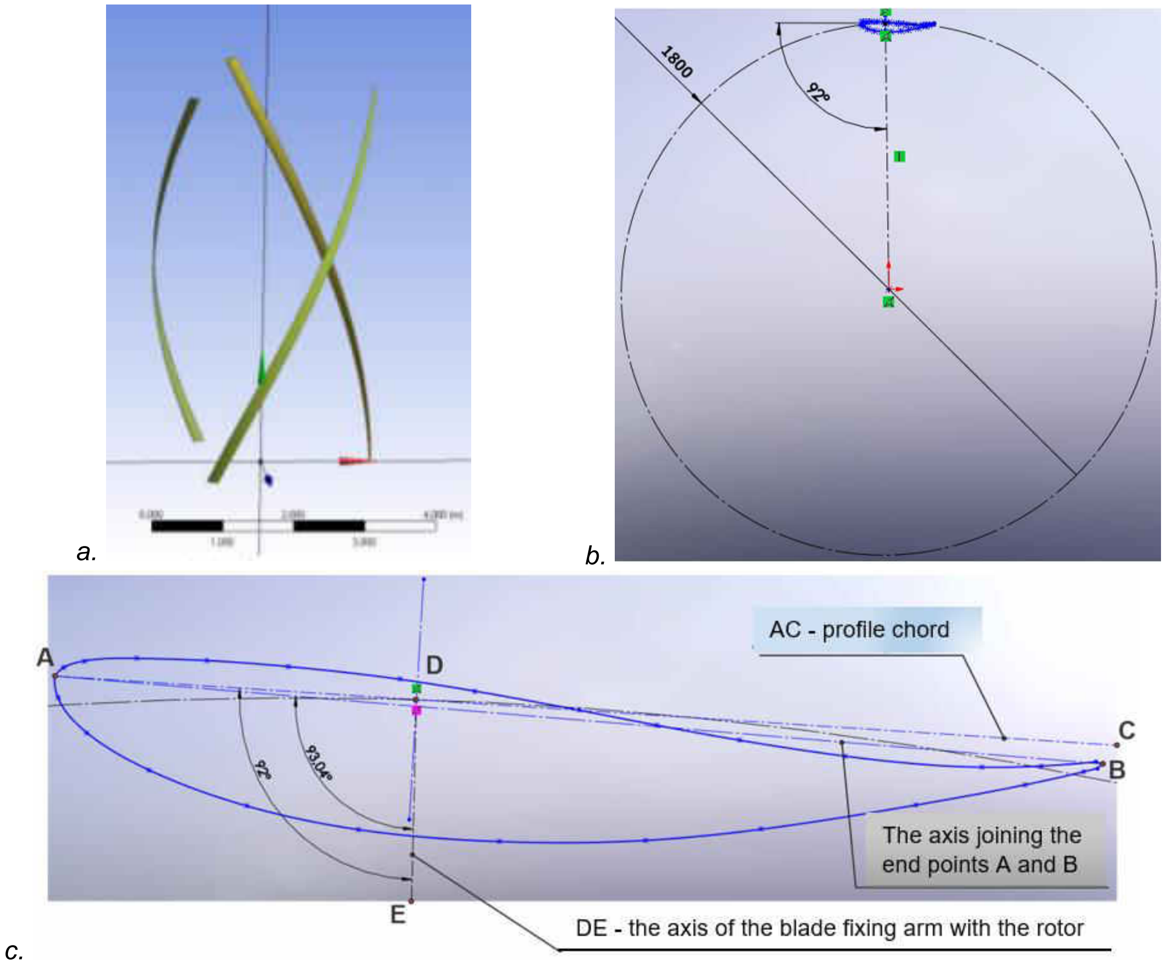

Fig. 2. CAD model of the helical rotor (a), the projection of the rotor in the plane (b) and the parameters of the aerodynamic profile of the blade

Angular velocity: $\omega := \frac{V_t}{R_t}$ = 30.8 s^{-1} (4);

Rotor speed $n := \frac{\omega \cdot 30}{\pi}$ = 294 min^{-1} (5);

Solidity $\sigma := \frac{N_p \cdot Lp \cdot c_p}{H_t \cdot D_t}$ = 0.42 (6);

Kinematic viscosity: $\nu := 1.460 \cdot 10^{-5} \frac{m^2}{s}$ (7);

Table 1: Rotor construction parameters

Parameter	Symbol	Value
Height, m	H_t	2.1
Turbine diameter, m	D_t	1.8
Length of the blade, m	L_p	2.25
Rapidity	λ	3.5
Aerodynamic profile chord, m	c_p	0,35
Blade number	N_p	3
Wind speed, m/s	$V_{inf.}$	11
Air density, kg/m³	r_{aer}	1.225
Estimated power for yield 0.33, W	P	1016

Angle of attack (fig. 3): $\alpha(\theta) := \mathrm{atan}\left(\frac{V_{ind} \cdot \sin(\theta)}{V_{ind} \cos(\theta) + R_t \cdot \omega}\right)$, θ = 0deg, 1...360 deg. (8)

Relative speed: $W_{rel}(\theta) := \sqrt{\left(V_{ind} \cdot \sin(\theta)\right)^2 + \left(V_{ind} \cdot \cos(\theta) + R_t \cdot \omega\right)^2}$; θ = 0deg,1...360 deg. (fig. 4). (9)

Load (C_l) and resistance (C_d) coefficients were determined using JavaFoil simulations (fig. 5).
Normal and tangential coefficients:

$$Cn_i := Cl_i \cdot \cos\left(\alpha\left(\theta 1_i\right)\right) + Cd_i \cdot \sin\left(\alpha\left(\theta 1_i\right)\right) \quad (10)$$

$$Ct_i := Cl_i \cdot \sin\left(\alpha\left(\theta 1_i\right)\right) - Cd_i \cdot \cos\left(\alpha\left(\theta 1_i\right)\right) \quad (11)$$

The parameters of the vertical-axis wind turbine are shown in Table 1 above.

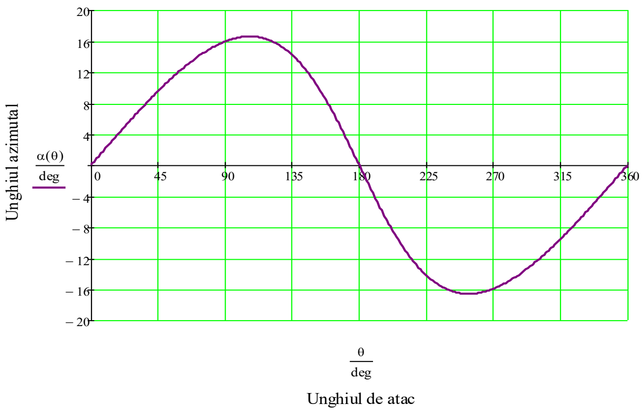

Fig. 3. Angle of attack as a function of azimuthal angle

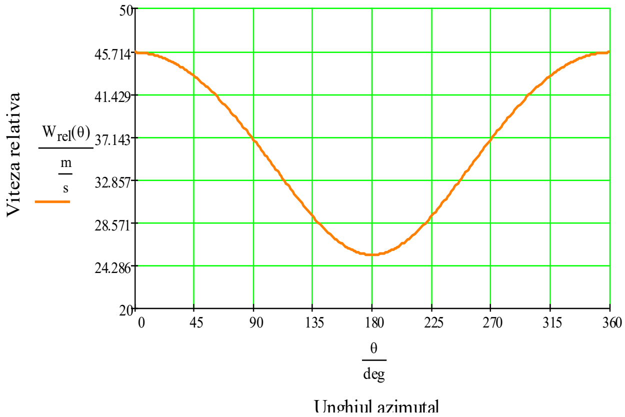

Fig. 4. Relative velocity as a function of azimuthal angle

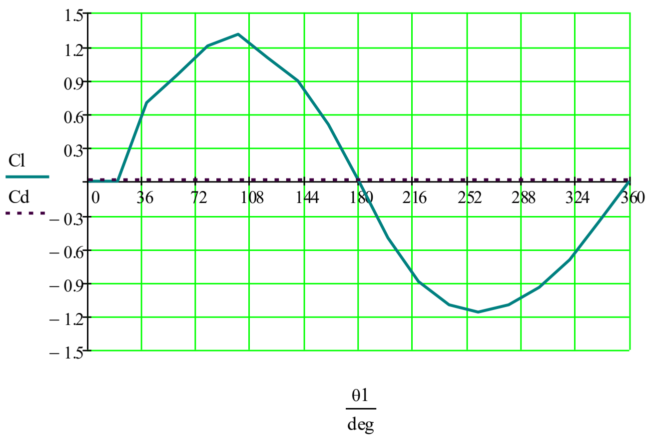

Fig. 5. C_l şi C_d as a function of azimuthal angle

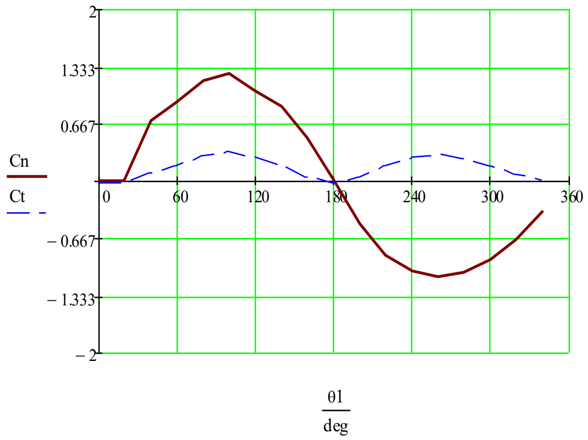

Fig. 6. C_n şi C_t as a function of azimuthal angle

3. CAD modeling of the rotor

ANSYS CFX software was used for the numerical simulation of the "*blade-fluid*" interaction. The mathematical model in the ANSYS CFX software is based on the continuity and momentum equations that are solved using the *k-epsilon* turbulence model (*solving the non-stationary Navier-Stokes equation*). The mathematical model used in the QBlade application is Double-Multiple Streamtube (DMS). This model was developed by Ion Paraschivoiu for the analysis of the performance of Darrieus type rotors. CAD models of the rotor, domain of the rotor (rotary domain) and fluid domain (static domain) were made using SolidWorks and then imported into ANSYS. Domain sizes are set, using the recommendations of the cited source [6]. The dimensions of the fluid domain are: length - 30 m, width - 18 m, height - 8 m (fig. 7, a). The dimensions of the rotor domain are: height 2.5 m, diameter 2.1 m. The rotor is placed at a distance of 5 m from the entry and in the middle compared to the four sides (fig. 7.b). To facilitate the setting of border conditions, the following named selections are created: entry, exit and openings. The three surfaces of the rotor domain are also defined, i.e., the caps and the cylindrical surface. The surfaces of the blades are also defined. This is done when making the CAD model of the rotor. These lines are very useful for setting placement dimensions around the blade. An interface is created between the rotor domain and the fluid domain (Fluid-Fluid). The mesh for the rotor domain and fluid domain is made separately (figure 7.c). The mesh for the fluid domain is as follows: the maximum face size and the Tet size for the fluid domain is 350 mm; The weaving method is automatic; Inflation is made at the interface with the rotor domain: height of the first layer - 120 mm, maximum layers – 6, and grow rate is 1.12. The size of the element of interface surface between the rotor and the domain is 90 mm. The number of items is 585632.

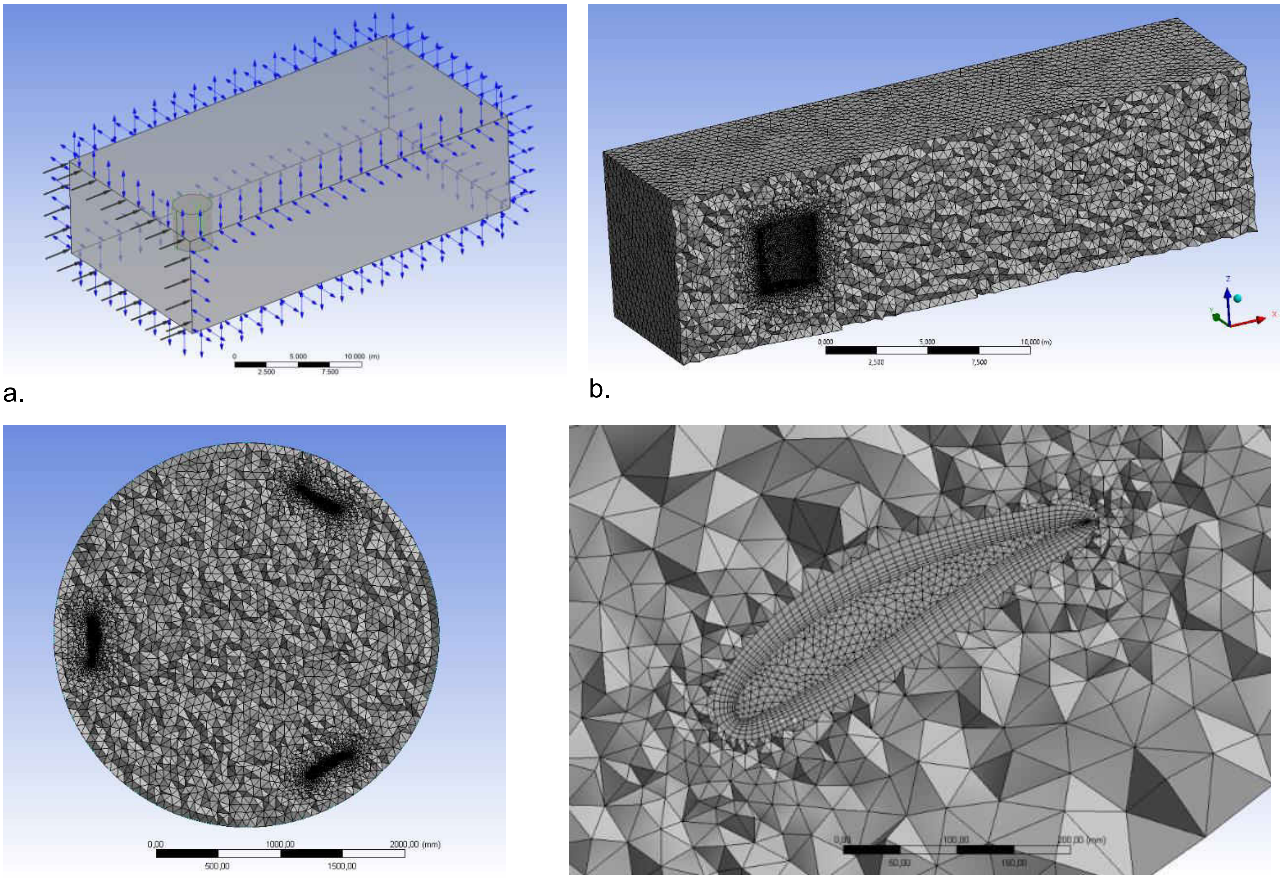

a. b.

c. d.

Fig. 7. Discretization of the domain around the blade (a), domain of the rotor (b), domain of the stator (c), and model of the computational domain of the vertical-axis wind rotor.

For the rotor domain, the maximum face size and Tet size of the element is 120 mm. The size of the element on the surfaces of the blades is 3 × 6 mm. In order to reproduce the phenomenon of the boundary layer on the blade surface, where strong fluctuations of the fluid velocity occur, prismatic finite elements were generated by extending them from the blade surface to the outside. This was achieved through the “*Inflation Layer*” process, which was imposed on the surface of the blade with the option “*Total Thickness*” with number of layers = 8, grow rate = 1.1 (relative thickness of two adjacent layers) and type of grow rate = geometric. Height of the first layer = 1 mm (fig. 7.d). The total number of elements is 5684368. When checking the quality of the meshes obtained, asymmetry and orthogonality are the most important. The recommendation is to have a maximum asymmetry less than 0.95 and a minimum orthogonality greater than 0.15.
The domain was discretized, using the "*Triangles*" method with maximum element dimensions of 16 mm. The "*Edge Sizing*" procedure with an element size of 0.8 mm was used for the perimeter of the aerodynamic profile. The "*Inflation*" procedure was also applied with the "*Total thickness*" option: "*Number of layers*" - 11; *Grow rate* - 1.17; "*Maximum thickness*" - 4 mm. A maximum limit of 2.5 mm has been set for interior domain elements. At the Setup stage, the "*Pressure-Based*" computational model in steady flow conditions ("*Steady*") was adopted. The “*K-epsilon Standard*” model with the “*Standard wall function*” option was used to simulate turbulence.
The reference areas for which the boundary conditions were specified (Inlet, Outlet, Internal, Walls) are indicated in figure 7. For Inlet the speed of 16 m / s was adopted, and for Outlet - Gauge pressure (Pascal) - 0. For the maximum residual values of the equations, available in the “*Monitors - Residual - Absolute Criteria*” section, a maximum value of 0.0001 has been set.

4. CFD solutions and results

The simulation results, displayed in Figure 8, show the current lines and the velocity distribution around the blade profiles. It is obvious that the blade, which passes through the descending area, will reduce the rotor torque, as the air flow speed decreases. One can note that the power lines form vortices behind the blades, which must be taken into account when placing wind turbines in wind farms. The power curve was obtained based on the simulations in the ANSYS CFX program (wind speed of 11 m / s, 294 rpm) (fig. 9). The convergence of power results was attested by monitoring the variables of interest. For a better illustration of the dependence on the wind speed, figure 10 shows power curves for V = 7, 8, 9, 10, 11, 12 m / s. The power curves were sketched using the average value of the resulting power for the corresponding wind speed.

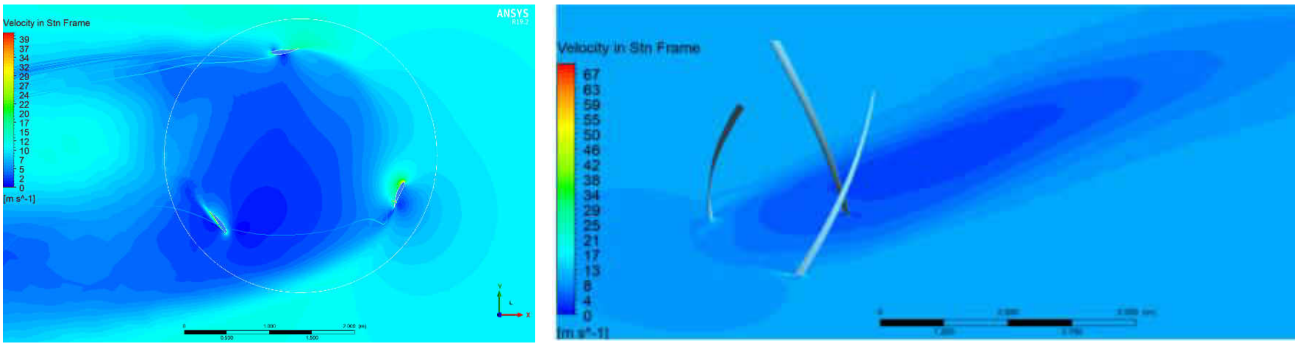

Fig. 8. Fluid velocity distribution around the rotor

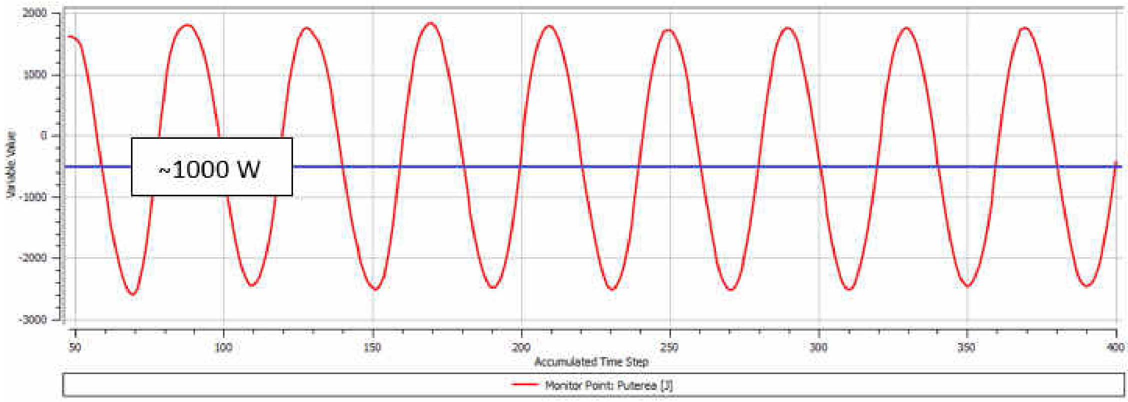

Fig. 9. Power curve obtained by simulations in the ANSYS CFX software (wind speed 11m / s, 294 rpm)

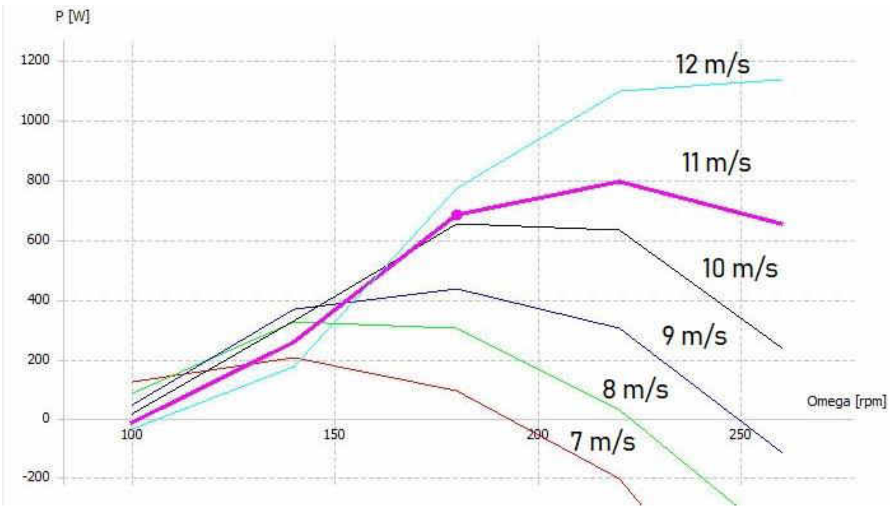

Fig. 10. Comparative power curves obtained based on simulations in the Qblade application

Based on the results of the calculations and CFD simulations performed, the hybrid experimental model of a vertical-axis wind turbine with helical-blade rotor (Figure 11) was designed and manufactured. The blades of the Darrieus and Savonius rotors were made of composite material, ensuring low mass and the required mechanical strength parameters. The Savonius rotor, installed inside the Darrieus rotor, has the function of a starter, thus lowering the starting speed of the Darrieus rotor to approx. 3-4 m / s, therefore ensuring the increase of the turbine efficiency at low wind speeds. The experimental model of the turbine was blown in a wind tunnel, validating, in the rough, the results obtained by CFD simulations and calculations.

Fig. 11. Experimental model of the Darrieus + Savonius hybrid vertical-axis wind turbine

5. Conclusions

- Vertical-axis wind turbines are advantageous compared to horizontal-axis wind turbines, especially in urban and suburban environments;
- The results of the simulations performed in the ANSYS CFX fluid flow dynamics analysis software indicate a very good accordance with the results obtained in the dedicated QBlade application;
- The use of helical blades ensures a low degree of unevenness of the rotor speed;
- The use of the Savonius rotor ensures the lowering of the starting speed of the Darrieus rotor.

Acknowledgments

This paper has been developed as part of a project co-financed by the European Union through the European Regional Development Fund, under Competitiveness Operational Programme 2014-2020, Priority Axis 1: Research, technological development and innovation to support economic competitiveness and business development, Action 1.1.4 - Attracting high-level personnel from abroad in order to enhance the R&D capacity, project title: *Establishing a high-level proficiency nucleus in the field of increasing renewable energy conversion efficiency and energy independence by using combined resources*, project acronym: CONVENER, Financial agreement no. 37/02.09.2016. European funding has also been granted, under Competitiveness Operational Programme POC 2014-2020, call POC-A1-A.1.1.3-H-2016, Financial agreement no. 253/02.06.2020, signed between INOE 2000 and the Ministry of Education and Research for the project titled "Horizon 2020 Support Center for European project management and European promotion PREPARE", MYSMIS2014 code 107874.

References

[1] Bostan, I., V. Dulgheru, I. Sobor, V. Bostan, and A. Sochirean. *Renewable energy conversion systems / Sisteme de conversie a energiilor regenerabile*. Chişinău, Tehnica-Info Publishing House, 2007.
[2] European Environment Agency. „EEA greenhouse gases – data viewer", April 13, 2021. Accessed September 6, 2021. https://www.eea.europa.eu/data-and-maps/data/data-viewers/greenhouse-gases-viewer.
[3] Maican, E. *Renewable energy systems / Sisteme de energii regenerabile*. Bucharest, PRINTECH Publishing House, 2015.
[4] Paraschivoiu, I., S. Ammar, and F. Saeed. „VAWT versus HAWT: a comparative performance study of 2–6 MW rated capacity turbines." *Transactions of the Canadian Society for Mechanical Engineering* 42, no. 4 (2018): 393-403, doi: 10.1139/tcsme-2017-0137.
[5] Dulgheru, V., C. Dumitrescu, L. Dumitrescu, R. Rădoi, and C. Cristescu. „*Wind system*"/„*Sistem eolian*". Patent no. A/00620 on 06.09.2017, OSIM, Romania.
[6] Mohamed, M. H., A. M. Ali, and A. A. Hafiz. „A CFD analysis for H-rotor Darrieus turbine as a low speed wind energy converter." *Engineering Science and Technology, an International Journal* 18, no. 1 (March 2015): 1-13.

A Review of Quantification of Noise in Engines

Dr. **Sujoy NAIR**[1], Dr. **Raman SINGH**[2,*]

[1,2] Jammu University, Jammu Kashmir, India

* Corresponding author's e-mail address: ramanjalali4@gmail.com

Abstract: *During the decade of 1970's, introduction of more stringent noise control regulations led to more attention being paid towards the acoustic performance of engines. Priede analyzed a relationship between development of in cylinder pressure and subsequent noise emissions from engines. Kamal focused his work on finite element analysis of individual engine components for the dynamic analysis of engines. Later based on various noise transfer paths, main bearing of connecting rod was found to be a major transmission path for the indirect component of combustion based noise.*

Keywords: *Noise, vibro acoustic*

1. Introduction

In modern days, multidisciplinary approaches are being utilized for evaluation of NVH performance of engines. Some of these methods include modal analysis, finite element techniques (FEA), boundary element method (BEM), statistical energy analysis (SEA), lumped mass approach as well as transfer path analysis (TPA).

Each of these methods have specific frequency ranges over which they are most reliable e.g. FEA is more suited in low frequency ranges, whereas TPA is more suitable for medium frequency ranges. SEA gives results that are more accurate in higher ranges. Evaluation of acoustic performance of engines can be performed both objectively as well as subjectively using these techniques [1-6].

Figure no 1 shows plots of in cylinder pressure spectra for two different types of engines [7]. A difference of about 20dB is seen at 1KHz frequency.

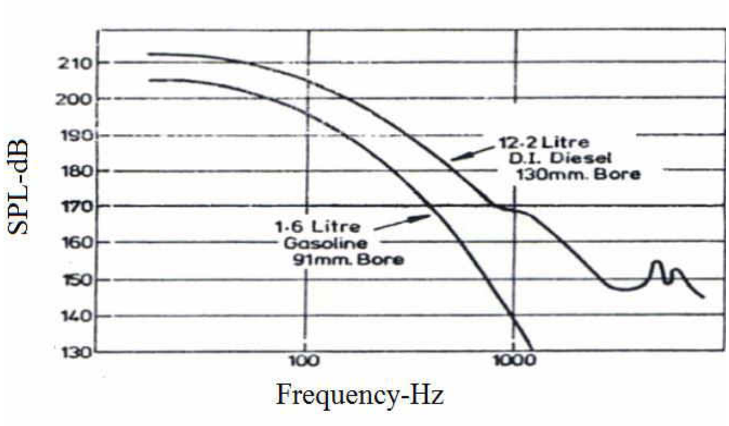

Fig. 1. In cylinder pressure spectrum

Based on various mathematical relationships, Anderton developed models to quantify the combustion-based noise according to type of engine [8]. It involves calculation of mechanical impedance Z(f) between the force applied at top of piston F(f) and average mean square root velocity v(f) of engine block. i.e.

$$Z(f) = \frac{\sqrt{V^2(f)}}{F(f)} \quad (1)$$

The average surface velocity V(f) may be expressed in terms of in cylinder pressure (p) and cylinder bore (B) as:

$$V(f) = \frac{p\pi B^2}{4Z(f)} \tag{2}$$

Further, the relationship of radiated acoustic power (W) from a surface may be written as:

$$W(f) = \rho CSV(f)\sigma = \frac{p^2}{\rho C} \tag{3}$$

Where σ is radiation efficiency and S is radiated surface area.
Combining the above relationships, we have:

$$W(f)=\sigma SC\rho\frac{p\pi B^2}{4Z(f)} \tag{4}$$

The intensity of radiated noise I(f) is given by:

$$I(f)=\sigma C\rho\frac{p\pi B^2}{4Z(f)} \tag{5}$$

In order to minimize the dependence of engine speed, various in cylinder pressure spectra were analyzed. Variations in these plots were observed like a straight line in frequency ranges 0.8KHz – 3KHz. The slope of pressure spectrum in this range was defined as combustion noise index (Ƶ) [2].

Using further analysis, it was shown that in cylinder pressure spectrum p(f) may be expressed as:

$$p^2(f)\sim(\frac{N}{f})^{Ƶ} \text{ Antilog}(3N) \tag{6}$$

Where N is engine RPM

From the above relationships, we have:

$$I(f)\,)\sim(\frac{N}{f})^{Ƶ} \text{ Antilog}(3N)\ \rho cS\sigma\frac{p\pi B^2}{4Z(f)} \tag{7}$$

Or

$$I(f)\,)\sim(\frac{N}{f})^{Ƶ} S\sigma\,\frac{B^4}{z(f)^2} \tag{8}$$

Overall Intensity I_O can be expressed by integration over a given frequency range $[f_1,f_2]$ as:

$$I_O\sim SN^{Ƶ}B^4\int_{f_1}^{f_2}\frac{\sigma}{f^{Ƶ}Z(f)^2} \tag{9}$$

Various empirical relationships have been developed at ISVR, University of Southampton for prediction of noise in terms of sound pressure levels for different types of engines. Some of these include [29]:

$$SPL_{\text{N.A. Direct Injection Diesel engines}} = 30*\log(N +50*\log(B) +106 \tag{10}$$

$$SPL_{\text{Turbocharged Diesel engines}} = 40*\log(N+50*\log(B)-135 \tag{11}$$

$$SPL_{\text{Indirect injection Diesel engines}} = 43*\log(N +60*\log(B)-176 \tag{12}$$

$$SPL_{\text{Petrol engines}} = 50*\log(N +60*\log(B)-203 \tag{13}$$

As compared to diesel engines, a gasoline engine operates at higher operational speeds has smaller bore and smaller reciprocating mass. Consequently, such an engine has lower in cylinder pressure and hence lower sound pressure levels of radiated noise as seen from figure no 2.

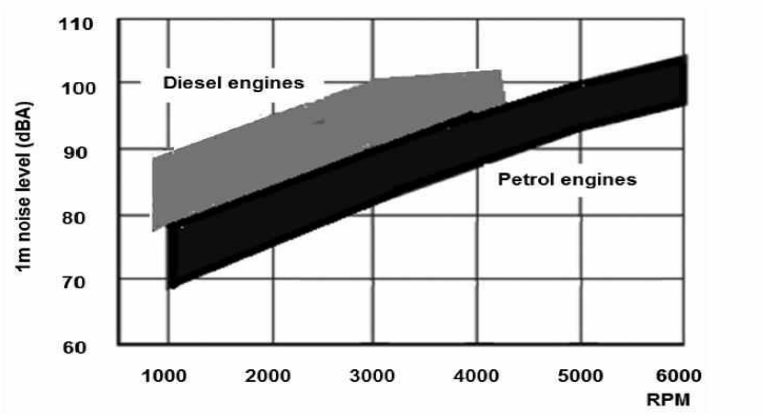

Fig. 2. Variations of sound pressure levels with engine speed

The diesel engine knocking refers to noise mainly in 500Hz-6000Hz range and is dominant under low speed idle operational conditions. Various moving parts in diesel engines are designed heavier and stronger as compared to gasoline engines in order to meet durability requirements under high operational pressures. Hence, the mechanical impacts in case of a diesel engine are stronger when compared to gasoline engines. There are additional sources of noise like turbochargers and operation of fuel injection pumps in case of a diesel engine. However, there are some sources of noise exclusively associated with operation of a gasoline engine. These include piston pin tickling noise under low speed conditions, clatter noise under cold operational conditions and slip stick piston noise originating from crankshaft [10-20].

2. Methods of quantification of noise

There are several techniques that have been used to identify various sources of noise in engines [3]. Some of these include selective shielding of parts, surface vibration method as well as acoustic intensity technique. Of these methods, the selective covering by lead is the most expensive as well as time consuming one. These techniques have been discussed further in the next part of this work.

a) **Selective lead covering method**-it is one of most reliable methods of source identification in field of engine acoustics. This method consists of measurement of noise emissions from engine using selective covering of engine parts with lead (which is a high transmission loss material). The increase in radiated noise is then noted by removing lead cover from the component. This procedure is repeated one by one for all major parts. Figure no 3 shows results of such a test that was performed on a 6 cylinder naturally aspirated diesel engine [3].

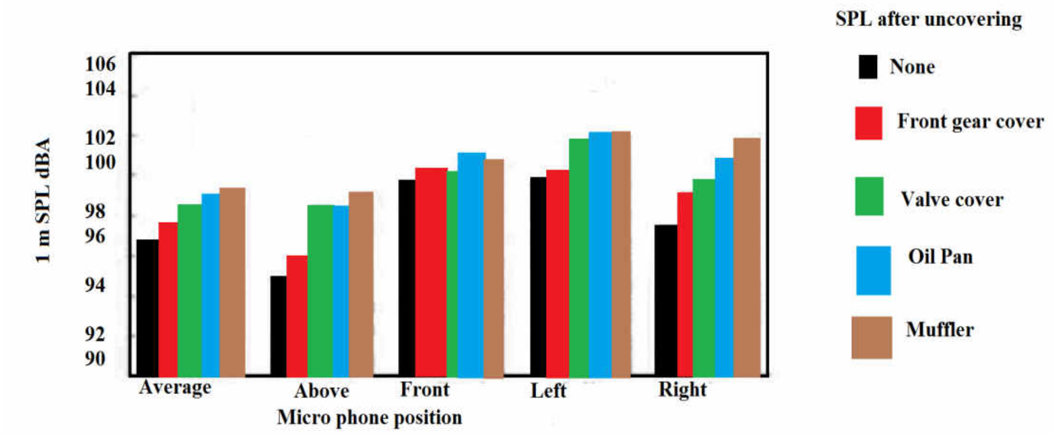

Fig. 3. Noise analysis using lead cover method

Total sound power level (SPL) emitted from this engine was found to be around 114dBA with valve cover, muffler, front gear cover and oil pan contributing about 21%, 10%, 8% and 7% respectively.

b) **Surface vibration method**-The A weighted sound power level of engine ($L_w[A]$) can be expressed in terms of acoustic impedance (ρc), surface velocity (u),radiation efficiency (σ)and surface area (S) by following relationship [3]:

$$L_w[A]= 10*\log(\rho c)+10*\log(S)+10* \log(\sigma)+10*\log (u) \quad (14)$$

The radiation efficiency is ability of surface vibrations to convert into air borne noise. The radiation efficiency can be estimated by considering engine as a radiating rigid sphere. This is also related to critical frequency of component, which may be defined as the frequency at which natural wavelengths of vibrations of given structure matches with those of radiated vibrations. At frequencies lower than the critical ones, the radiation efficiency is less than unity and vice versa.

The dominant range of critical frequency for components of a typical diesel engine lies in range 400-800Hz. The radiation efficiency rises at an approximate rate of 40d B/decade in ranges lesser than critical frequency. The value of critical frequency occurs when kr ≈ 4, where k is wave number and r is radius of an arbitrary sphere that has same volume as that of engine under consideration

Measurement of surface vibrations can be best done by mounting accelerometers on engine block. Positioning of accelerometers must be carefully done, as surface vibrations vary with wall thickness. Hence proper balancing between less and strong sensitive measurement points is necessary. The surface velocity can be calculated by using Fourier transformations (FT) to first convert acceleration data into frequency domain and then carrying out integration.

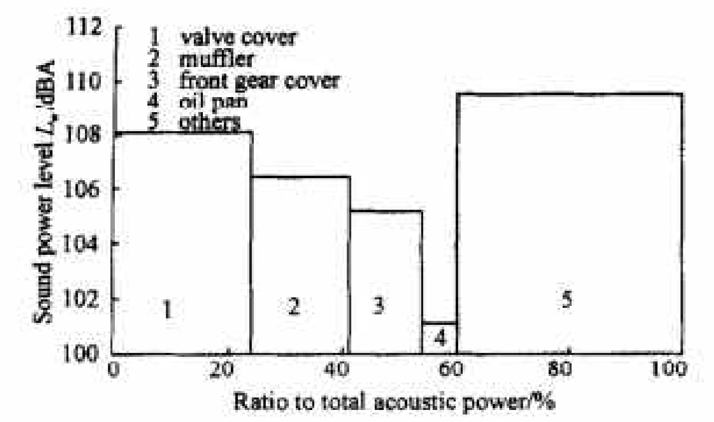

Fig. 4. Noise analysis using vibrational analysis method

Figure no 4 shows the results of contributions of various components as obtained by surface velocity method [6]. It can be seen that larger contributions occur from valve cover, muffler shell, gear cover and oil pan cover.

c) **Use of Spectro- filters** [3]

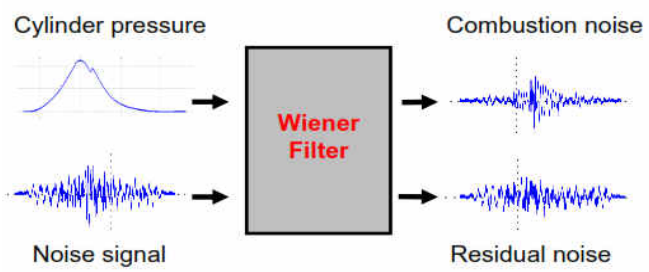

Fig. 5. Application of Wiener filter for estimation of combustion noise

Noise emissions from diesel engines has several contributing sources of which combustion based noise is a major one. Residual noise due to various other sources is shown in figure no 5. If the in cylinder pressure signal is known, these two sources can be separated using suitable Wiener Spectro-filters. These types of filters extract noise sources that are coherent with in cylinder pressure signals, hence providing an estimation of combustion based noise.
Wiener filter has a single input response P(t) giving a single output response C(t) as seen from figure no 6. The impulse response function has been denoted by H(t). The system is corrupted by external component M(t). This model can be represented by following relationships:

$$C(t)=P(t)*H(t) \tag{15}$$

$$G(t)=M(t)+C(t) \tag{16}$$

The Spectro-filter H(t) can be estimated from following equations:

$$W(f) = \frac{S_{PD}(f)}{S_{PP}(f)} \tag{17}$$

$$W(t)=IFFT[W(f)] \tag{18}$$

In these equations $S_{PP}(f)$ denotes the auto spectrum of P(t), whereas $S_{PD}(f)$ denotes the cross spectrum of P(t) and M(t). Convolution of input P(t) with W(t) gives an estimate of C(t) .i.e.

$$C^{\sim}(t)=P(t)*W(t) \tag{19}$$

$$G^{\sim}(t)=E(t)- C^{\sim}(t) \tag{20}$$

In case of a mono cylinder engine C(t) denotes the combustion noise, P(t) denotes in cylinder pressure developed, M(t) denotes the mechanical based noise, E(t) denotes total noise emissions and H(t) denotes the relationship function between in cylinder pressure and noise emissions as shown in figure no 6,7.

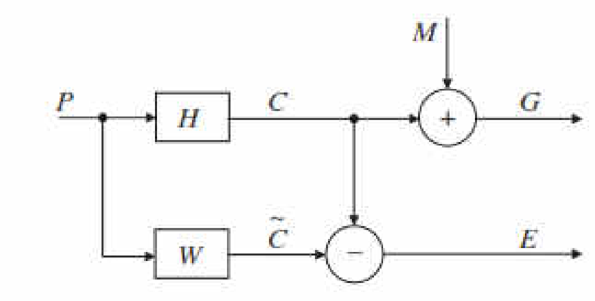

Fig. 6. Engine noise model (single cylinder)

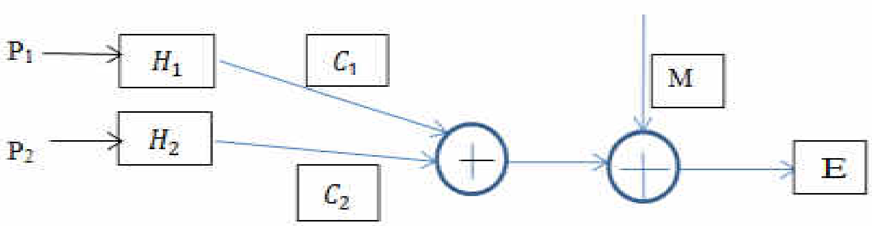

Fig. 7. Engine noise model (dual cylinder)

In case of a dual cylinder engine, figure no 7 shows the noise model. This is a multiple inputs and a single output (MISO) system. The combustion noise C(t) can now be considered as sum of the individual components produced by each cylinder i.e.

$$pC(t)=C_1(t)+C_2(t) \tag{21}$$

Various cyclo-stationary signals were used for calculation of Wiener filter as described above. These values were computed by subtraction of average values computed over a large number of cycles from original signals. The average values of signals have very reduced level in high frequency ranges (above 800Hz). As a result, the accuracy of Wiener filter is high in this range. Hence, these are well suited for analyzing noise emissions from a diesel engine as a major portion of energy of signals lies in this range.

References

[1] Kaisan, Muhammad Usman, Latifat Ovaiyoza Yusuf, Ibrahim Umar Ibrahim, Shitu Abubakar, and Sunny Narayan. "Effects of Propanol and Camphor Blended with Gasoline Fuel on the Performance and Emissions of a Spark Ignition Engine." *American Chemical Society (ACS) Omega* 5, no. 41 (2020): 26454−26462.
[2] Grujic, I., N. Stojanovic, R. Pesic, A. Davinic, and S. Narayan. "Numerical analysis of IC engine operation with high pressure hydrogen injections." *Transactions of FAMENA* 44, no. 1 (2020): 55-56.
[3] Mahroogi, Faisal O, and S. Narayan. "A recent review of hybrid automotive systems in Gulf Corporation Council region." *Proceedings of Institute of Mechanical Engineers Part D: Journal of Automotive Engineering* 233, no. 14 (2019): 3579-3587, DOI: 10.1177/0954407019836055.
[4] Abubakar, S., F.O. Anafi, M.U. Kaisan, S. Narayan, S. Umar, and U.A. Umar. "Comparative analyses of experimental and simulated performance of a mixed-mode solar dryer." *Proceedings of Institution of Mechanical Engineers, Part C: Journal of Mechanical Engineering Science* 234, no. 7 (2020): 1393-1402.
[5] Kaisan, M.U., S. Abubakar, B. Ashok, Dhinesh Balasubramanian, S. Narayan, Ivan Grujic, and Nadica Stojanovic. "Comparative analyses of biodiesel produced from jatropha and neem seed oil using a gas chromatography–mass spectroscopy technique." *Biofuels* 12, no. 7 (2021): 757-768, DOI: 10.1080/17597269.2018.1537206.
[6] Narayan, Sunny, and Vipul Gupta. "Numerical Analysis of Secondary Motion of Piston Skirt in Engines." *International Journal of Acoustics and Vibrations* 23, no. 4 (2018): 557-565.
[7] Narayan, Sunny. "A review of diesel engine acoustics." *FME Transactions* 42, no. 2 (2014): 150-154, DOI:10.5937/fmet1402150N.
[8] Narayan, S., Sasa Milojevic, and Vipul Gupta. "Combustion monitoring in engines using accelerometer signals." *Journal of Vibroengineering* 21, no. 6 (2019): 1552-1563.
[9] Mahroogi, Faisal O, S. Narayan, and Vipul Gupta. "Acoustic transfer function in gasoline engines." *International Journal of Vehicle Noise and Vibration (IJVNV)* 14, no. 3 (2018): 270-280.
[10] Narayan, S. "Wavelet analysis of diesel engine noise." *Journal of Engineering and Applied Sciences* 8, no. 8 (2013): 255-259.
[11] Narayan, S. "Analysis of Piston Slap Motion." *International Journal of Applied Mechanics and Engineering (IJAME)* 20, no. 2 (May 2015): 445-450, DOI: https://doi.org/10.1515/ijame-2015-0030.
[12] Narayan, Sunny. "Piston Slap Noise in engines." *International Journal of Applied Engineering Research* 8, no. 14 (2013): 1695-1700.
[13] Narayan, Sunny. "Effect of dwell time on noise radiated from diesel engine." *International Journal of Applied Engineering Research* 8, no. 11 (2013): 1339-1347.
[14] Kaisan, Muhammad Usman, Shitu Abubakar, Muhammed Mustapha M, and S. Narayan. "Determination of Wear Metals Debris Concentration in Aircraft Engines." *International Journal of Recent Technology and Engineering (IJRTE)* 8, no.2 (2019):1289-1292, DOI: 10.35940/ijrte.B1917.078219.
[15] Narayan, S., Ali Sulaiman Alsagri, and Vipul Gupta. "The design and analysis of hybrid automotive suspension system." *International Journal of Mechanical and Production Engineering Research and Development (IJMPERD)* 9, no. 4 (Aug. 2019): 637-642.
[16] Mahroogi, Faisal O., and S. Narayan. "Design and analysis of Double Wishbone suspension systems for automotive applications." *International Journal of Mechanical and Production Engineering Research and Development (IJMPERD)* 9, no. 4 (Aug. 2019): 1433–1442.
[17] Stojanovic, Nadica, Nouby M. Ghazaly, Ivan Grujić, Jasna Glišović, and Sunny Narayan. "Influence of Size of Ventilated Brake Disc's Ribs on Air Flow Velocity." *International Journal of Advanced Science and Technology* (*IJAST)* 29, no.1 (2020): 637-647.
[18] Mahroogi, Faisal O., and S. Narayan. "Effects of dampers on piston slapping motion." *International Journal of Vehicle Noise and Vibration (IJVNV)* 16, no. 1/2 (2020): 46 – 57, DOI: 10.1504/IJVNV.2020.112432.
[19] Narayan, S., and Vipul Gupta. "Numerical Model of Combustion Noise generation in Combustion Engines." *International Journal of Advanced Science and Technology (IJAST)* 29, no. 5 (2020): 8852-8858.
[20] Narayan, S., and V. Gupta. "Frequency characteristics of in cylinder pressure of a gasoline engine." *Journal of Applied Engineering Science* 19, no.1 (2021): 92-97, DOI: https://doi.org/10.5937/jaes0-27156.

Research regarding Electro-Pneumatic Systems with Pneumatic Motor

Lecturer Dr. eng. **Iulian Claudiu DUȚU**[1], Dr. eng. **Tiberiu AXINTE**[2,*],
Dipl. Eng. **Lidia CALANCEA**[2], Dipl. Eng. **Cătălin FRĂȚILĂ**[2],
Dipl. Eng. **Mihai DIACONU**[2], Dipl. Eng. **Remus COJOCARU**[3]

[1] Politehnica University of Bucharest, Romania

[2] Research Center for Navy, Romania

[3] Princess Cruises, USA

*tibi_axinte@yahoo.com

Abstract: *In this paper, we study electro-pneumatic systems with air motors. Besides the pneumatic motors, the cylinders are the actuators which are the most used in electro-pneumatic systems. The study of pneumatic and electro-pneumatic circuits is performed in the FluidSim from Festo. At the beginning, we make simple pneumatic systems with single or two air motors. We continue with simple and complex electro-pneumatic systems that have air motors. The pneumatic motors are generally used for the development of the following installations: pump drivers, conveyor drivers, mixing equipment, pharmaceutical packaging, tension devices, hose reels, winches, hoists, turntables, etc.*

Keywords: *FluidSim, pneumatic, electrical, systems, air motor*

1. Introduction

A pneumatic motor (an air motor) is a type of motor that does mechanical work by expanding compressed air. The air motors generally convert the compressed air energy to mechanical work through either linear or rotary motion.
The air motor was first applied to the field of transportation from Challiot (France) in 1840.
In research, the pneumatic motor can be used for electro-pneumatic arm development.

Symbol	Description
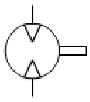	The pneumatic motors are categorized into the groups of piston motors, turbines, gear motors and sliding vane motors.

Fig. 1. The pneumatic motor

The pneumatic motors can be piston air motors or vane air motors.

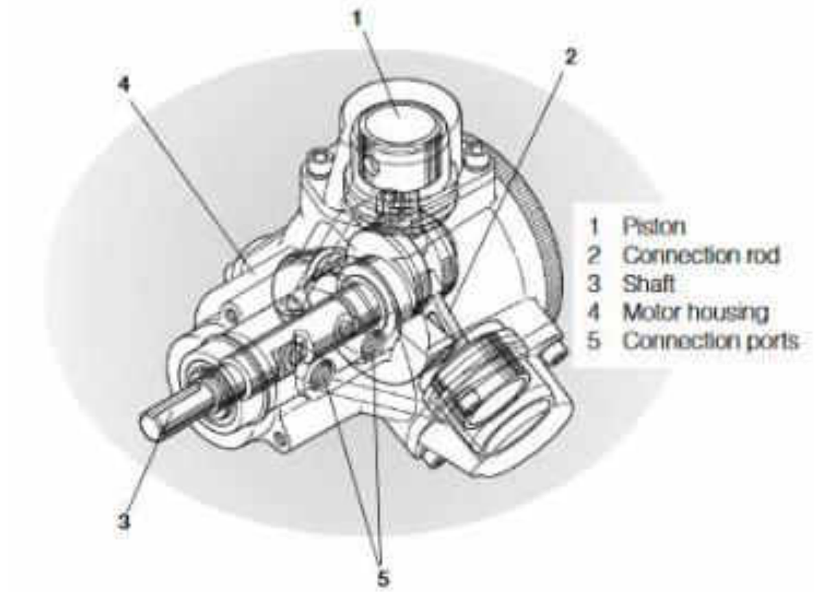

Fig. 2. Radial air motor. Components.

The main components of radial air motor, [1]:
- Piston;
- Connection rod;
- Shaft;
- Motor housing;
- Connection ports.

The relationship that defines the equilibrium of torque in rotary drive is, [2]:

$$M_{PV} - M_{ext} - \mathrm{f} \cdot \omega - \mathrm{I} \cdot \varepsilon = 0 \tag{1}$$

Where:
- M_{PV} - pressure and swept volume dependent torque.
- M_{ext} - external torque.
- f - friction.
- ω- angular velocity.
- I – moment of inertia.
- ε – angular acceleration.

The pressure and swept volume dependent torque is:

$$M_{PV} = \frac{(P_1 - P_2) \cdot V}{2 \cdot \pi} \tag{2}$$

- P_1 – initial pressure;
- P_2 – final pressure;
- V – volume.

2. The pneumatic motor in circuits

An air motor is a type of motor which does mechanical work by expanding compressed air, [3].

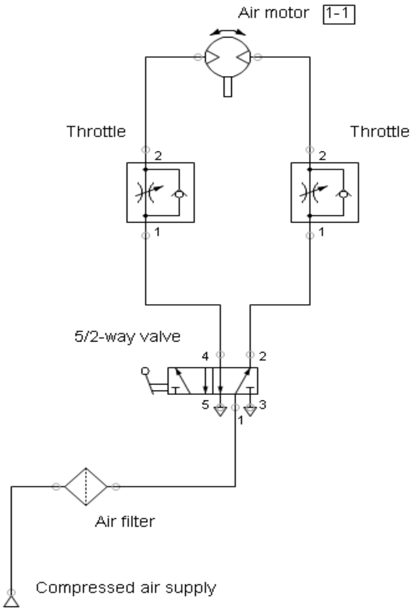

Fig. 3. Pneumatic system with an air motor. Scheme 1.

The pneumatic system with the air motor 1-1 has the following components:

Description	Number of components
Air motor	1
Throttle	2
5/2-way valve	1
Air filter	1
Compressed air supply	1

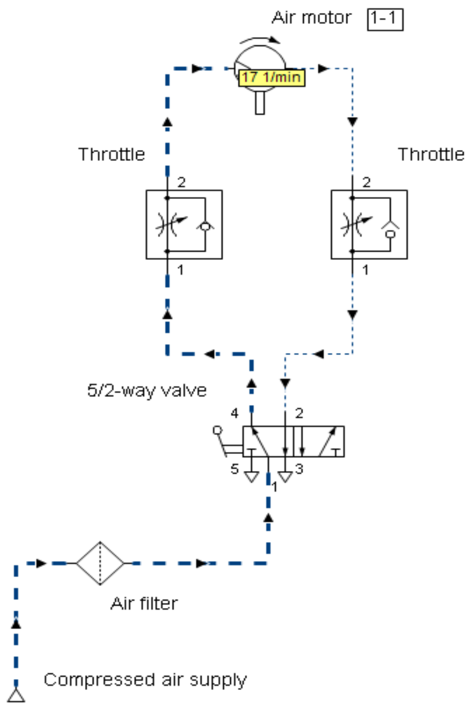

Fig. 4. Pneumatic system with an air motor. Simulation.

The pneumatic system opens if the lever is pushed from 5/2-way valve. In our case, the volumetric flow rate in the air motor 1-1 is 17 l/min, Fig. 4.

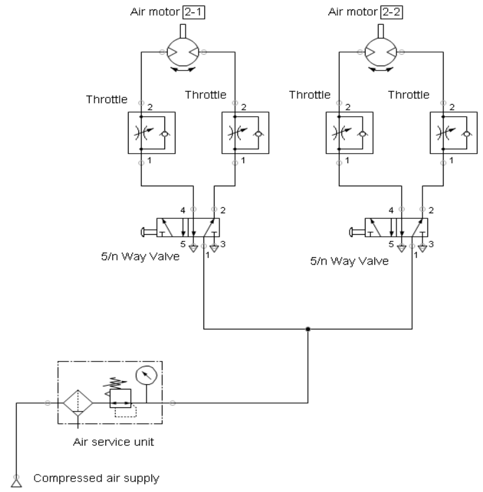

Fig. 5. Pneumatic system with two air motors. Scheme 2.

The pneumatic system with two air motors: 2-1 and 2-2, in scheme 2, has the following devices:

Description	Number of components
Air motor	2
Throttle	4
5/2-way valve	2
Air service unit	1
Compressed air supply	1

The two air motors are independent. They can start at the same time or successively. The shafts rotate in a different direction. Therefore, they can rotate clockwise or counterclockwise, [4].
At air motor 2-1, the shaft rotates clockwise. However, at the air motor 2-2, the shaft rotates counterclockwise, Fig. 6.

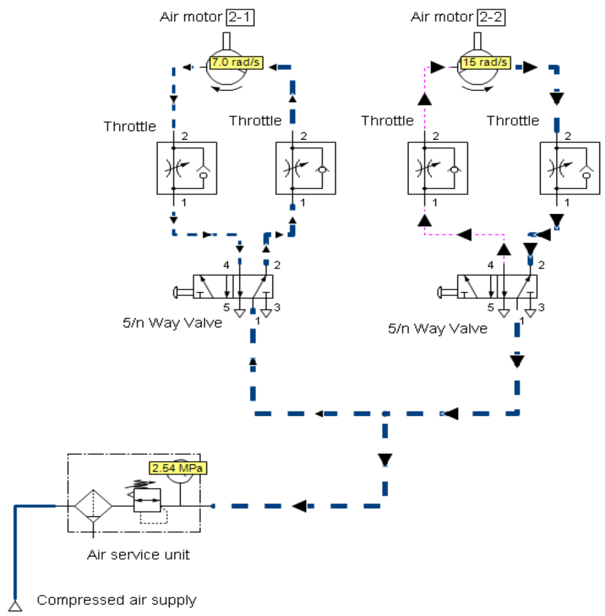

Fig. 6. Pneumatic system with two air motors. Simulation.

The air service unit pressure gauge indicates 2.54 MPa. Rotational speed from the air motor 2-1 is $\omega_{2-1} = 7\ rad/s$ and rotational speed from the air motor 2-2 is $\omega_{2-2} = 15\ rad/s$, Fig. 6.

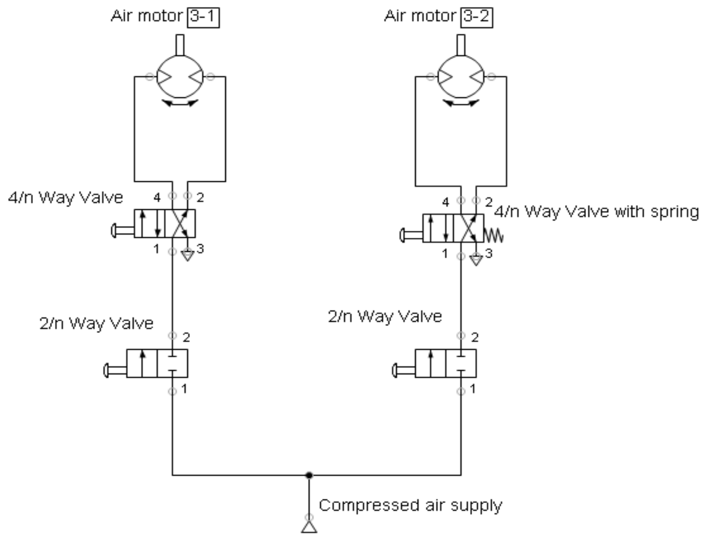

Fig. 7. Pneumatic system with two air motors. Scheme 3.

The pneumatic system with two pneumatic motors air motors: 3-2 and 3-1, in scheme 3, has the following devices:

Description	Number of components
Air motor	2
4/n way valve	1
4/n way valve with spring	1
2/n way valve	2
Compressed air supply	1

The directional control valves type 2/n way valve are safety devices, Fig. 7.

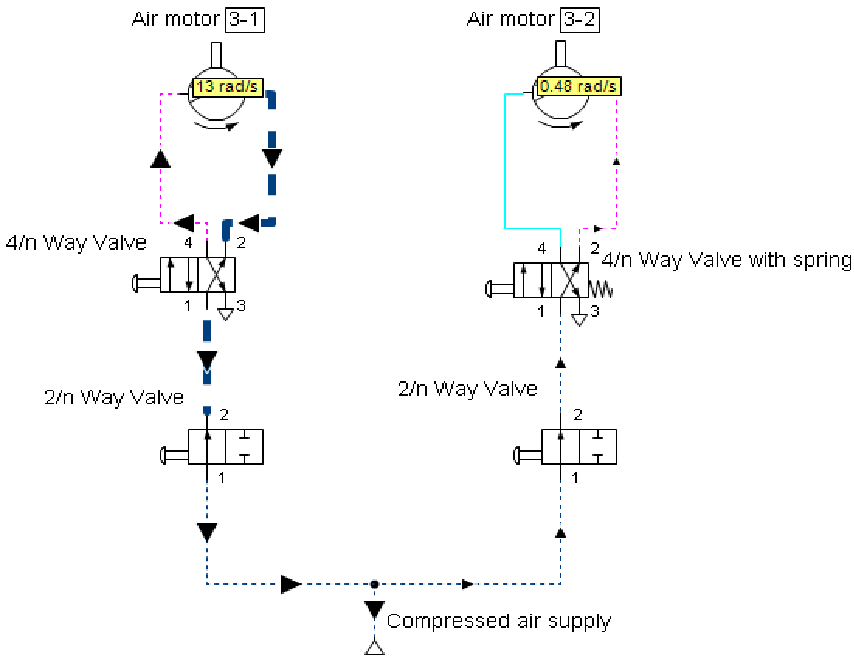

Fig. 8. Pneumatic system with two air motors. Simulation.

Rotational speed from pneumatic motors are represented by two diagrams, Fig. 9

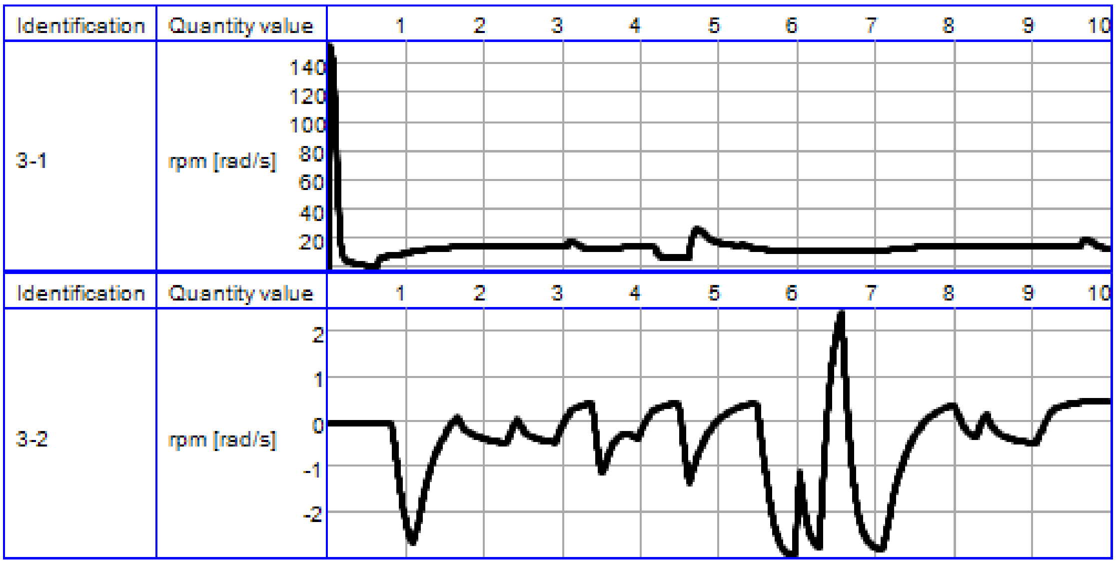

Fig. 9. Scheme 3. Diagrams of the pneumatic motors.

The diagrams of the two pneumatic motors do not resemble each other at all, Fig. 9.

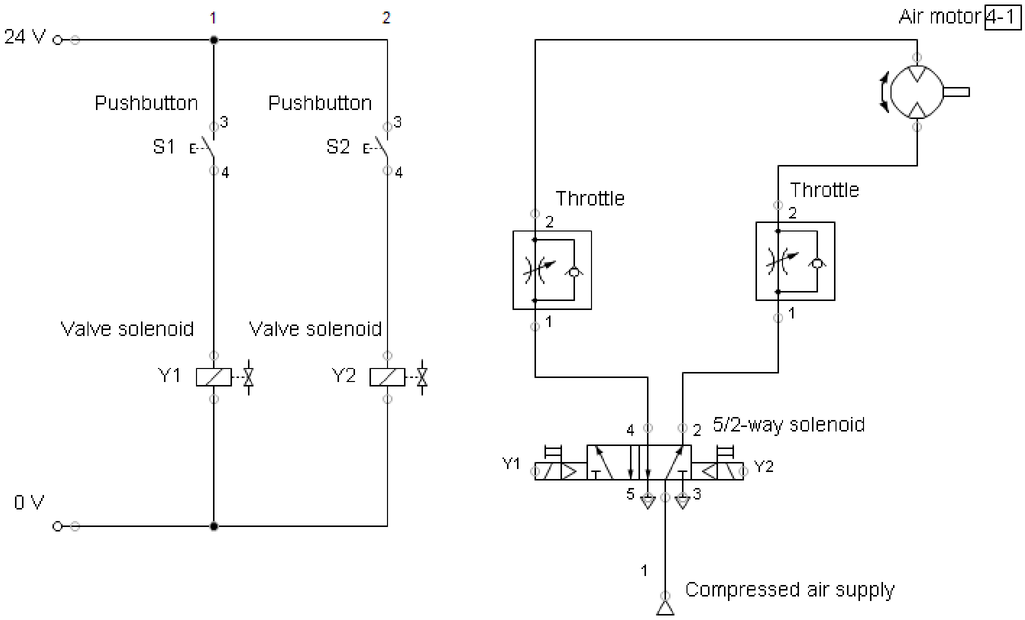

Fig. 10. Electro-pneumatic system with an air motor. Scheme 4.

Scheme 4 represents the first electro-pneumatic circuit in the manuscript. The devices used in the electro-pneumatic system are:

- Pneumatic devices:

Description	Number of components
Air motor	1
Throttle	2
5/2 way solenoid	1
Compressed air supply	1

➢ Electrical devices:

Description	**Number of components**
Solenoid valve	2

If we press the S1 button, the shaft rotates counterclockwise. The rate of rotation for the S1 button is $\omega_{4-1\,a} = 3.1\ rad/s$, Fig. 11.

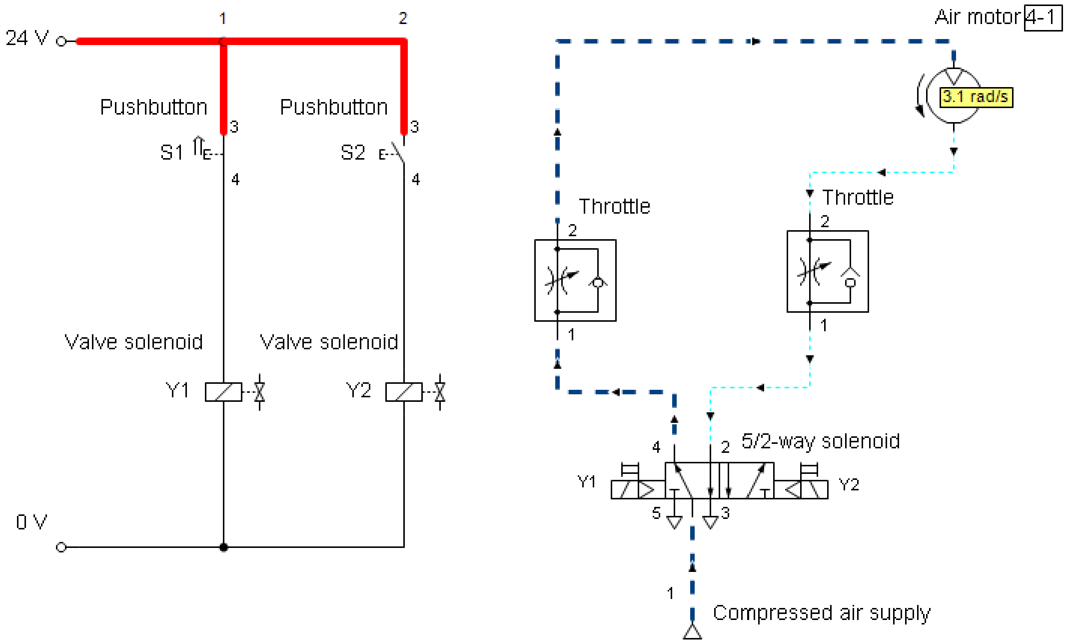

Fig. 11. Counterclockwise rotation shaft. Scheme 4.

After that, we press the S2 button; the shaft rotates clockwise. The rate of rotation for the S2 button is $\omega_{4-1\,b} = 3.1\ rad/s$, Fig. 12.

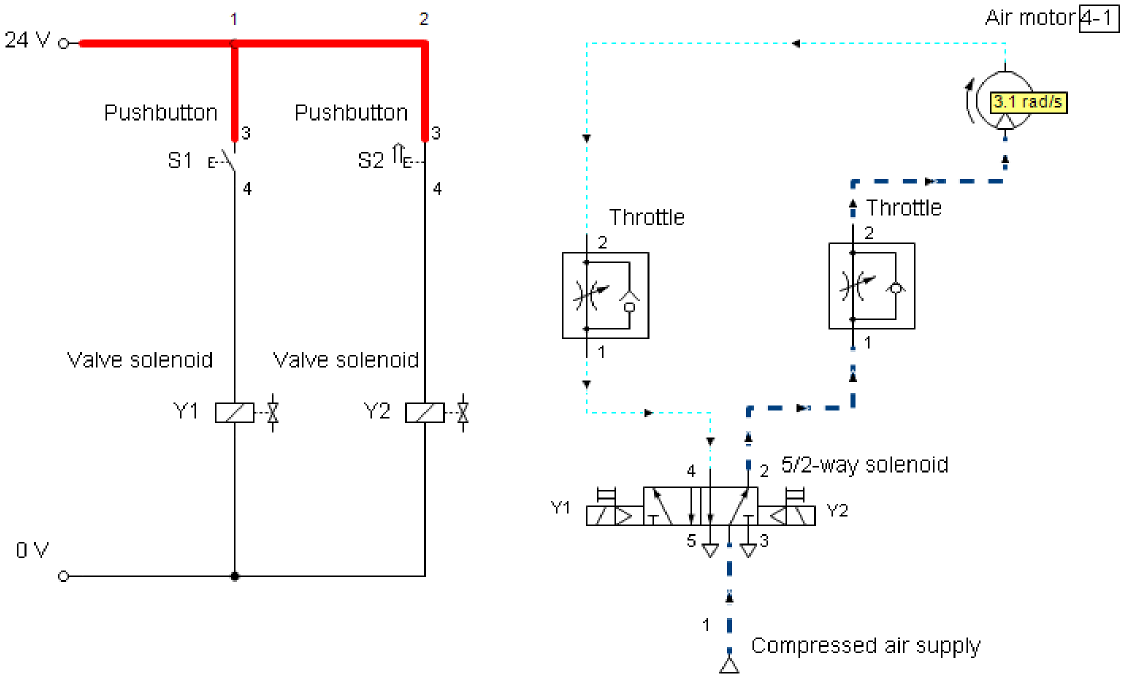

Fig. 12. Clockwise rotation shaft. Scheme 4.

The rotational speed in both directions are equal, [5].
For the pneumatic motor 4-1: $\omega_{4-1\,a} = \omega_{4-1\,b} = 3.1\ rad/s$, Fig. 11 and Fig. 12.

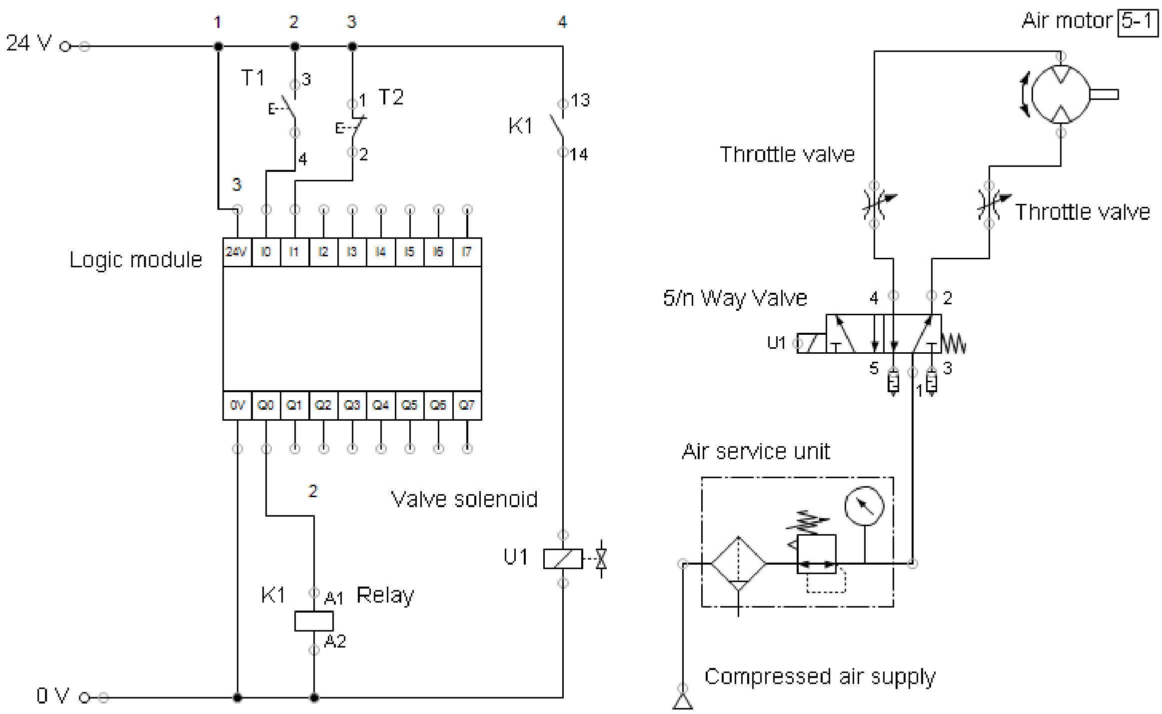

Fig. 13. Electro-pneumatic system with an air motor and logic module. Scheme 5.

At scheme 5, the logic module is introduced in the electrical one, Fig. 13.
The main parts of scheme 5 are:

- Pneumatic parts

Description	Number of components
Air motor 5-1	1
Throttle valve	2
5/2 way valve	1
Air service unit	1
Compressed air supply	1

- Electrical parts

Description	Number of components
Solenoid valve	1
Relay	1
Logic module	1

However, in logic modules there are two digital components from digital technology: latching relay and NOT, Fig. 14.

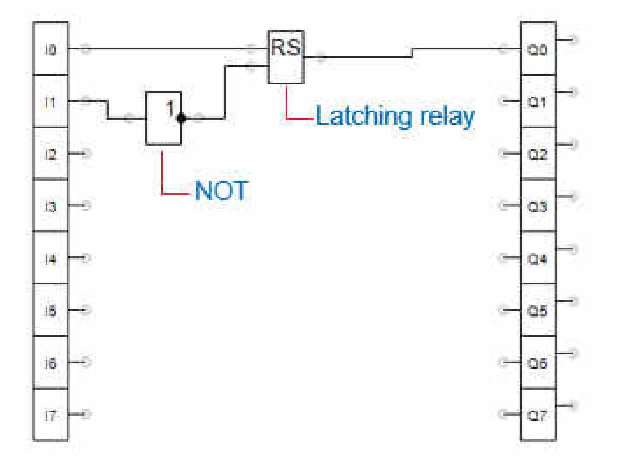

Fig. 14. Components parameters of logic module. Scheme 5.

The electro-pneumatic system shown in scheme 4 opens when the T1 button is pressed. In this case, the shaft from air motor 5-1 rotates counterclockwise. The rotational speed is $\omega_{5-1\,a} = 1.5\ rad/s$. The pressure gauge from the air service unit indicates 0.399 MPa, Fig. 15.

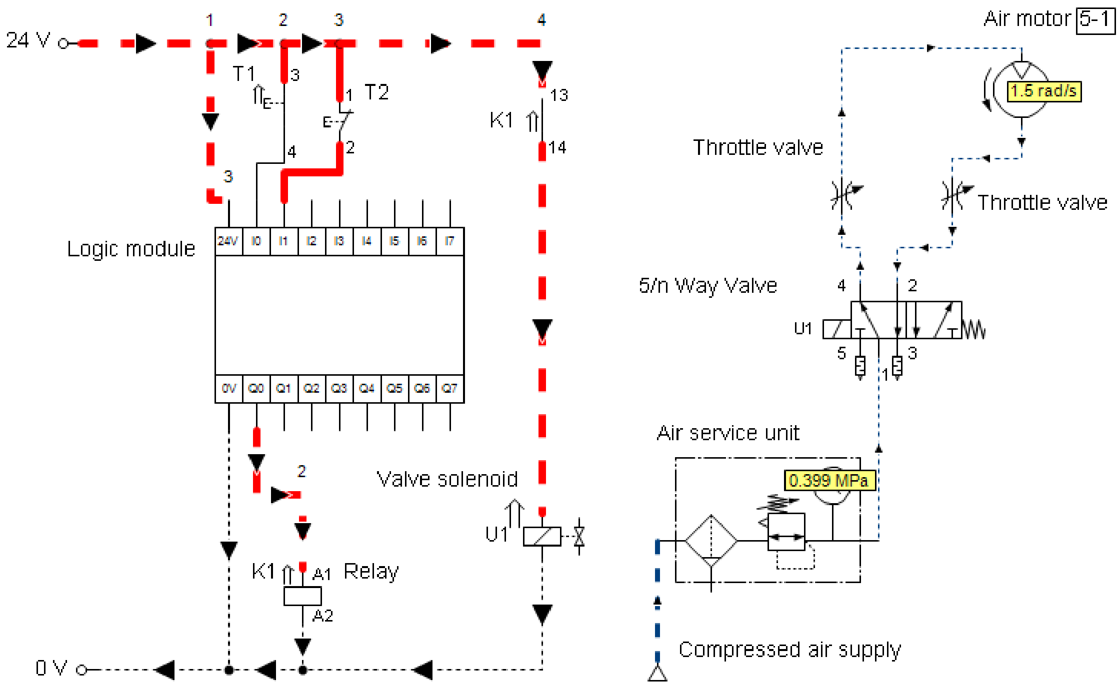

Fig. 15. Counterclockwise rotation shaft .Scheme 5.

However, to try to change the direction of the air motor 5-1, one must press T2 button.
In this case, the shaft from the air motor rotates clockwise, [6].
The rotational speed is $\omega_{5-1\,b} = 1.7\ rad/s$, Fig. 16.

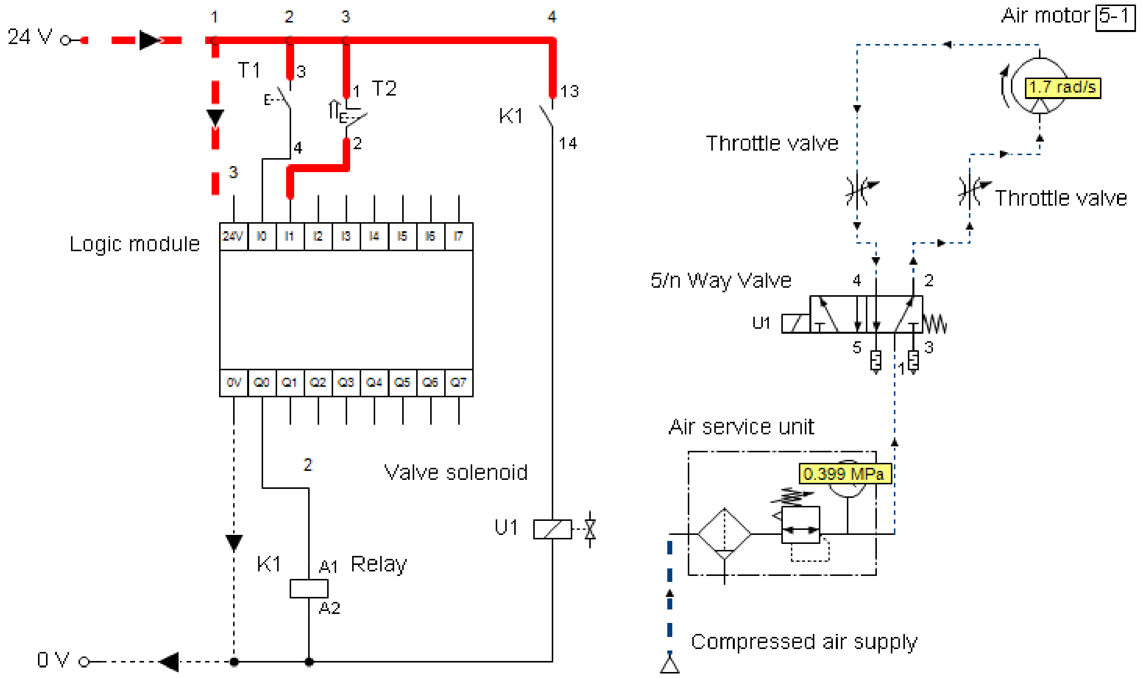

Fig. 16. Clockwise rotation shaft. Scheme 5.

3. Conclusions

The advantages of pneumatic motors are the following: non-electrical sparking, cool running, mounting flexibility, capability to operate in all positions and variable directions.
Some electro-pneumatic systems use mini air motors in small installations.
The electro-pneumatic systems that use air motors are operated in safety conditions for operators.
The high rotation speed for shafts from air motors can lead to increased productivity if it is used in industry.
From this perspective, the determination of such characteristics is very useful and the created pneumatic models can be used in technical research.
The pneumatic motors from Festo are efficient alternatives to electric motors. Their air motors provide excellent horsepower and easily adjusted controls.
In the future, we will try to develop electro-pneumatic schemes that use several types of actuators, meaning air motor with cylinder or semi-rotary actuator.

References

[1] Dvorak, L., K. Fojtasek, and V. Rehacek. “Experimental equipment for measuring of rotary air motors parameters.” *EPJ Web of Conferences* 143, DOI: 10.1051/epjconf/201714302019 (2017): 02019.
[2] www.festo.com.
[3] Panaitescu, M., M. Dumitrescu, and F. V. Panaitescu. “Indoor air quality monitoring universal device.” *IOP Conference Series: Materials Science and Engineering* 916 (2020): 012081.
[4] Dumitrache, C.L., and D. Deleanu. “Sloshing effect, Fluid Structure Interaction analysis.” *IOP Conference Series: Materials Science and Engineering* (2020): 012030.
[5] Curca, E., R. Damian, O. Radu, and V. Rosca. “Modeling and simulation of hydro-acoustic signal propagation in the Romanian Black Sea coast.” *IOP Conference Series: Earth and Environmental Science* 172 (2018): 012015, DOI: 10.1088/1755-1315/172/1/012015.
[6] Degeratu, M. *Dimensional analysis, similarity and modeling. Guide for applications in fluid mechanics and hydraulics / Analiză dimensională, similitudine și modelare. Îndrumar pentru aplicații în mecanica fluidelor și hidraulică*. Bucharest, Publishing House of the Romanian Academy of Scientists (AOSR), 2015.

Combustion Process Analysis in Engines Using Vibration Signals

Dr. **Faisal O. MAHROOGI**[1], Dr. **S. NARAYAN**[2]

[1]Faculty of Mechanical Engineering, Islamic University of Medina, Saudi Arabia

[2]Faculty of Mechanical Engineering, Qassim University, Saudi Arabia

* Corresponding author's e-mail address: rarekv@gmail.com

Abstract: *This work analysis the scope of non-intrusive measurements by engine vibration monitoring. These signals complex in nature due to contributions of various sources like valve operations, fuel pump operation, combustion events and piston motion. The vibration signals obtained from tests has been analysed into various components. Tests were done to select an optimum location for placement of accelerometer to measure engine block vibrations, which are sensitive to combustion contribution due to rapid rise in cylinder pressure. A suitable range of frequency has been identified in which there is high correlation between engine block vibrations and the cylinder pressure using time frequency analysis methods.*

Keywords: *Automotive; Noise; Acoustic*

1. Introduction

There are generally three phases of injection process used in diesel engines, namely pre-injection period, main-injection period & post injection period. There is a delay period between instant at which fuel is injected inside the combustion chamber and actual start of ignition process. Greater this delay period, more is the temperature achieved during course of combustion and hence better conditions exist for NOx formation. In order to shorten this delay period, a small amount of fuel is pre-injected before main injection occurs during the phase of pre-mixed combustion. Torque and power produced in engine mainly depends on the duration of main injection period. It is advantageous to vary the injected fuel mass with time in order to reduce the specific consumption of fuel. This is achieved by rate shaping as seen in figure no 1. Rate shaping curve may be rectangular, step or boot type in shape. Post-injection of fuel is done in order to reduce the soot emissions and in some cases may be useful for exhaust gas recirculation treatment [1-12].

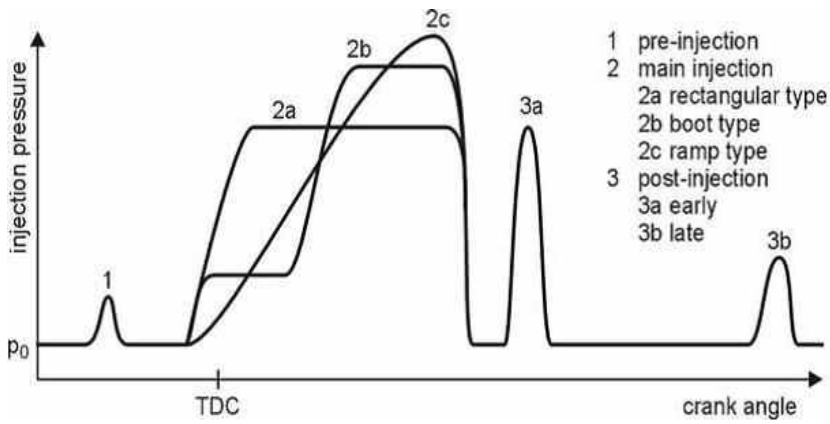

Fig. 1. Multiple injection methods adopted for modern diesel engines [1]

The amount of fuel injection during pre-injection period is denoted by Q_{pre}(mm^3per stroke), whereas the amount of fuel injected during main-injection period is denoted by Q_{main}(mm^3per stroke).
Various methodologies used to diagnose working of combustion engines are as follows:

A. Vibrations- location of transducer to monitor vibrations is a major issue as there are chances of due contamination of signals due to environmental issues. Frequency analysis, peak and RMS values are effective to monitor imbalances, bearing damage or shaft misalignments [1-11].
B. Noise emissions- Noise levels are perceived by the humans as air pressure oscillations reaching ears which lead to motion of the ear drums. It provides information about injection faults, wear, and improper valve operation.
C. In cylinder pressure- it is effective to monitor injector faults, wear, valve operational problems, incorrect injection timings and hence overall combustion efficiency of engines. However, higher temperatures conditions make various pressure sensors expensive with short life span time [12].
C. Noise emissions - Various sound features can be analyzed by means of sound pressure levels (SPL). In order to obtain the levels that bear a closer relationship to loudness judgment, three different networks of frequency weighting (A, B, and C) filters have been incorporated into various sound level meters with the A weighting most closely matching the hearing capacity of human ears [13].
Various signal processing methods that may be used for effective condition monitoring of engines includes:
A. Power spectral density function (PSD)- This function (Ψ^2) provides the frequency composition of data in terms of its mean square values [14]. The average square values approach mean square values as $T \rightarrow \infty$.

$$\text{i.e. } \Psi^2 (\omega, \Delta\omega) = \text{Lim}_{\Delta x \rightarrow \infty} \int x^2 (t)\, dt / T \quad (1)$$

B. Time frequency analysis -The Fourier transformation of a function f(t) in frequency domain can be represented as:

$$f(\omega)= \int x(t)e^{-i\omega t}\, dt \quad (2)$$

This analysis is useful as long as frequency content of signals do not vary with time.
Hence time frequency analysis or wavelet analysis are more suitable for analysis of transient signals [15]. The short time-frequency analysis (STFT) of signal may be represented as:

$$\text{STFT } (\tau,f)= \int x(t)\, h^*(t-\tau)\, e^{-i\omega t}\, dt \quad (3)$$

Where x(t) is input signal & h(t-τ) is window

The presented work aims at study of engine block vibrations for combustion process monitoring using time and frequency domain processing techniques.

2. Literature review

Combustion process plays an important role in emissions, NVH and engine power output. Hence, new methods of diagnosis have been developed to monitor this process and to relate the injection methods using non-intrusive sensors. Chamber oscillation are caused due to rapid rise in pressure gradient due to ignition of air-fuel mixture. Use of microphones is one of most important non-intrusive methods are and concerns of contact with high temperature surfaces is avoided. However, there may be signal contamination due to other sources superimposed [12-14]. Accelerometer signals have been analyzed to define the frequencies of cylinder pressure and vibration signals [15]. Cylinder pressure was reconstructed using vibration measurements are presented [16-20]. In [19] the various events have been analyzed using surface vibrations in engines.

The depletion of fossil fuels in modern times has pressed for need to find methods to save consumption of fuel [20]. Nadija et al. [13] presented an overview of automotive NVH engineering, classifying power train-related NVH, road- and tire-related NVH and wind related NVH. They also discussed brake and chassis, squeak and rattle noise. Automotive industries are concerned to minimize noise and vibration level for marketing [37]. Dynamic features of vibrations and instability of the front-end accessory drive belt system was investigated. Various challenges in NVH testing of engines that constitute complexities to the development were explored.

3. Materials and methods

Tests were done on a single cylinder HARTZ engine having specifications as presented in Table no 1. A fully opened electronic control unit connected to computer was used to manage the injection system with aim to control operational parameters. The engine was coupled with a synchronous motor of SIEMENS 1PH7 make thus allowing to control speed and load. The in cylinder pressure was monitored by an AVL transducer having specifications shown in Table 2. Block vibrations were measured by means of a Endveco7240C type Mono axial accelerometer having features accelerometer are presented in Table no 3. Engine testing speed of 2000 RPM,3000 RPM and load values of 80%, 100% was chosen with an aim to cover complete engine operational conditions. Main operational parameters are listed in Table no 4.

Table 1: The features values of engine

Type	Diesel Engine
Make	HARTZ
No of cylinders	1
Stroke	65mm
Displacement	0.243 liter
Compression	22:1
Maximum Power	3.5kW@4400RPM
Bore	69mm
Maximum Torque	10N-m @2000RPM

Table 2: Pressure Transducer Specifications

Range	0-250Bar
Sensitivity	20pC/Bar
Resonance Frequency	160kHz

Table 3: Accelerometer Transducer Specifications

Range	1000g
Sensitivity	3pC/g
Resonance Frequency	90kHz

Table 4: Fuel injection Specifications

Case	Injection pressure	Q_{pre}	Q_{main}	SOI_{pre}	SOI_{main}	Load	Speed
1	700	1	15.4	19.3°	6.02°	80%	2000RPM
2	700	1	16.7	20°	6°	100%	2000RPM
3	700	1	17.8	22.4°	9°	80%	3000RPM
4	700	1	14.6	18.2°	9.5°	100%	3000RPM
5	--	--	--	--	--	--	3000RPM

4. Results and discussions

Low frequency components in cylinder pressure curve are related to compression curve, whereas higher order harmonics are related to sudden rise in cylinder pressure. The motored condition can be used a baseline for combustion comparison as it contains contribution only due to motion of engine parts (figure 2−11).

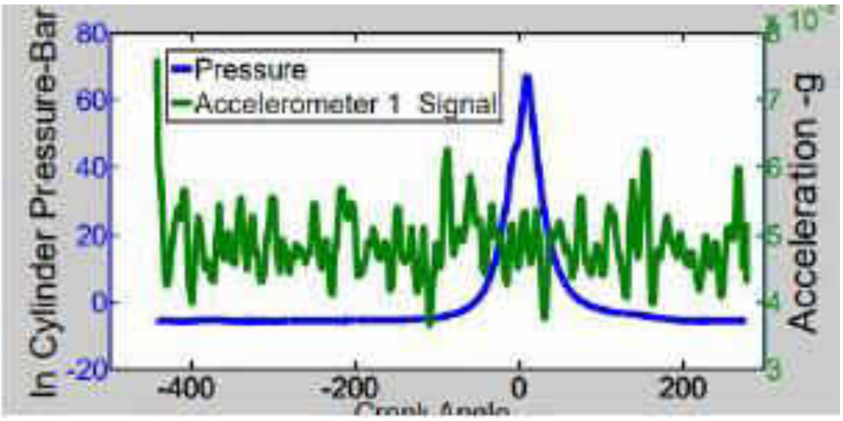

Fig. 2. Comparison of signals (Case 1)

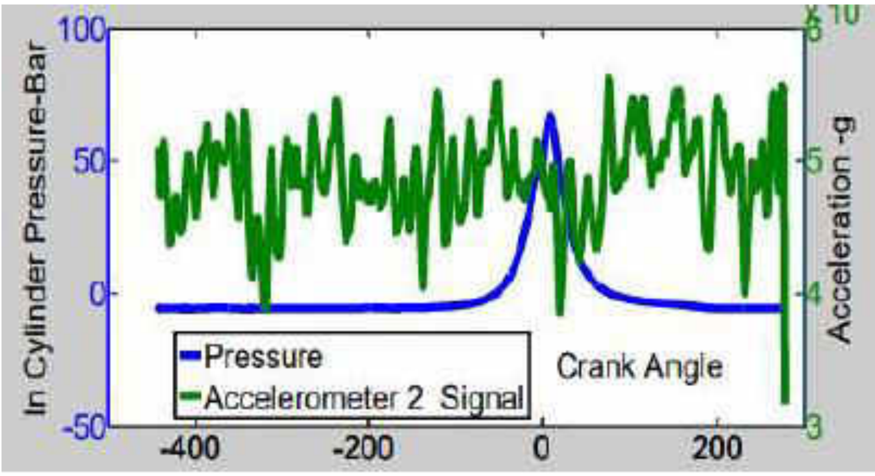

Fig. 3. Comparison of signals (Case 1)

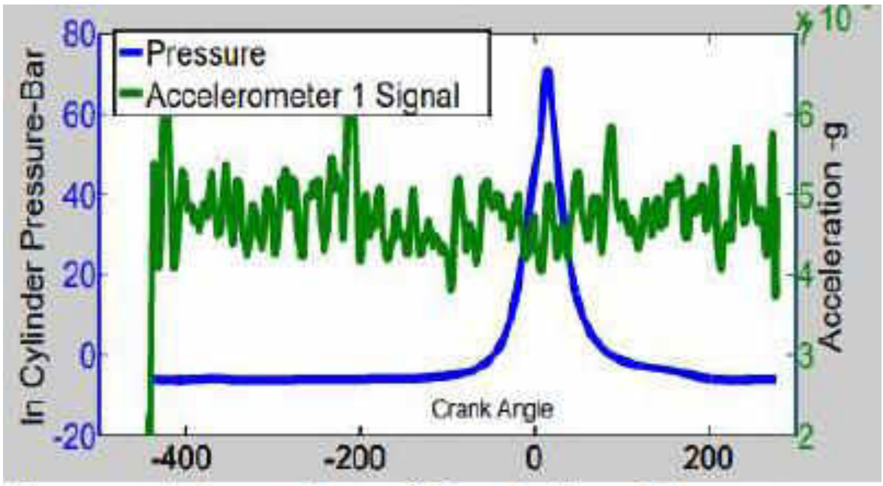

Fig. 4. Comparison of signals (Case 2)

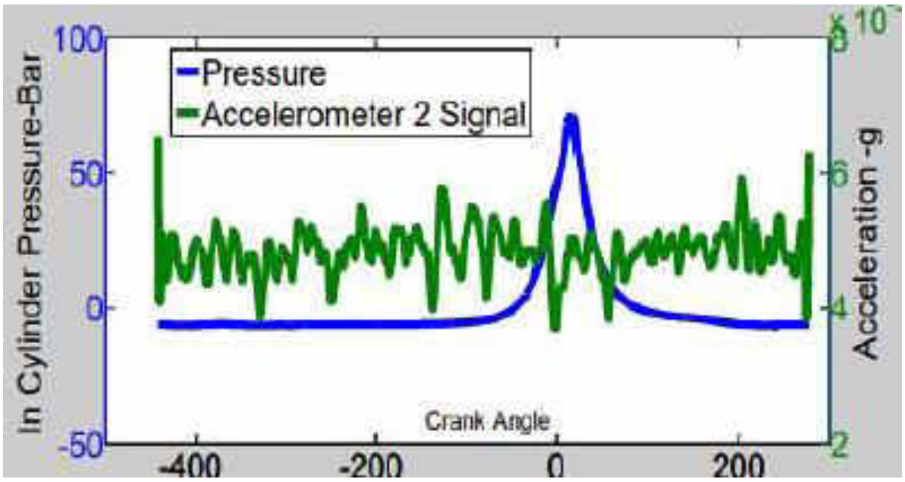

Fig. 5. Comparison of signals (Case 2)

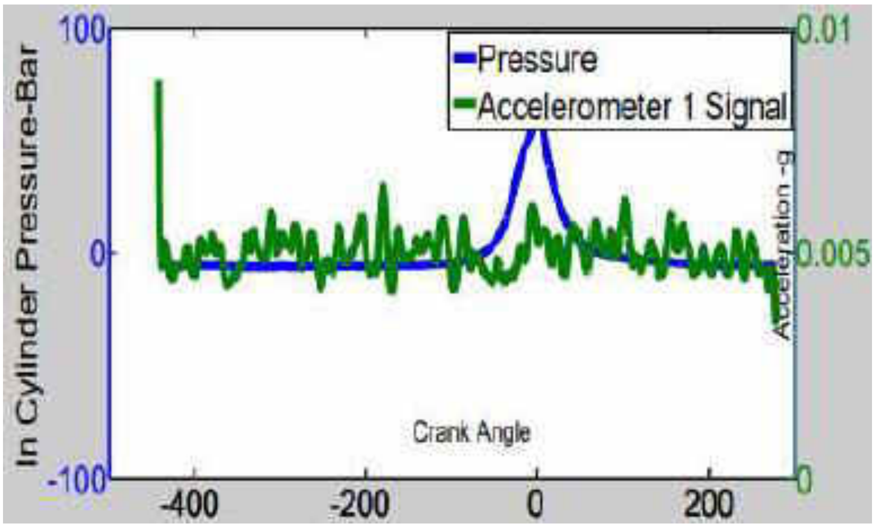

Fig. 6. Comparison of signals (Case 3)

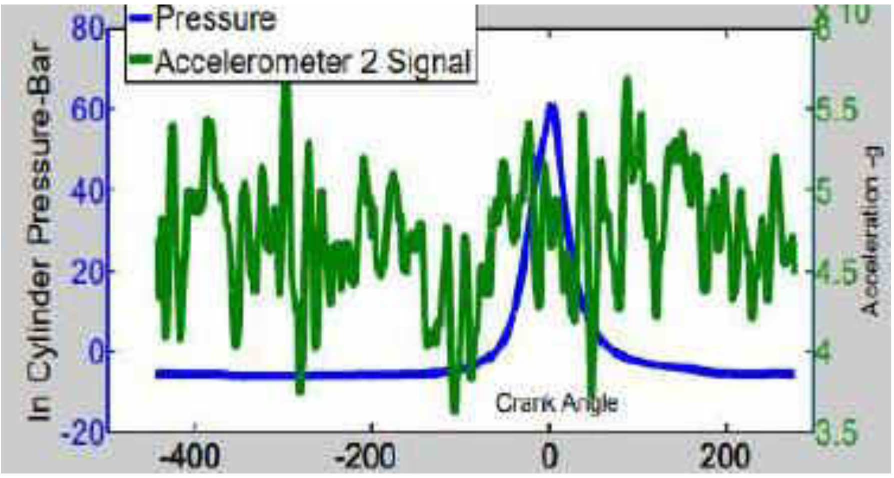

Fig. 7. Comparison of signals (Case 3)

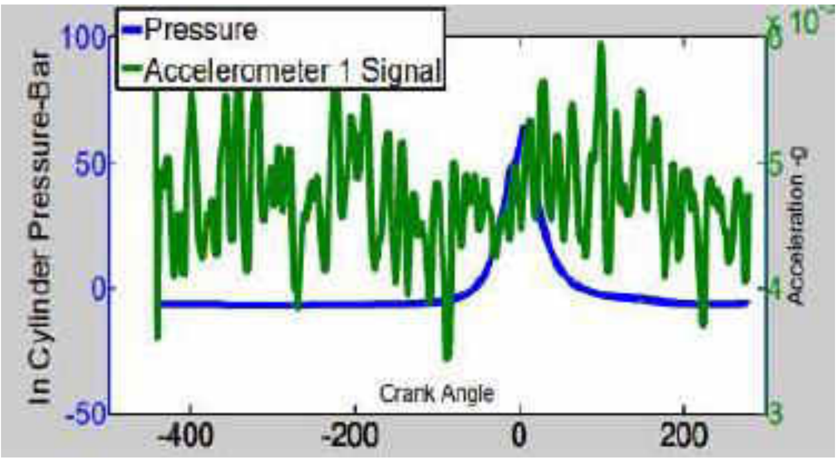

Fig. 8. Comparison of signals (Case 4)

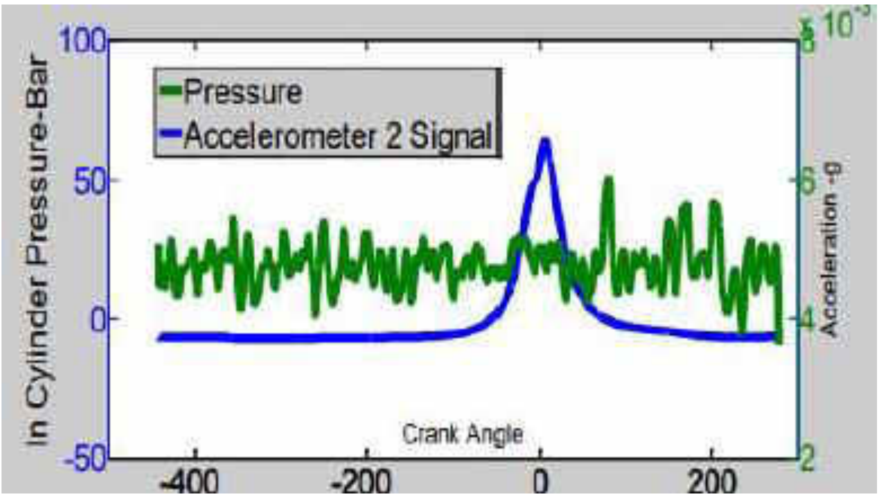

Fig. 9. Comparison of signals (Case 4)

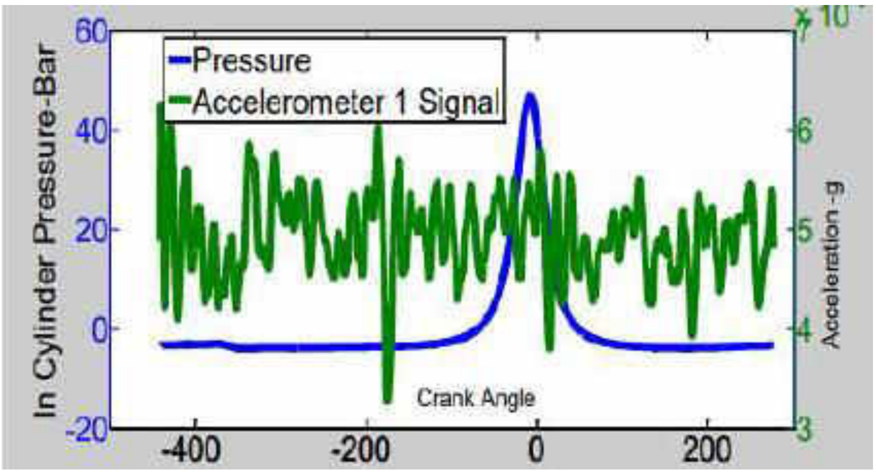

Fig. 10. Comparison of signals (Case 5)

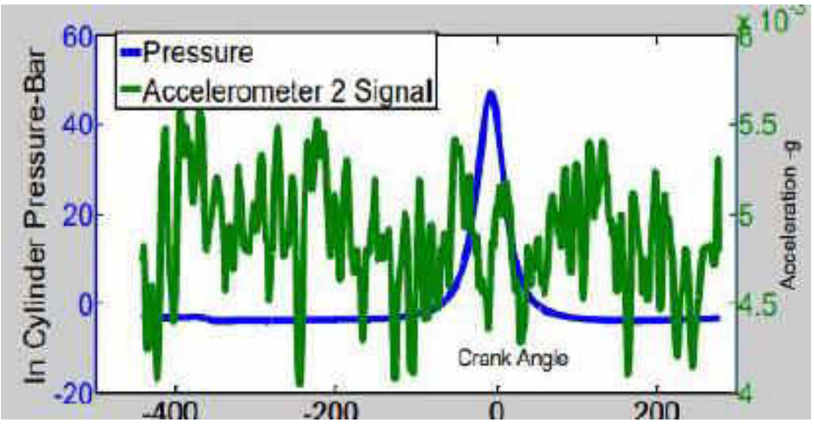

Fig. 11. Comparison of signals (Case 5)

Further frequency peaks can be observed in range 500Hz-1kHz regardless of operational conditions which can be considered as direct contribution due to combustion process. It has been proved that at low frequency ranges there is high structural attenuation upto1 kHz which decays and then again rises with frequency. This is responsible for low vibrations in engine block in spite of rapid rise in cylinder pressure. Also, all signals show same trends without concerning loading conditions (figure 12−16).

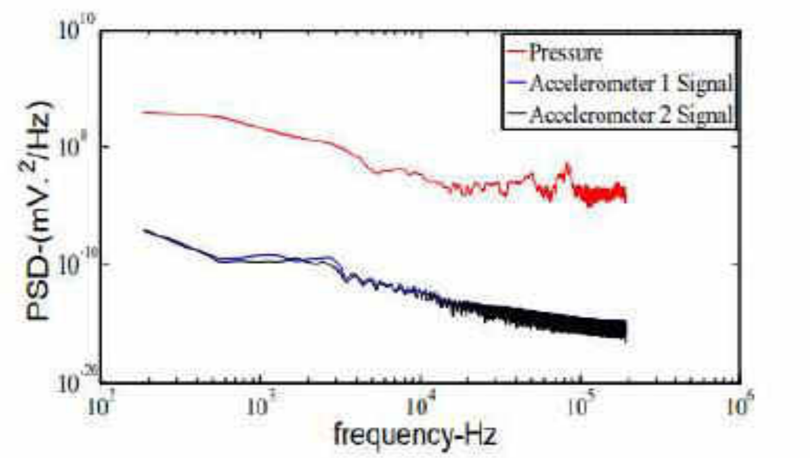

Fig. 12. Comparison of signals (Case 1)

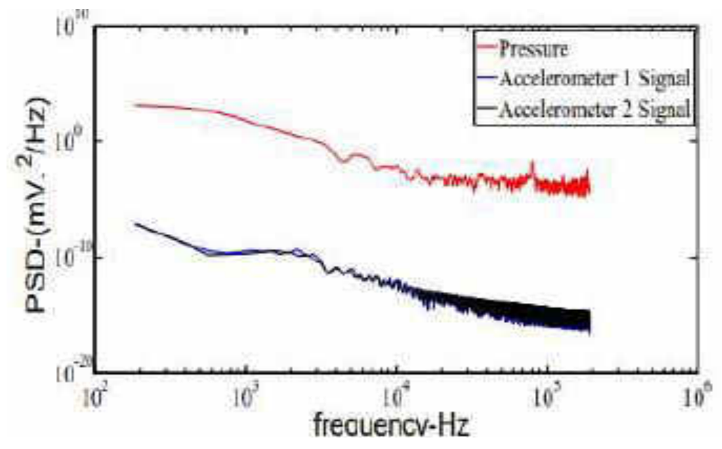

Fig. 13. Comparison of signals (Case 2)

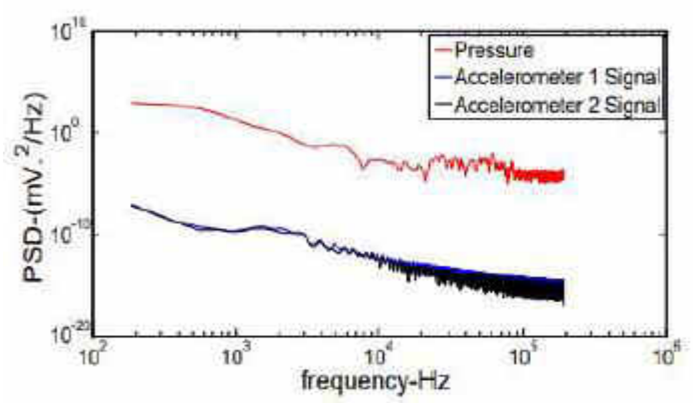

Fig. 14. Comparison of signals (Case 3)

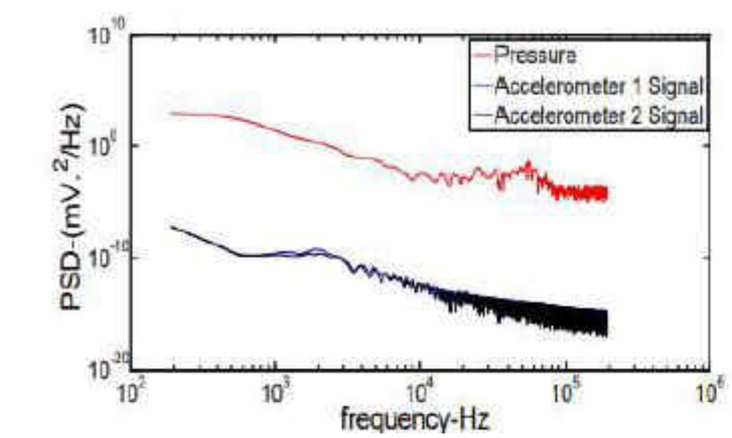

Fig. 15. Comparison of signals (Case 4)

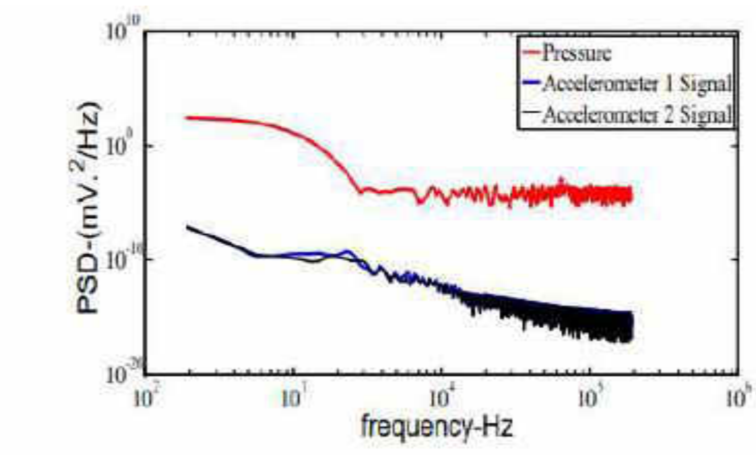

Fig. 16. Comparison of signals (Case 5)

Hence, coherence plots were drawn between cylinder pressure and accelerometer signals. Coherence function can be defined as ratio of product of cross spectral density of input signal (cylinder pressure) and output signals (accelerometer) to product of spectral densities of each signals. The range of this function varies from 0 to 1. Figures 17-21 show plots of squared magnitude of coherence functions between in cylinder pressure and both accelerometer positions for the given testing conditions.

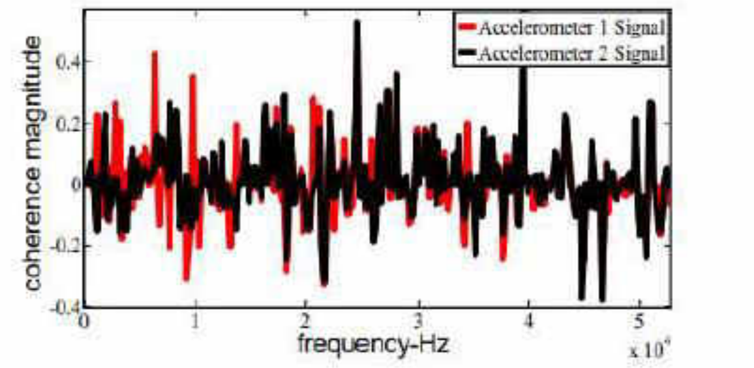

Fig. 17. Coherence signals (Case 1)

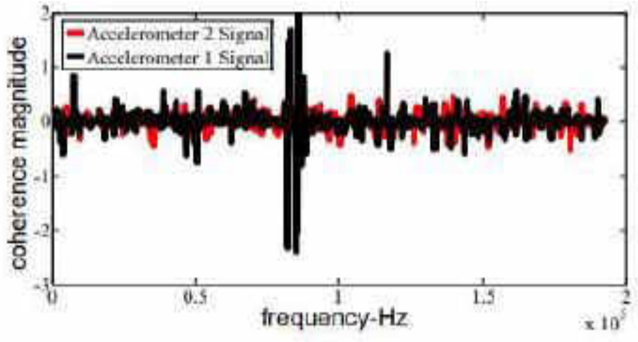

Fig. 18. Coherence signals (Case 2)

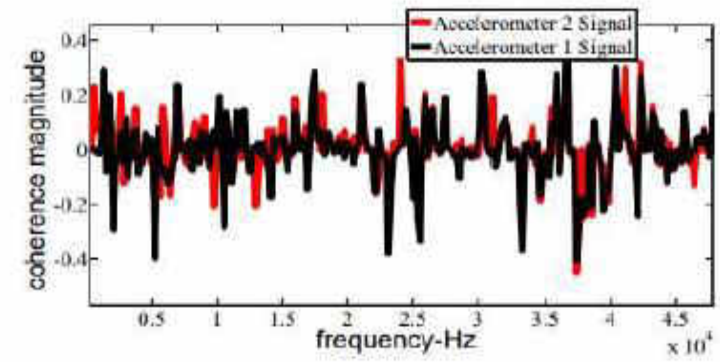

Fig. 19. Coherence signals (Case 3)

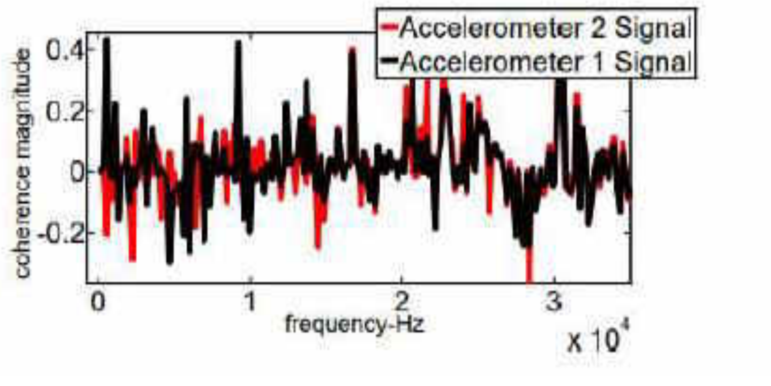

Fig. 20. Coherence signals (Case 4)

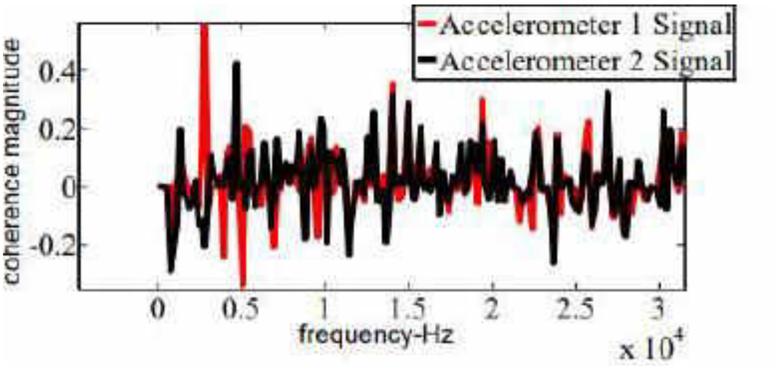

Fig. 21. Coherence signals (Case 5)

From these plots, it is clear that accelerometer signals along horizontal direction exhibit low coherence with cylinder pressure signals due to contamination of signals by other noise sources like piston slap. In addition, high values of coherence function between cylinder pressure and vertical accelerometer signals were exhibited in frequency range 500Hz-1100Hz. Table 5 shows maximum squared values of coherence functions for test cases in this frequency range.

Table 5: Coherence Specifications

Case	Value
1	0.84
2	0.85
3	0.86
4	0.81
5	0.83

In order to further analyzed signals, time-frequency analysis of pressure signals was done for the given testing conditions with focus in the frequency band defined earlier. The results obtained in figures 22-26 highlight higher frequency amplitudes near Top dead canter position, which denotes combustion events.

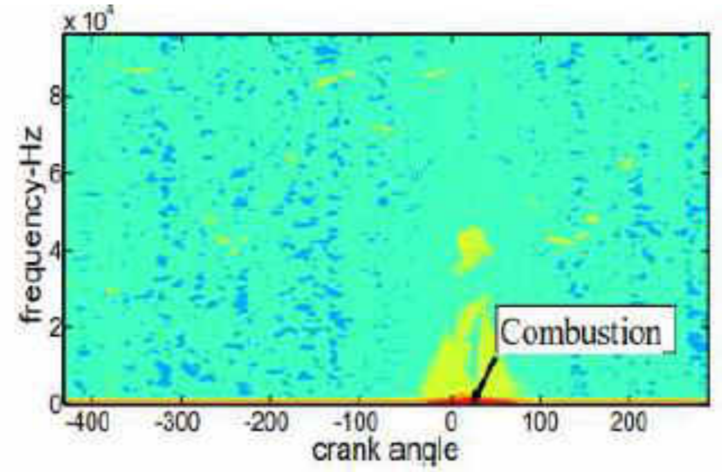

Fig. 22. Coherence signals (Case 1)

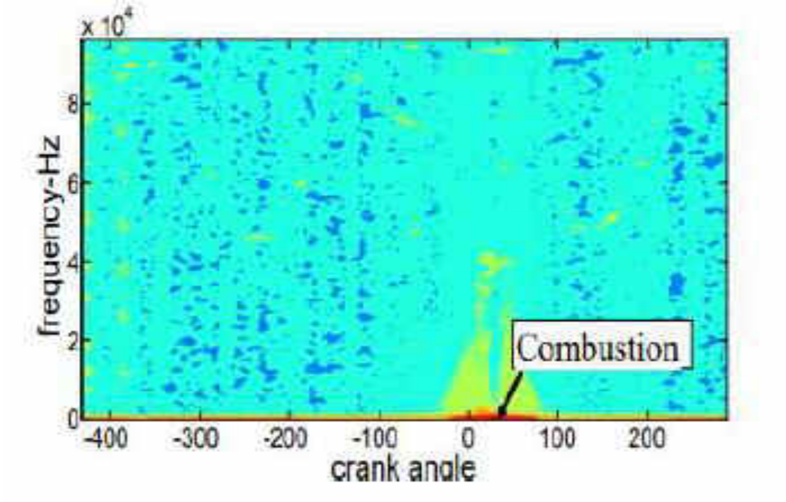

Fig. 23. Coherence signals (Case 2)

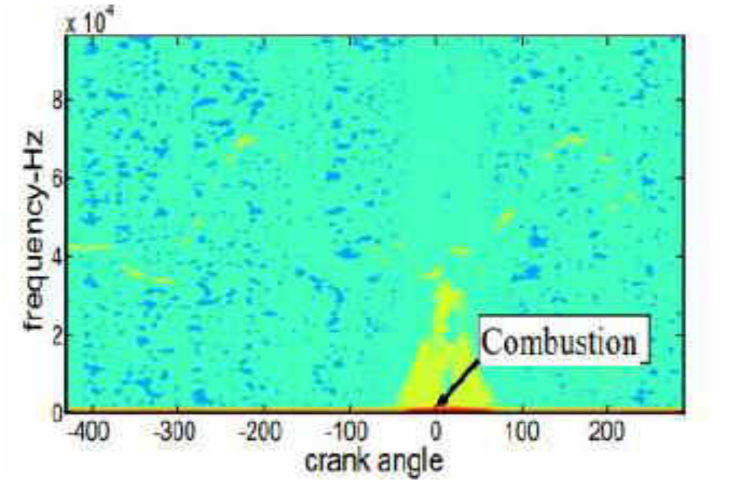

Fig. 24. Coherence signals (Case 3)

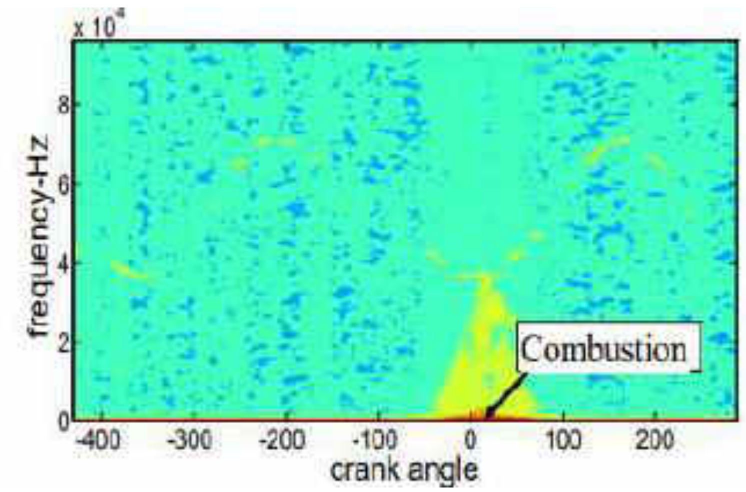

Fig. 25. Coherence signals (Case 4)

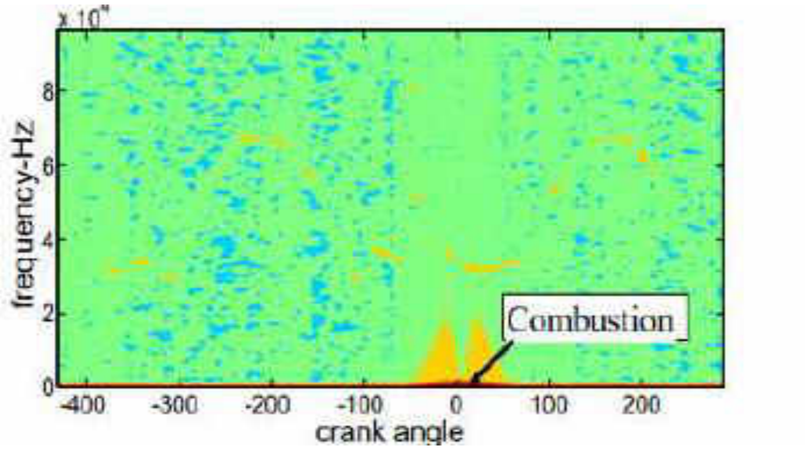

Fig. 26. Coherence signals (Case 5)

5. Conclusions

The work in this paper investigates the scope of use of block vibration signals as a means of condition monitoring of combustion process. Power spectral density plots showed the distribution of energy of various signals. Coherence analysis was used to define a frequency range in which cylinder pressure signals have strong relationship with engine block vibrations. The results have shown that accelerometer signals along vertical direction are most sensitive towards combustion process. The results showed minimum variations with change in the engine operational conditions, which demonstrate the suitability of engine block vibration for condition monitoring of engines.

References

[1] Grujic, I., N. Stojanovic, R. Pesic, A. Davinic, and S. Narayan. "Numerical analysis of IC engine operation with high pressure hydrogen injections." *Transactions of FAMENA* 44, no. 1 (2020): 55-56.
[2] Mahroogi, Faisal O, and S. Narayan. "A recent review of hybrid automotive systems in Gulf Corporation Council region." Proceedings of Institute of Mechanical Engineers Part D: Journal of Automotive Engineering 233, no. 14 (2019): 3579-3587, DOI: 10.1177/0954407019836055.
[3] Narayan, Sunny, and Vipul Gupta. "Numerical Analysis of Secondary Motion of Piston Skirt in Engines." *International Journal of Acoustics and Vibrations* 23, no. 4 (2018): 557-565.
[4] Narayan, Sunny. "A review of diesel engine acoustics." *FME Transactions* 42, no. 2 (2014): 150-154, DOI:10.5937/fmet1402150N.
[5] Narayan, S., Sasa Milojevic, and Vipul Gupta. "Combustion monitoring in engines using accelerometer signals." *Journal of Vibroengineering* 21, no. 6 (2019): 1552-1563.
[6] Mahroogi, Faisal O, S. Narayan, and Vipul Gupta. "Acoustic transfer function in gasoline engines." International Journal of Vehicle Noise and Vibration (IJVNV) 14, no. 3 (2018): 270-280
[7] Narayan, S. "Wavelet analysis of diesel engine noise." *Journal of Engineering and Applied Sciences* 8, no. 8 (2013): 255-259.
[8] Narayan, S. "Analysis of Piston Slap Motion." *International Journal of Applied Mechanics and Engineering (IJAME)* 20, no. 2 (May 2015): 445-450, DOI: https://doi.org/10.1515/ijame-2015-0030.
[9] Narayan, Sunny. "Piston Slap Noise in engines." *International Journal of Applied Engineering Research* 8, no. 14 (2013): 1695-1700.
[10] Narayan, Sunny. "Effect of dwell time on noise radiated from diesel engine." *International Journal of Applied Engineering Research* 8, no. 11 (2013): 1339-1347.
[11] Mahroogi, Faisal O., and S. Narayan. "Effects of dampers on piston slapping motion." *International Journal of Vehicle Noise and Vibration (IJVNV)* 16, no. 1/2 (2020): 46 – 57, DOI: 10.1504/IJVNV.2020.112432.
[12] Kaisan, Muhammad Usman, Latifat Ovaiyoza Yusuf, Ibrahim Umar Ibrahim, Shitu Abubakar, and Sunny Narayan. "Effects of Propanol and Camphor Blended with Gasoline Fuel on the Performance and Emissions of a Spark Ignition Engine." *American chemical society (ACS) Omega* 5, no. 41 (2020): 26454−26462.
[13] Narayan, S., Ali Sulaiman Alsagri, and Vipul Gupta. "The design and analysis of hybrid automotive suspension system." *International Journal of Mechanical and Production Engineering Research and Development* 9, no. 4 (Aug. 2019): 637-642.

[14] Mahroogi, Faisal O., and S. Narayan. "Design and analysis of Double Wishbone suspension systems for automotive applications." *International Journal of Mechanical and Production Engineering Research and Development (IJMPERD)* 9, no. 4 (Aug. 2019): 1433–1442.
[15] Narayan S. "Analysis of noise emitted from diesel engines." *Journal of Physics: Conference Series* 662 (2015): 012018, doi:10.1088/1742-6596/662/1/012018.
[16] Mahroogi, Faisal O., and S. Narayan. "Dynamic analysis of piston secondary motion using FEM method." *Proceedings of the 26th International Congress on Sound and Vibration ICSV26*, July 7-11, 2019, Montréal, Canada, 5323-5330.
[17] Narayan, S. "Effects of Various Parameters on Piston Secondary Motion." *SAE Technical Paper* 2015-01-0709, (March 2015), DOI: https://doi.org/10.4271/2015-01-0079.
[18] Stojanovic, Nadica, Jasna Glisovic, Ivan Grujic, S. Narayan, Sasa Vasiljevic, and Bojana Boskovic. "Experimental and numerical modal analysis of brake squeal noise." *Mobility & Vehicle Mechanics* 44, no. 4 (2018): 73-85.
[19] Stojanovic, Nadica, Ivan Grujic, Jasna Glisovic, A. Alempijevic, S. Narayan, and Muhammad Usman Kaisan. "Numerical Stress Analyses of Cardan Joint for Agricultural Machinery." *Tractors and power machines* 23, no. 1-2 (December 2018): 66-70.
[20] Grujic, Ivan, Nadica Stojanovic, Jovan Dorić, Jasna Glisovic, S. Narayan, and Aleksandar Davinić. "Engine load impact on maximum value of normal force in piston mechanism." *Tractors and power machines* 23, no. 1-2 (December 2018): 10-16.

A Review of NVH Testing of Engines

Dr. **Raman SINGH**[1,*], Dr. **Sujoy NAIR**[2]

[1,2] Jammu University, Jammu Kashmir, India

* Corresponding author's e-mail address: ramanjalali4@gmail.com

Abstract: *The presented work establishes benefits of using various intrusive as well as non-intrusive methods to analyze pressure, noise and vibrations signals from a dual cylinder diesel engine. This work investigated the effects of change in various injection parameters on development of in cylinder pressure, noise emissions and engine block vibrations. Various contributing NVH sources in engines include flow noise, combustion based noise, mechanical noise, etc. Amongst these sources, the contributions due to combustion based noise and piston lateral motion are of prime importance. Hence, a major portion of this work was dedicated towards discussion of these two aspects of engine acoustics.*

Keywords: *Noise, vibro acoustic*

1. Introduction

Diesel engines constitute a major source of power for various ships, buses, trains as well as road machinery. About one fifth of the total energy consumption in U.S.A. goes towards operating these engines [1], and hence demand for these engines is growing fast as compared to gasoline engines [2]. Sales of vehicles using diesel engines reached peak during the decade of 1980′s in U.S.A. due to major oil crises as depicted in figure no 1 [1].

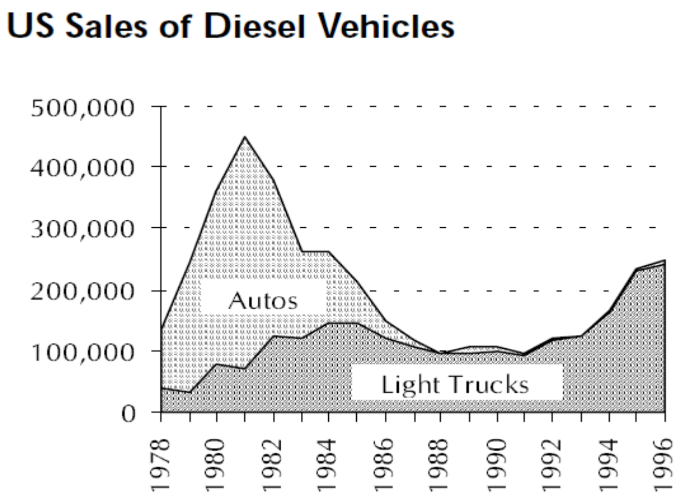

Fig. 1. Trends in sales of various diesel engine based automobiles in U.S.A.

Various projections at that time had predicted that an increase of about 20% in sales would be achieved at the end of decade [3]. However, due to variations in the fuel costs, falling prices of petrol and various problems associated with operations of diesel engines led to fall in their overall sales [4, 5].

Gasoline engines use spark ignition system for initiation of fuel reaction when compared with diesel engines (which are based on the compression ignition of fuel-air mixture). Diesel engines operate at higher compression ratios, thus allowing more useful work output during course of their operation. Combustion in these type of engines can be made to take place away from chamber walls, thus helping in reduction of overall heat release rate. In addition, there are various throttling as well as pumping losses associated with operation of petrol engines. These are some of the major reasons for their lesser cycle efficiency when compared with diesel engines. Overall fuel efficiency of a diesel engine may pass over 40% in case of medium sized engines and 50% for larger ones (which are generally used in marine propulsions) [6].

The above-discussed factors have hence led to renewal of interest of various automotive companies towards development of diesel engines. Sales data of diesel engines based automobiles in Europe have indicated that about a quarter of new automobiles were powered using these engines [7, 8]. In France, diesel engines accounted for almost half of total engine sales [9]. Sales of diesel engine based cars in Japan have almost tripled in past [10]. Several commercial vehicle suppliers have now started to manufacture their own diesel engines. Table no 1 shows the market share of diesel engines supplied by various automotive manufacturers in U.S.A.

Table 1: Supply of diesel engines by various manufacturer, Year-2013 [11]

Automotive Make	Engine Make	Market Share
Hino	Hino	100%
Freightliner	Cummins	62.3%
	Detroit Diesel	37.0%
	Mercedes Benz	0.7%
International	Cummins	7.2%
	Navistar	92.8%
Volvo	Cummins	13.6%
	Volvo	86.4%
Western Star	Cummins	21.2%
	Detroit Diesel	78.8%
Mack	Cummins	6.0%
	Mack	94.0%
Peterbilt	Cummins	65.2%
	PACCAR	34.8%

Recently several key technologies like direct injection (D.I.) systems, recirculation of exhaust gas as well as turbocharging are being introduced for further development of diesel engines [12]. Other methods include use of pre-mixed and homogenous charge compression ignitions systems [13-15]. However, higher period of pre-mixed combustion in these methods may lead to higher noise emissions from engines. Hence, various merits of using a diesel engine may be lost over their poor performance over various noise, vibration and harness benchmarks.

2. Summary of various sources of noise in combustion engines

Vehicle noise and vibrations can have a bad effect on overall performance of automobiles. These aspects also form important benchmarks for perception of customers while choosing a vehicle as parameters of comfort levels and vehicle reliability. In automotive collective term of noise, vibration and harness (NVH) is used to indicate the unwanted sounds and vibrations [16]. NVH is a term commonly used for the branch of engineering related to vehicle refinement in terms of sound and vibration performance as experienced by its occupants. A layout of vehicle consists of several units which includes chassis, power train, heating, ventilation and air conditioning systems (HVAC) as well as various electronics systems [17].

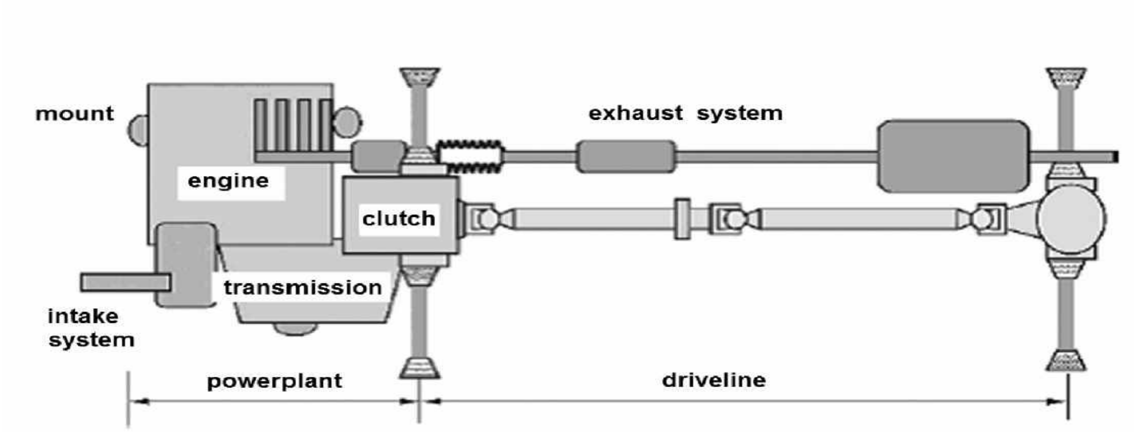

Fig. 2. Powertrain system

Figure no 2 depicts powertrain showing an engine block, transmission systems, clutch, driving systems as well as intake and exhaust systems.

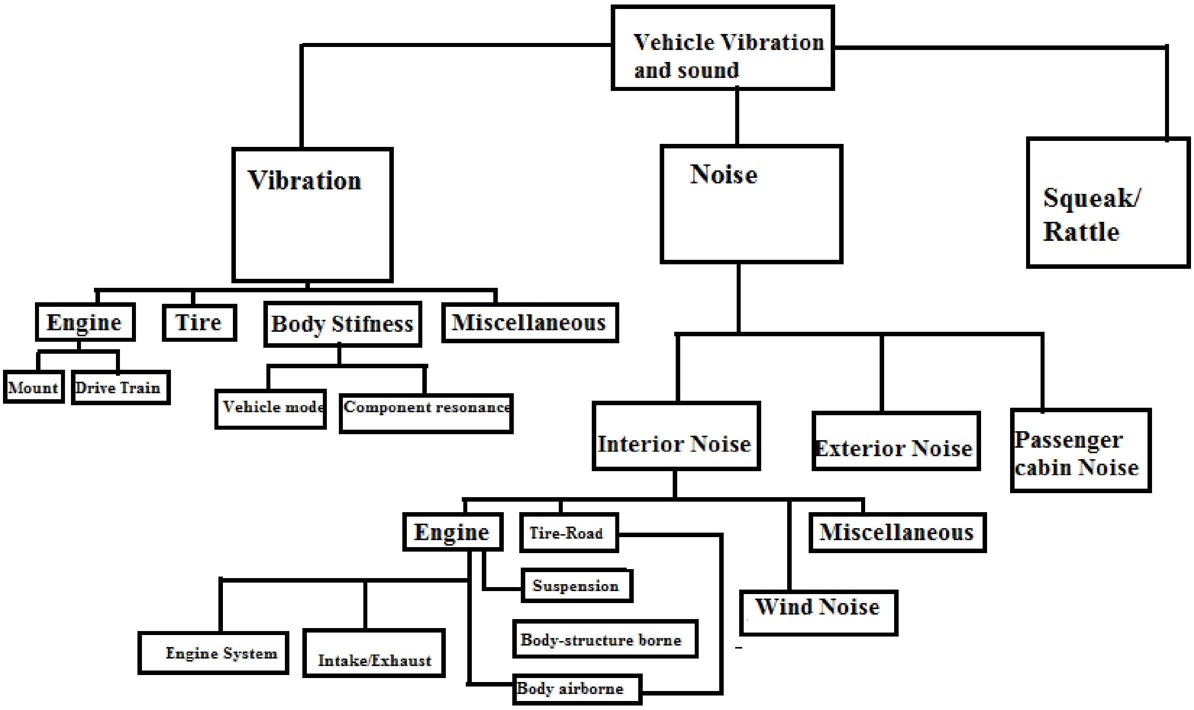

Fig. 3. Noise and vibration sources in an engine

Various sources of vibrations in an automobile may be further classified as external or internal one as depicted in figure no 3. The internal sources are due to variable pressure acting on piston head as well as inertia of various moving parts. The external ones refer to vibrations due to unbalanced moments and variable engine torque. Further various sources of noise in an engine may be classified as motion dependent noise, combustion based noise and aerodynamic noise etc. as shown in figure no 4 [18].

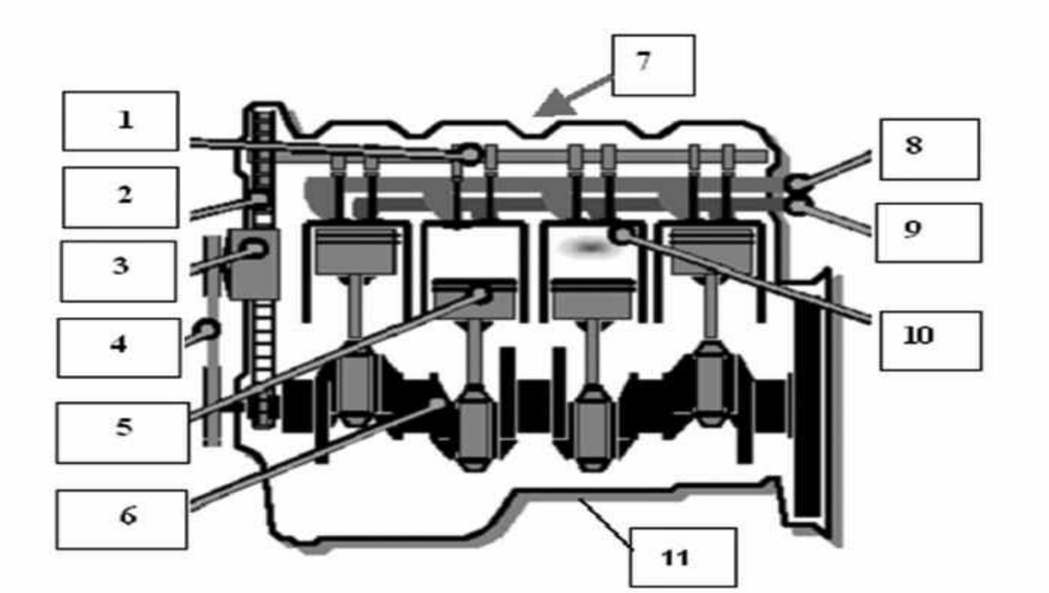

Fig. 4. Schematic representation of various sources of noise (1:valve train, 2:chain drive, 3-4:acessory noise, 5:piston slap, 6:bearing noise, 7:cover noise, 8:intake noise, 9:exhuast noise,10:combustion noise,11:oil pan noise)

Combustion based noise can be analyzed by monitoring the speed of combustion process taking place inside combustion chambers, crank angle positions corresponding to 50% mass fraction burnt (CA50), 100% mass fraction burnt (CA100), location and amplitude of maximum in cylinder pressure developed (P_{max}) and maximum value of its derivative $(\frac{dP}{d\phi})_{max}$.

Combustion based noise is generated as an impulsive pressure wave due to combustion process impacts on the wall of liner and piston head [19]. The intensity of this noise is proportional to the square of in cylinder pressure developed. This noise can be further classified as direct or indirect type [20]. Direct one is related to the development of in cylinder pressure, whereas the indirect part refers to portion that is transferred to structure from the combustion chamber.
Motion based noise which is proportional to operational speed of engine arises due to relative motion of parts or various inertial forces resulting in impacts. This includes noise due to piston motion, bearing noise, cam noise, oil pump noise, timing belt and chain noise as well as structural noise of cover [20]. This type of noise can be estimated by running engine under motored condition assuming that other components such as flow-based noise are neglected.

Aerodynamic noise includes contributions due to intake noise, exhaust noise and noise due to motion of fan. Various vibrations due to transmissions and driveline also contribute separately. There are also other noise sources, which include squeak and rattle of engine body system. Noise levels experienced by passengers inside the vehicle are not only dependent on various sources but also on the engine structure and acoustic transfer functions. Various sources have typical frequency ranges as shown in table no 2 [20]. Wind and road tire noise lie in the medium frequency ranges [20].
Range of various frequencies not only depends upon operational conditions, but also on the configurations of engines. Hence, identification and estimation of specific frequency must be done by proper testing procedure. By comparison of fundamental frequency and harmonics of individual noise sources, contributions of each source can be estimated. A typical beak up of contributions from various engine surfaces for a V6 engine using this technique is shown in table no 3 [22].

Table 2: Frequency ranges of various noise sources

Noise source	Approximate frequency range	Effecting factor
Combustion Noise	500-8000Hz	In cylinder pressure
Piston Slap	2000-8000Hz	Speed, piston design
Valve Operation	500-2000Hz	Valve type ,Engine speed
Fan Noise	200-2000Hz	Speed, number of Blades
Intake Flow Noise	50-5000Hz	Turbulence
Exhaust Flow Noise	50-5000Hz	Turbulence
Injection Pump Operation	2000Hz	Pump features
Gear Noise	4000Hz	Speed, Number of teeth
Accessory Belt-Chain Noise	3000Hz	Engine speed, misalignment, number of teeth

Table 3: Noise analysis from a V6 engine

Part	dB Sound Pressure Levels
Engine Block	78.7
Cylinder Head	76
Crank Case	79
Engine Base	78
Intake Manifold	77
Cam Cover	78
Front Cover	77
Exhaust Manifold	74
Oil Pan	73

Its effects can lead to temporary or permanent hearing damage and can impair workers' efficiency. Individuals suffering from poor hearing, whether it is due to their age or illness, can have their problems made worse by exposure to higher levels of noise at work. It can also lead to accidents due to limited speech communication, misunderstanding oral instructions and masking the sounds of approaching danger or warnings.

References

[1] Kaisan, Muhammad Usman, Latifat Ovaiyoza Yusuf, Ibrahim Umar Ibrahim, Shitu Abubakar, and Sunny Narayan. "Effects of Propanol and Camphor Blended with Gasoline Fuel on the Performance and Emissions of a Spark Ignition Engine." *American chemical society (ACS) Omega* 5, no. 41 (2020): 26454−26462.
[2] Grujic, I., N. Stojanovic, R. Pesic, A. Davinic, and S. Narayan. "Numerical analysis of IC engine operation with high pressure hydrogen injections." *Transactions of FAMENA* 44, no. 1 (2020): 55-56.
[3] Mahroogi, Faisal O, and S. Narayan. "A recent review of hybrid automotive systems in Gulf Corporation Council region." Proceedings of Institute of Mechanical Engineers Part D: Journal of Automotive Engineering 233, no. 14 (2019): 3579-3587, DOI: 10.1177/0954407019836055..
[4] Abubakar, S., F.O. Anafi, M.U. Kaisan, S. Narayan, S. Umar, and U.A. Umar. "Comparative analyses of experimental and simulated performance of a mixed-mode solar dryer." *Proceedings of Institution of Mechanical Engineers, Part C: Journal of Mechanical Engineering Science* 234, no. 7 (2020): 1393-1402.
[5] Kaisan, M.U., S. Abubakar, B. Ashok, Dhinesh Balasubramanian, S. Narayan, Ivan Grujic, and Nadica Stojanovic. "Comparative analyses of biodiesel produced from jatropha and neem seed oil using a gas

chromatography–mass spectroscopy technique." *Biofuels* 12, no. 7 (2021): 757-768, DOI: 10.1080/17597269.2018.1537206.

[6] Narayan, Sunny, and Vipul Gupta. "Numerical Analysis of Secondary Motion of Piston Skirt in Engines." *International Journal of Acoustics and Vibrations* 23, no. 4 (2018): 557-565.

[7] Narayan, Sunny. "A review of diesel engine acoustics." *FME Transactions* 42, no. 2 (2014): 150-154, DOI:10.5937/fmet1402150N.

[8] Narayan, S., Sasa Milojevic, and Vipul Gupta. "Combustion monitoring in engines using accelerometer signals." *Journal of Vibroengineering* 21, no. 6 (2019): 1552-1563.

[9] Mahroogi, Faisal O, S. Narayan, and Vipul Gupta. "Acoustic transfer function in gasoline engines." *International Journal of Vehicle Noise and Vibration (IJVNV)* 14, no. 3 (2018): 270-280.

[10] Narayan, S. "Wavelet analysis of diesel engine noise." *Journal of Engineering and Applied Sciences* 8, no. 8 (2013): 255-259.

[11] Narayan, S. "Analysis of Piston Slap Motion." *International Journal of Applied Mechanics and Engineering (IJAME)* 20, no. 2 (May 2015): 445-450, DOI: https://doi.org/10.1515/ijame-2015-0030.

[12] Narayan, Sunny. "Piston Slap Noise in engines." *International Journal of Applied Engineering Research* 8, no. 14 (2013): 1695-1700.

[13] Narayan, Sunny. "Effect of dwell time on noise radiated from diesel engine." *International Journal of Applied Engineering Research* 8, no. 11 (2013): 1339-1347.

[14] Kaisan, Muhammad Usman, Shitu Abubakar, Muhammed Mustapha M, and S. Narayan. "Determination of Wear Metals Debris Concentration in Aircraft Engines." *International Journal of Recent Technology and Engineering (IJRTE)* 8, no.2 (2019):1289-1292, DOI: 10.35940/ijrte.B1917.078219.

[15] Narayan, S., Ali Sulaiman Alsagri, and Vipul Gupta. "The design and analysis of hybrid automotive suspension system." *International Journal of Mechanical and Production Engineering Research and Development (IJMPERD)* 9, no. 4 (Aug. 2019): 637-642.

[16] Mahroogi, Faisal O., and S. Narayan. "Design and analysis of Double Wishbone suspension systems for automotive applications." *International Journal of Mechanical and Production Engineering Research and Development (IJMPERD)* 9, no. 4 (Aug. 2019): 1433–1442.

[17] Stojanovic, Nadica, Nouby M. Ghazaly, Ivan Grujić, Jasna Glišović, and Sunny Narayan. "Influence of Size of Ventilated Brake Disc's Ribs on Air Flow Velocity." *International Journal of Advanced Science and Technology* (*IJAST)* 29, no.1 (2020): 637-647.

[18] Mahroogi, Faisal O., and S. Narayan. "Effects of dampers on piston slapping motion." International Journal of Vehicle Noise and Vibration (IJVNV) 16, no. 1/2 (2020): 46 – 57, DOI: 10.1504/IJVNV.2020.112432.

[19] Narayan, S., and Vipul Gupta. "Numerical Model of Combustion Noise generation in Combustion Engines." *International Journal of Advanced Science and Technology (IJAST)* 29, no. 5 (2020): 8852-8858.

[20] Narayan, S., and V. Gupta. "Frequency characteristics of in cylinder pressure of a gasoline engine." *Journal of Applied Engineering Science* 19, no.1 (2021): 92-97, DOI: https://doi.org/10.5937/jaes0-27156.

ISSN 1453 – 7303 **"HIDRAULICA" (No. 3/2021)**
Magazine *of Hydraulics, Pneumatics, Tribology, Ecology, Sensorics, Mechatronics*

Strategy for Implementation and Use of Monitoring Systems for Gear-Motors

Dipl. Eng. **Paul LĂCĂTUȘ[1],** Dipl. Eng. **Mihai IONEL[1*],**
PhD Eng. **Gabriela MATACHE[2],** Dipl. Eng. **Valentin BARBU[2]**

[1] S.C. CORNER PROD S.R.L.

[2] Hydraulics and Pneumatics Research Institute INOE 2000-IHP

* office@cornerprod.ro

Abstract: *The article describes the strategy of implementation and use of a monitoring system that specifically targets the moto reducer assemblies used in many equipment and machinery in various fields. The article presents the architecture of a monitoring system and how to achieve the system. The testing of the system on a firewood-breaking equipment made within a project developed by the company together with INOE 2000-IHP is also presented.*

Keywords: *System monitoring, moto reducer, maintenance*

1. Introduction

In recent years, the increase in the technical and technological level has had a strong impact on all branches of industry. At the same time, mass production imposed the maximum reduction of the operating costs of machinery, production lines. This is how the phrase "Maintenance free" appeared more and more frequently without maintenance, or "Low Maintenance", with low maintenance, in the marketing plan of the products. This phrase is based on the consideration of a normal period of life of a product, strict operating conditions. Real life shows us, however, that the equipment is used far beyond the normal period declared by the manufacturer and the operating conditions often exceed the limits imposed by the manufacturer and designer. This brings to the fore the maintenance of the equipment, which, however, must be done in the conditions of limiting the operating costs. It has been shown that the "fault intervention" strategy, reactive maintenance, is a particularly expensive one, especially given by the costs of equipment downtime, loss of production.
The widely used maintenance strategies are periodic, corrective maintenance and predictive maintenance. Periodic maintenance is based on maintenance schedules given by the manufacturer with periodical revisions, changes of parts and consumables. Periodic maintenance imposes important operating costs given by the downtime, the change of some subassemblies and consumables before reaching the necessary wear due to the operating conditions, or the failure of the equipment between the revision periods due to the exceeding of some technological limits in operation [1].

2. Predictive maintenance

Predictive maintenance is based especially on adapting the schedules of maintenance actions based on the real operating conditions and the real condition of the equipment in order to prevent failure and reduce both maintenance costs and costs imposed by repairing after defect of an equipment.
In order to have an efficient predictive maintenance, the essential condition is the correct monitoring of the equipment, the target both in terms of operating conditions and in terms of the state of real wear and probability of failure.
Monitoring in operation by non-invasive means is essential to obtain the statistical data necessary for a correct evaluation necessary for planning predictive maintenance.
Monitoring in operation requires the reading of some operating and operating parameters continuously with an acquisition rate that is relevant for the tracking wear phenomena.

3. Monitoring a moto reducer

The monitoring of a moto reducer is done throughout its life in order to verify the operating conditions, to estimate the usages and the life span, to replace the worn elements, in order to preserve the characteristics necessary for the good functioning. After mounting the moto reducer in the installation, the alignment of the axes, noise and vibration of the system are checked. Both before and after the run-in (where necessary), the most important parameters are checked in the void and in the load, namely the working temperature and the absorbed currents that correspond to a certain moment necessary for the application. These measured initial parameters allow us to report the values measured later to the initial values and to detect wear and tear of certain components, aging or oil leakage, decommissioning of auxiliary equipment such as forced ventilation, cooling installations, accidental loads, etc. [1].
The reducers contain gears that undergo wear over time; wearing and tearing are influenced by the number of cycles, speed, and operating temperature, type of lubricant, the number of starts-stops and the number of changes in direction. If the wear of the cemented gears is hardly noticeable, at the molten gears the wear is more pronounced and can be checked by checking the clearance.
The gears are mounted in the housing together with their axes on the bearings. Bearings also suffer wear and tear that are depending on the number of cycles, speed, applied forces, their position relative to the oil bath, the lubricant used, and the lubrication mode of the bearing.
Lubrication of gears and bearings is made depending on the type of gear, gauge and shape of the reducer, mounting position. The oil is also subject to wear and is influenced primarily by the working temperature and the maximum working temperature [2].
Periodic checking of the seals is then required. Seals on moving axles are the most exposed to wear and depend on the spindle speed at the contact points, the type of lubrication and the quality of the lubricant, the temperature and working conditions (dust, aggressive environments, sun).
It is checked the mounting of the motor on the reducer, the correct tightening of the screws, the wear of the input shaft and the wedges, the absence of abnormal vibrations and noises, the output shaft from the reducer and the alignment with the driven machine.
In the motor, the absorbed current is measured on each phase and checked with the one listed on the engine label but also with the one initially measured when the empty and load tests were made and the operating temperature is measured and checked compared to the initially measured temperature.
Two parameters are those that monitor the moto reducer behavior very well: the effective power and the working temperature. Sharp changes in them are signs of wear and tear of the engine. Parallel interpretation of the power and temperature measured over a long period of time can create a model for determining the type of wear existing in the gear motor.
Classic monitoring is done (visual – monthly), oil change (if applicable) between 3000 and 10000 hours of operation. Next, we propose a monitoring system with the recording of the electrical parameters for the motor and the temperature at several points of the reducing motor assembly.

4. Architecture of the monitoring system

The monitoring systems in operation are based on an architecture with distinct layers of data acquisition and processing taken from the target equipment. The system uses a set of sensors that take information from the system in operation, archive the acquire data in a database from where it is read and processed in order to obtain high-level data useful in maintenance and production management.
The arch must be open, scalable, and capable of being expanded with new sensors, new recorded sizes and new processing modes for finding top-level data relevant to the state of operation and use of the system under control. The architecture is structured on several functional levels that cover specific functionalities within the monitoring system.
The architecture of the system has three main levels:

1. Sensor system
2. Communication network
3. Data processing module

5. Levels

5. 1 Sensor system

The sensors transform the monitored specific sizes into electrical signals that can be taken further for monitoring.
The sensors used in this application are sensors with WiFi communication produced by Shelly Cloud Bulgaria. The sensors used are intelligent sensors based on SoC microcontrollers, system on a chip, from express if's ESP8266 family. These sensors run an application that allows them to have a WEB interface for configuration and monitoring. ESP8266 systems have also implemented a TCP/IP stack and hardware needed to connect to a Wifi network in the 2.4 GHz band [3], [4]. At this level of system development, two types of electrical and temperature sensors are used.

1. **Electrical sensors**

The electrical sensor is Shelly 3EM that allows measuring the voltage in the three-phase supply network of the motor as well as the current consumed by each phase. For reading the current, current transformers are used transducers capable of correct measurement up to 120 A.

The sensor acquires all six of these vector sizes with a cadence of two measurements per minute. All the sensor makes the necessary calculations to indicate the power consumed on each phase and the power factor. It is also possible an accumulation to indicate an energy used over a certain period of time.

2. **Thermal sensors**

The thermal sensor is Shelly 1 with temperature measuring mode that allows the acquisition of three temperatures, in three points with semiconductor sensors of type 18S20 in cases with IP67 degree of protection. Temperatures are read with a cadence of one measurement per minute.

3. **Other types of sensors**

The system is open and can take signals from other types of sensors as long as they can communicate in the WiFi network with an open API or on one other of the protocols supported in the system.

5. 2 Communication network

The communication network used in the application is a local WiFi network, used only by the application components.
Communication is done in TCP/IP network protocol. Over the TCP/IP protocol, the sensors communicate with the upper level through the MQTT open protocol. MQTT is a publish/subscribe protocol in which a data source, a sensor in our case publishes information to an MQTT Broker. The MQTT broker is a software that records all data sources, receives the information sent by the data sources and publishes it to all destinations that have subscribed to a particular topic. The MQTT protocol is in agnostic protocol to the content, thus being able to transmit various types of information organized only on data topics. All components of the monitoring system connect to a local network that ensures communication between them.
The local LAN network is controlled by the microtik Hap Lite RB941 Access Point router that ensures the management of network functions:

1. Authentication of clients in the WiFi network
2. Automatic allocation of addresses in the local network through DHCP protocol
3. Network Address Translation function to be able to connect the local network to the internet
4. Firewall function to protect the internal network from attacks from the Internet
5. Port forwarding function to make available resources from the local network to the Internet to allow access to data collected and processed by the system from the Internet

All sensors connect to the WiFi network and automatically receive IP addresses from the Microtik router [5].

5. 3 Data processing module

The data processing module is implemented with a SoB, raspberry pi 4 on board system with 4GB of RAM that provides all the necessary functions for the application:

1. Data collection
2. Storage
3. Data processing.

On the Raspberry Pi runs the Raspbian operating system along with the applications necessary to ensure the above functions. In order to ensure easy replication of the system, a solution was chosen to use docker containers with the necessary applications. Under these conditions, only a compose file for the Docker Compose applications required to replicate the application. The compose file that was written specifically for this application has the YAML format. It allows downloading from the internet the necessary Docker containers and linking them to ensure the operation of the application.
The management of the installed containers can be done through the web interface of the Portainer-CE application.
The use of containers for the various applications necessary for the monitoring system was made in the idea of an easier replication process of such systems and the generation of systems adapted in more detail to the requirements of various applications of the end users.

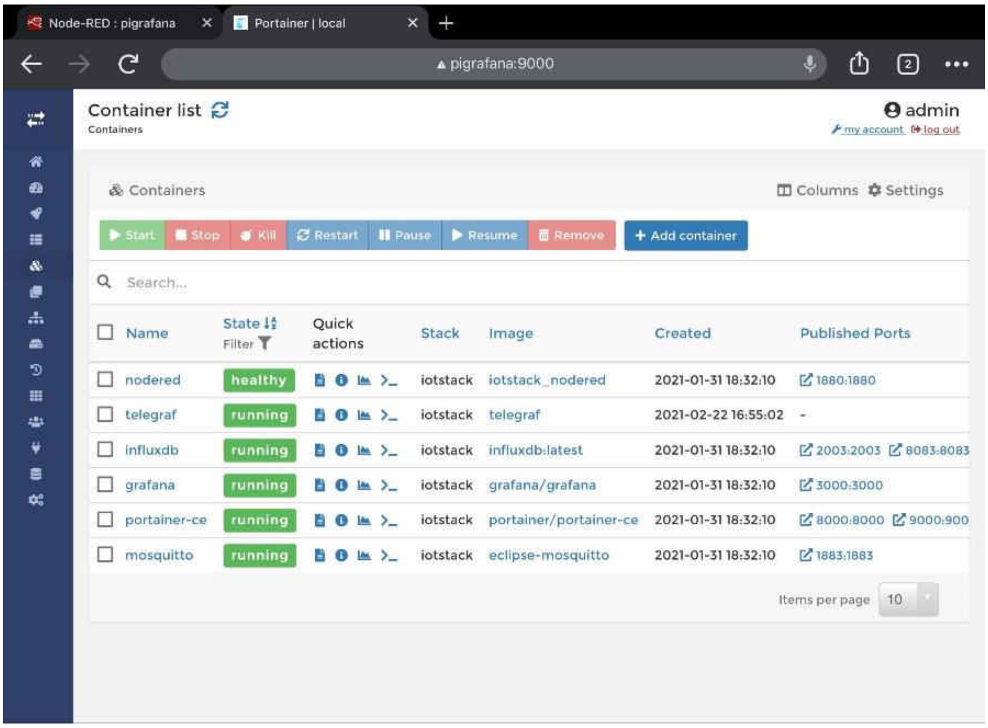

Fig. 1. Application with web interface for container management Portainer CE

5.3.1 Data collection operation

The data collection function allows retrieving data from sensors with the cadence of one measurement per minute. Each sensor is programmed to transmit once a minute the data measured by MQTT protocol.
In order to use the MQTT protocol, it is necessary to use a Broker that takes the data published by the sensors and transmits it to the applications that have subscribed for receiving the data in question. The MQTT broker is provided by the open source Mosquitto application that runs in a Docker container [6].

Within the data collection function is also the node-red opensource application that allows the graphic realization and running of NodeJS applications. The function of the Node Red module is to connect to the MQTT Broker and process the primary data received from the sensors in order to be stored in a database in a unitary way.

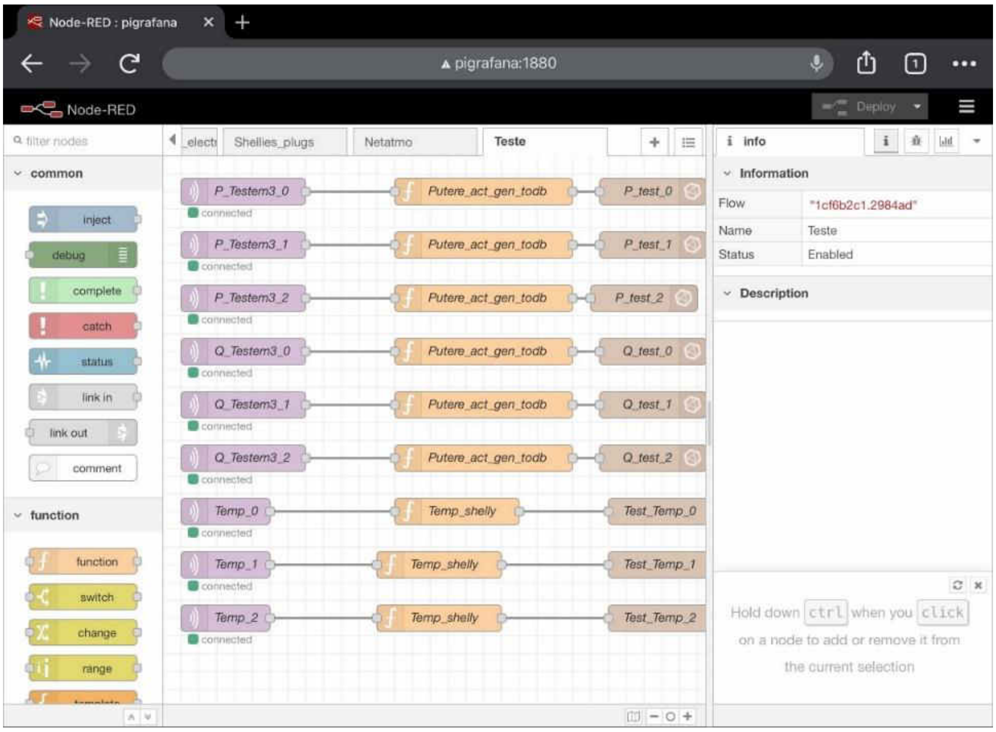

Fig. 2. Node-Red graphics application

5.3.2. Storage function

The storage function is provided by a temporal database of type InfluxDB that retrieves the data processed primary by the Node-Red module to apply it a timestamp and stores it. InfluxDB also runs in a Docker container and stores the data on the 64GB SD card in the Raspberry Pi. The InfluxDB database is of the opensource type with a high similarity with SQL databases.

5.3.3. Data processing function

Most of the data processing function is provided by the opensource Grafana application. Grafana is connected to the InfluxDB database, retrieves the data and displays it based on "dashboard" programmed specifically for this application in public web pages. The Grafana app can be programmed to give warnings and alarms when exceeding certain thresholds specified for the measured data.

The data in the InfluxDB database can be processed through specific mediation functions, maximum memorization.

Grafana was scheduled in this case to determine certain abnormal cases such as:

1. Exceeding the phase current absorbed by the motor
2. Uneven current consumption in motor phases
3. Uneven voltages applied to the engine
4. Exceeding normal operating temperatures at various points of the main motor assembly.

The values of the alarm thresholds can be easily modified depending on the specific requirements of the use of the motor [7], [8].

The alarms are stored by Grafana and are sent in various ways to a user designated to evaluate the system's operation. In our case, notifications are sent by e-mail and through the Telegram instant messaging system using a so-called BOT, a message transmission robot. These alarms, alerts can be received on any portable device running a Telegram client or email.

6. System realization

The monitoring system is made in two separate boxes with a sufficient degree of protection for placement within the monitored application.

6.1 Monitoring module

The monitoring module is placed near the monitored conductive motor assembly, and the connection of the motor is made through it to take over the current voltage electric parts necessary for the analysis.

Fig. 3. Monitoring module

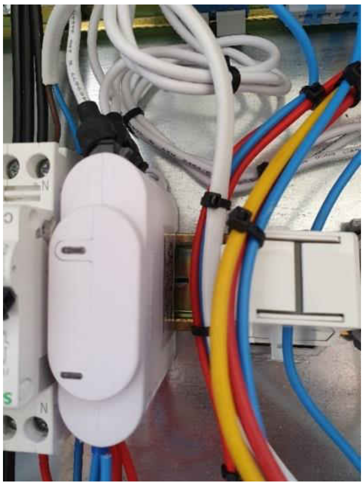

Fig. 4. Electrical size transducer

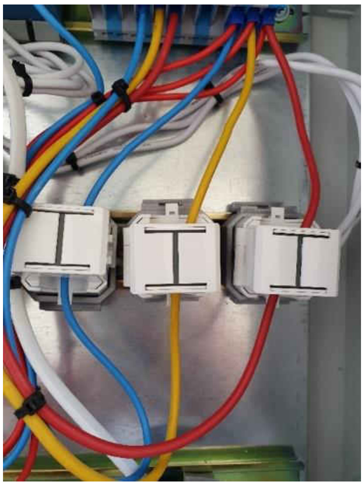

Fig. 5. Current transformers 120A

For the acquisition of temperatures, a device is used that reads OneWire sensors and transmits the readings also read via WiFi to the control module.

Fig. 6. Temperature transducer

Fig. 7. OneWire IP67 temperature sensor

6.2 Control module

In the control module take place the recording, processing, primary analysis of the data measured and stored in the database.

Fig. 8. Control module

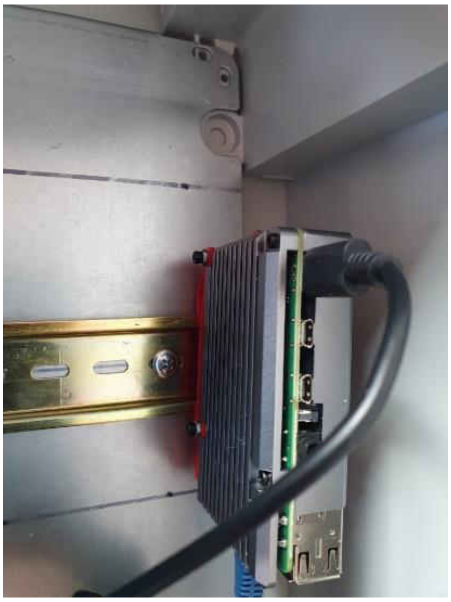

Fig. 9. The Processing Computer Raspbarry Pi 4

The continuous control module the router that ensures Wifi communication with the rest of the monitoring modules and the Single Board Computer of Raspberry Pi 4 type that stores the data and processes it according to the processing levels described above.

7. System testing

The testing was done in this case on a moto reducer assembly with a 2.5 Kw motor and a molten reducer. The electrical sizes and temperatures at various engine charges were read. The data was acquired in the control module and was displayed in the panels generated by Grafana [9].

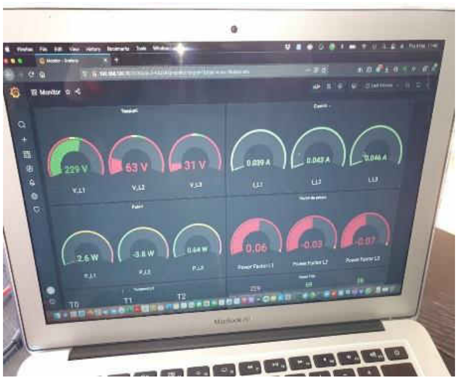

Fig. 10*.* Tested system

Fig. 11. Tests and measurements

Fig. 12. Measurements of current, voltage, powers, power factor

Fig. 13. Various data display panels

8. Conclusions

The monitoring system allows the acquisition and recording of the main electrical parameters and temperatures from a main motor assembly, their storage in a temporal database and their graphic display at the same time with the alarm of exceeding some predetermined values.

Acknowledgments

This paper has been developed as part of a project co-financed by the European Union through the European Regional Development Fund, under Competitiveness Operational Programme 2014- 2020, Priority Axis 1: Research, technological development and innovation (R&D&I) to support economic competitiveness and business development, Action 1.2.3 – Partnerships for knowledge transfer, project title: *Eco-innovative technologies for recovery of biomass wastes*, project acronym: ECOVALDES, SMIS code: 105693-594, Financial agreement no. 129/23.09.2016.

References

[1] Bucșa, Ioan, and Nicolae Cristofor. *The technician's guide for the design of machinery and equipment /Îndrumătorul tehnicianului proiectant de mașini și utilaje*. Bucharest, Technical Publishing House, 1967.
[2] Georgescu, G.S. *Guide for mechanical workshops /Îndrumător pentru ateliere mecanice*. Bucharest, Technical Publishing House, 1978.
[3] http://www.screwlogsplitter.com.
[4] https://woodsplitterplans.com.
[5] https://www.youtube.com/watch?v=W66YcaJfqhI. "DR RapidFire Splitter at work".
[6] https://www.loaderplans.com/log-splitter.
[7] https://wematik.de.
[8] https://logsplitterplans.com.
[9] http://dirtyhandtools.com.

A Review of Structural Attenuation in Combustion Engines

Dr. **S. NARAYAN**[1*], Dr. **Raman SINGH**[2]

[1] Qassim University, Saudi Arabia

[2] Jammu University, Jammu Kashmir, India

* rarekv@gmail.com

Abstract: *The rate of pressure (which mainly depends on the ignition delay period) and quantities of combustion gas formed during this period are a key parameter to analyze combustion-based noise. A shorter delay period means lesser amount of combustible gas formed and hence lesser combustion noise. Hence, delay period must be reduced as much as possible for effective reduction of combustion noise. Structure and layout of engine also plays a significant role. There are many approaches to control combustion noise. One of these includes reducing cylinder pressure spectrum typically in middle and high frequency ranges. Other include reducing ignition delay period or number of combustible gases formed during this period. Increasing the stiffness of parts, use of turbo charging process and use of split injection methods have also proved to be other effective methods*.
Increase in the compression ratio and chamber temperature may shorten this delay period. However, an increase in compression ratio can cause a rise in noise due to slapping motion of skirt. Various parameters of fuel injection system like instance of fuel injection, injection pressure, number of nozzles and fuel supply rate also affect the combustion noise. Increasing the pressure of injection or engine speed leads to an increase in the amount of fuel accumulated during the delay period resulting in rise of combustion noise.

Keywords: *Engine structure, acoustics, noise control*

1. Introduction

A technique to quantify combustion-based noise has been proposed by [1]. The combustion-based noise was most dominant in frequency range of 800Hz- 4kHz [2]. Acoustic measurements of noise outside the engine may be used for combustion noise analysis only when the engine is operated in such a way that contribution of combustion events towards the noise emissions becomes predominant. This can be achieved either by either advancing injection timing or by changing Cetane number of fuel. Alkyl blended fuel were used to maximize in cylinder pressure so that combustion noise becomes dominant [1].
Structural attenuation of engine structure also plays a vital role in determination of combustion-based noise. Values of structure response functions was found to fall by about 10dBA in 500Hz - 5kHz frequency range [1]. More recently, AVL has developed a noise meter which is based on analysis of engine indicator diagram [3]. Good correlation was observed when data from this noise meter was compared with results obtained from computer programming. Figure no 1 shows structural response functions of a group of 9 engines as recorded by an AVL noise meter [1]. The response of direct injection high-speed diesel engines falls by 12dB over 5kHz frequency range [1]. Further Shu was able to predicted this transfer function by setting an explosive charge inside cylinder which was locked at fixed crank angle position as seen from figure no 2 [4]. Different functions for various designs of combustion chambers and different amounts of explosion charges have also been compared in his work.
All the methods discussed above use expensive and time-consuming methodologies to analyze the transfer function of combustion noise, consequently an alternative method of analysis has been analyzed which involves use of Cepstrum analysis.
Cepstrum analysis is an important method of signal processing which has wide applications in source separation [5]. Psychoacoustic analysis of noise emissions from a S.I. engine has been carried out using Cepstrum analysis [6]. This methodology has also proved effective for cylinder pressure reconstruction [43], fault detection in gears [7] and condition monitoring of engines [8].

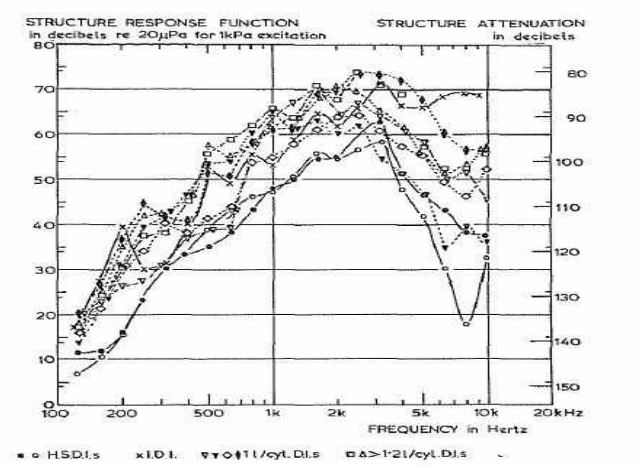

Fig. 1. AVL structural response function and structural attenuation

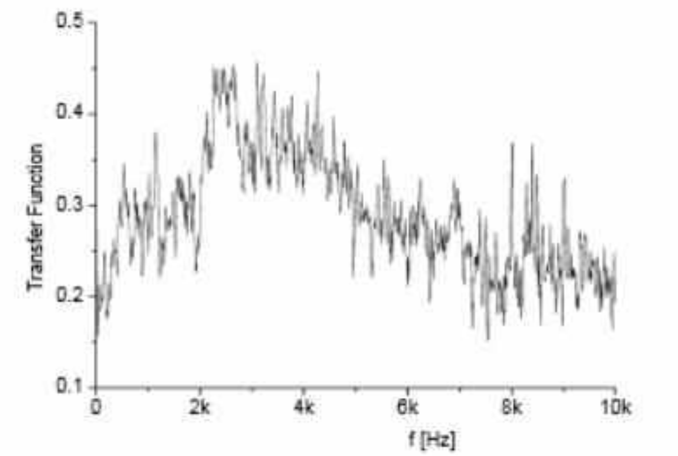

Fig. 2. Transfer function obtained by explosive charge

Mathematically Cepstrum can be defined as inverse spectrum of logarithmic power spectrum [9-20], i.e.

$$C_a(q) = |IFFT[\log[G_x(f)]]| \tag{1}$$

Where q is frequency in milliseconds & G_x denotes the Fourier transformation of function.
Since auto power spectrum density function is even, both its inverse Fourier transformations & Fourier transformations are equal. i.e.

$$C_x(q) = |FFT[\log [G_x(f)]]| = IFFT[\log [G_x(f)]] \tag{2}$$

As a noise source x(t) reaches a measuring point as an output signal y(t) after passing through a system represented by h(t), the information may be expressed by following equation:

$$y(t) = x(t).h(t) = \int x(\tau)h(t-\tau)dt \tag{3}$$

Taking Fourier transformation, we have:

$$G_y(f) = G_x(f) * G_h(f) \tag{4}$$

Further, taking logarithm and Fourier transformations on both sides this equation gets modified as:

$$\log(G_y(f)) = \log(G_x(f)) + \log(G_h(f)) \tag{5}$$

$$FFT[\log(G_y(f))] = F[FT\log(G_x(f))] + FFT[\log(G_h(f))] \tag{6}$$

Or

$$IFFT[\log(G_y(f))]=IFFT[\log(G_x(f))]+IFFT[\log(G_h(f))] \tag{7}$$

$$C_y(q) = C_x(q)+ C_h(q) \tag{8}$$

Structural response function for motored condition was evaluated taking noise emissions as output signal and in cylinder pressure as input. In case of firing conditions, the rate of heat release was taken as input parameter.

2. Experimental

Experiments were conducted on a KPKN2520 type, single cylinder diesel kirloskar rig having specifications as presented in table 1. Cases C was taken as reference base testing cases with fuel injected at 3600 RPM engine speed and 700 Bar injection pressure. 1mm^3/stroke of fuel was injected during pre -injection period as well as main injection period at crank angle positions 6° and 10° before top dead center positions of for this case.

Table 1: Engine specification

Type	Single cylinder DI 4 stroke diesel engine
Cooling	Air cooled
Rated power	3.75kW@1500RPM
Bore X Stroke	80mm X 110mm
Compression ratio	17.5:1

An AVL GU13P type piezoelectric transducer was used to acquire the instantaneous in-cylinder pressure data having various features enlisted in Table 2.

Table 2: Pressure transducer specifications

Range	0-200Bar
Sensitivity	15.8pC/Bar
Resonant frequency	130kHz

Various block vibrations were recorded by Endveco7240C make Mono axial accelerometers having features shown in table 3.

Table 3: Accelerometer transducer specifications

Range	0-1000g
Sensitivity	15.8pC/Bar
Resonant frequency	90kHz

A 4939 type Bruel and Kjaer free-field ¼″ make microphone having a preamplifier (type 2670) was used to acquire various noise emission signals. Main features of this transducer are shown in table 4.

Table 4: Microphone transducer specifications

Range	28-164dB
Sensitivity	4mV/Pa
Resonant frequency	4-100kHz

3. Results and discussions

Figures no 3-5 show the plots of this transfer function as obtained by Cepstrum analysis for various test case.

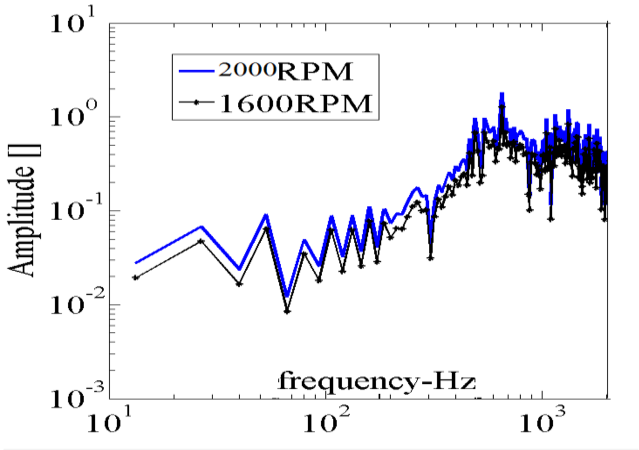

Fig. 3. Structural Attenuation Function (Motored)

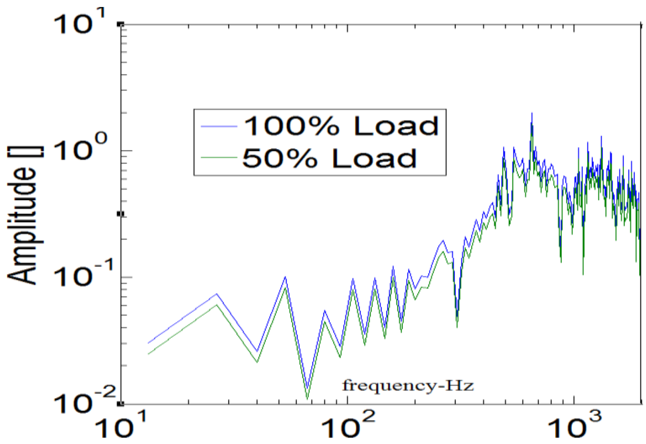

Fig. 4. Structural Attenuation Function (1600RPM)

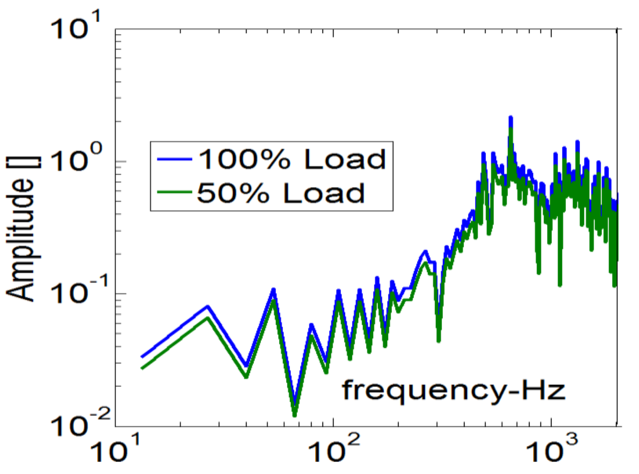

Fig. 5. Structural Attenuation Function (2000RPM)

It is clear from plots that noise transfer function for various cases showed same trends with higher values above 1kHz range. At low frequency ranges, various parts of engine have high rigidity and hence radiation efficiency is very low. In mid frequency ranges, longitude modes of vibrations in piston, connecting rod and crank shaft dominates which gradually increases the structural response of engine. In higher ranges, the radiation efficiency increases which may be attributed due to various Cast Iron parts. Several engines may use same materials for various parts; hence, various engines of different make having same size may show same variations in response function. The curves obtained by Cepstrum analysis show a significant difference in high frequency ranges above 1kHz. These variations may be attributed to differences in the designs of cylinder heads, engine block and cover, which also play a vital role.

Further neglected flow induced noise, the overall noise emissions (ON) from engine can be written as sum of direct combustion noise (CN) and motion-based noise (speed dependent), i.e.

$$ON = CN(H_1) + MN \tag{9}$$

Where H_1 is structural attenuation factor of combustion noise.
Assuming that mechanical noise levels (motored conditions) do not change significantly, the combustion noise levels for the given testing conditions were evaluated using transfer functions previously described as seen in figures no 6, 7.

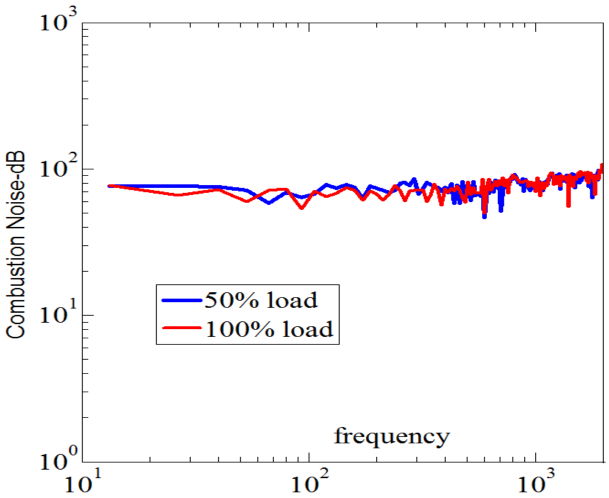

Fig. 6. Combustion noise -1600RPM

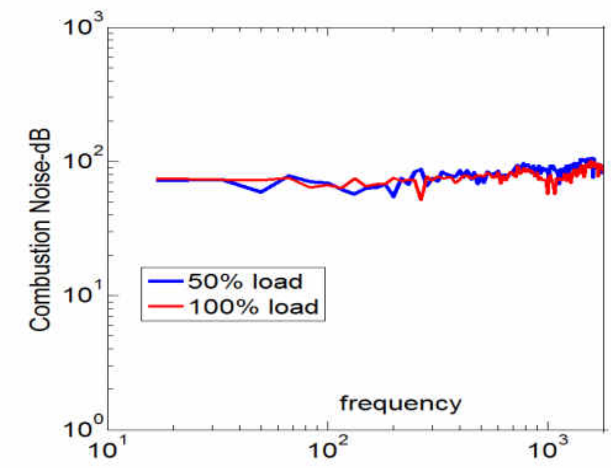

Fig. 7. Combustion noise -2000RPM

These plots are characterized by peaks in high frequency ranges which may be attributed to resonance of engine structure. Speed of engine showed no significant effects on the combustion noise levels, however increase of engine load caused a slight increase as the fuel was injected closer to TDC position and hence greater combustion noise emissions.

References

[1] Abubakar, S., F.O. Anafi, M.U. Kaisan, S. Narayan, S. Umar, and U.A. Umar. "Comparative analyses of experimental and simulated performance of a mixed-mode solar dryer." *Proceedings of Institution of Mechanical Engineers, Part C: Journal of Mechanical Engineering Science* 234, no. 7 (2020): 1393-1402.

[2] Narayan, S., Ali Sulaiman Alsagri, and Vipul Gupta. "The design and analysis of hybrid automotive suspension system." *International Journal of Mechanical and Production Engineering Research and Development (IJMPERD)* 9, no. 4 (Aug. 2019): 637-642.

[3] Mahroogi, Faisal O., and S. Narayan. "Design and analysis of Double Wishbone suspension systems for automotive applications." *International Journal of Mechanical and Production Engineering Research and Development (IJMPERD)* 9, no. 4 (Aug. 2019): 1433–1442.

[4] Grujic, I., N. Stojanovic, R. Pesic, A. Davinic, and S. Narayan. "Numerical analysis of IC engine operation with high pressure hydrogen injections." *Transactions of FAMENA* 44, no. 1 (2020): 55-56.

[5] Narayan, Sunny. "Correlation between in cylinder pressure and noise emissions from Diesel engines." *Journal of KONES Powertrain and Transport* 22, no. 1 (2015): 243-254.

[6] Narayan, Sunny, and Vipul Gupta. "Numerical Analysis of Secondary Motion of Piston Skirt in Engines." *International Journal of Acoustics and Vibrations* 23, no. 4 (2018): 557-565.

[7] Narayan, Sunny. "Piston Slap Noise in engines." *International Journal of Applied Engineering Research* 8, no. 14 (2013): 1695-1700.

[8] Narayan, S. "Analysis of Piston Slap Motion." *International Journal of Applied Mechanics and Engineering (IJAME)* 20, no. 2 (May 2015): 445-450, DOI: https://doi.org/10.1515/ijame-2015-0030.

[9] Narayan, S. "Modeling of Noise Radiated from Engines." *SAE Technical Paper* 2015-01-0107, (2015), doi:10.4271/2015-01-0107.

[10] Narayan, S., Sasa Milojevic, and Vipul Gupta. "Combustion monitoring in engines using accelerometer signals." *Journal of Vibroengineering* 21, no. 6 (2019): 1552-1563.

[11] Narayan, S. "Wavelet analysis of diesel engine noise." *Journal of Engineering and Applied Sciences* 8, no. 8 (2013): 255-259.

[12] Mahroogi, Faisal O., and S. Narayan. "Effects of dampers on piston slapping motion." *International Journal of Vehicle Noise and Vibration (IJVNV)* 16, no. 1/2 (2020): 46 – 57, DOI: 10.1504/IJVNV.2020.112432.

[13] Narayan, Sunny. "Effect of dwell time on noise radiated from diesel engine." *International Journal of Applied Engineering Research* 8, no. 11 (2013): 1339-1347.

[14] Narayan S. "Analysis of noise emitted from diesel engines." *Journal of Physics: Conference Series* 662 (2015): 012018, doi:10.1088/1742-6596/662/1/012018.

[15] Kaisan, Muhammad Usman, Latifat Ovaiyoza Yusuf, Ibrahim Umar Ibrahim, Shitu Abubakar, and Sunny Narayan. "Effects of Propanol and Camphor Blended with Gasoline Fuel on the Performance and Emissions of a Spark Ignition Engine." *American Chemical Society (ACS) Omega* 5, no. 41 (2020): 26454−26462.

[16] Kaisan, M.U., S. Abubakar, B. Ashok, Dhinesh Balasubramanian, S. Narayan, Ivan Grujic, and Nadica Stojanovic. "Comparative analyses of biodiesel produced from jatropha and neem seed oil using a gas chromatography–mass spectroscopy technique." *Biofuels* 12, no. 7 (2021): 757-768, DOI: 10.1080/17597269.2018.1537206.

[17] Mahroogi, Faisal O, and S. Narayan. "A recent review of hybrid automotive systems in Gulf Corporation Council region." *Proceedings of Institute of Mechanical Engineers Part D: Journal of Automotive Engineering* 233, no. 14 (2019): 3579-3587, DOI: 10.1177/0954407019836055.

[18] Mahroogi, Faisal O, S. Narayan, and Vipul Gupta. "Acoustic transfer function in gasoline engines." *International Journal of Vehicle Noise and Vibration (IJVNV)* 14, no. 3 (2018): 270-280.

[19] Mahroogi, Faisal O., and S. Narayan. "Dynamic analysis of piston secondary motion using FEM method." *Proceedings of the 26th International Congress on Sound and Vibration ICSV26*, July 7-11, 2019, Montréal, Canada, 5323-5330.

[20] Narayan, S. "Effects of Various Parameters on Piston Secondary Motion." *SAE Technical Paper* 2015-01-0709, (March 2015), doi:10.4271/2015-01-0079.

Program: POC 2014 - 2020, Ctr. nr. 37/ 02.09.2016, MySMIS103396-768
Crearea unui nucleu de competenţă de înalt nivel în domeniul creşterii eficienţei de conversie a energiilor regenerabile şi a autonomiei energetice prin utilizarea combinată a resurselor, CONVENER

PROTOTIP SISTEM COMBINAT PENTRU PRODUCEREA ENERGIEI ELECTRICE

Produsul executat la nivel de prototip este un sistem combinat pentru producerea energiei electrice folosind surse regenerabie (solară și eoliană); produsul poate furniza energie electrică pentru o locuință izolată (care nu este conectată la rețeaua de electricitate comună) sau pentru o locuință alimentată cu energie electrică de la un generator cu motor termic, caz în care se reduce consumul de combustibil.

Conținutul acestui material nu reprezintă în mod obligatoriu poziția oficială a Uniunii Europene sau a Guvernului României. www.fonduri-ue.ro Pentru informații detaliate despre celelalte programe cofinanțate de Uniunea Europeană, vă invităm să vizitați www.fonduri-ue.ro.

CONSTRUCȚIA PROTOTIPULUI:
1. Sub-sistemul solar fotovoltaic (SSV) - se compune din 6 panouri fotovoltaice (1600 x 1000 mm) cu puterea de 300 W fiecare, montate fix, în 2 grupuri de câte 3 panouri fiecare.

2. Sub-sistemul eolian (SE) - produce energie electrică prin conversia inițială a energiei vântului în energie mecanică, aceasta fiind convertită în energie electrică cu ajutorul unui generator.
Conversia energiei eoliene se realizează cu 2 turbine amplasate pe un ax comun și legate printr-un cuplaj unisens: Turbina interioară, de tip Savonius, are 2 pale înclinate (Diametru turbină: 500 mm; Înălțime turbină: 980 mm); Turbina exterioară, de tip Darrieus, are ca elemente de bază 3 pale vertical drepte cu înălțimea de 2,7 m (Tipul profilului în secțiune: asimetric, tip WORTMANN FX 63 - 137; Lungimea coardei palei: 700 mm; Amplificarea turației arborelui turbinei cu un mecanism cu 2 trepte egale, cu roți și curele dințate; Factorul total de amplificare: 6).

3. Sub-sistemul de stocare a energiei (grupul de baterii) - (SSE) - se compune din 4 baterii, fiecare având o capacitate de 220 Ah și o tensiune la borne de 12 Vcc.

4. Unitatea de gestionare a energiei (GE) - este un echipament electronic, capabil să gestioneze puteri de până la 3000 VA (2400 W). Echipamentul este la bază un controler solar care permite asocierea unei a doua surse regenerabile (turbină eoliană) și permite conectarea cu rețeaua comună de electricitate (230 Vca).

UNIUNEA EUROPEANĂ

GUVERNUL ROMÂNIEI

Instrumente Structurale 2014-2020

COD: SCEE - 3.0
SCEE - Sistem Combinat pentru producerea Energiei Electrice
3.0 - puterea electrică instalată (3.000 VA)

CARACTERISTICI TEHNICE:
Putere maximă panouri fotovoltaice: 1800 W
Putere maximă turbină eoliană: 1000 W
Energia maximă stocată în acumulatori: 10,560 kW
Putere maximă invertor: 3000 VA /2400 W
Tensiunea la ieșirea din invertor: 230 Vca
Frecvența la ieșirea din invertor: 50 Hz

Proiect cofinanțat din Fondul European de Dezvoltare Regională prin Programul Operațional Competitivitate 2014-2020

Program: POC 2014 - 2020, Ctr. nr. 37/ 02.09.2016, MySMIS103396-768
Crearea unui nucleu de competenţă de înalt nivel în domeniul creşterii eficienţei de conversie a energiilor regenerabile şi a autonomiei energetice prin utilizarea combinată a resurselor, CONVENER

PROTOTIP SISTEM COMBINAT PENTRU PRODUCEREA ENERGIEI TERMICE

Produsul executat la nivel de prototip este un sistem combinat pentru producerea energiei termice care asociază două surse de energie regenerabilă, prin captarea şi conversia energiei termice solare şi a energiei termice generate prin gazeificarea biomasei, în scopul asigurării continuităţii livrării de energie termică, indiferent de factorii atmosferici.
Sistemul este conceput pentru a produce apă caldă menajeră pentru o locuinţă mono-familială, dar poate fi folosit, în anumite condiţii, şi pentru a aduce aport la încălzire, prin creşterea temperaturii agentului termic primar.
Este destinat utilizării:
a. în locaţiile izolate, unde nu există reţea comună de furnizare a energiei termice şi nici alte posibilităţi de asigurare a energiei termice;
b. în locaţiile în care energia termică este asigurată cu diverse sisteme clasice (sobe, boilere care funcţionează cu lemne sau electricitate, gaz, peleţi, brichete etc.); în acest caz, sistemul se poate folosi şi pentru reducerea cheltuielilor pentru asigurarea energiei termice.

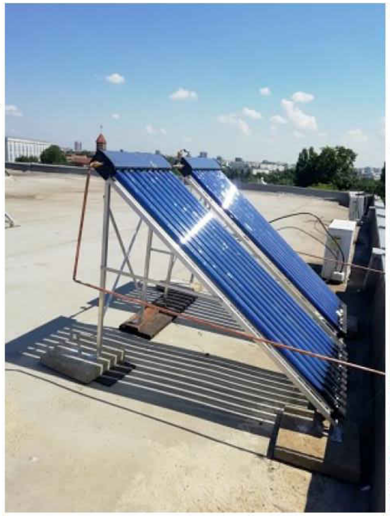

Conţinutul acestui material nu reprezintă în mod obligatoriu poziţia oficială a Uniunii Europene sau a Guvernului României. www.fonduri-ue.ro Pentru informaţii detaliate despre celelalte programe cofinanţate de Uniunea Europeană, vă invităm să vizitaţi www.fonduri-ue.ro.

Proiect cofinanţat din Fondul European de Dezvoltare Regională prin Programul Operaţional Competitivitate 2014-2020

UNIUNEA EUROPEANĂ — GUVERNUL ROMÂNIEI — Instrumente Structurale 2014-2020

COD: SCET - 10.0.
SCET - Sistem Combinat pentru producerea Energiei Termice
10.0 - puterea termică instalată (10 kW)

CONSTRUCŢIA ŞI CARACTERISTICILE TEHNICE:
Sistemul are în componenţă următoarele sub-sisteme:
1. Sub-sistemul solar termic (ST)
2. Sub-sistemul care utilizează biomasa (SB)
3. Sub-sistemul de stocare a energiei termice (SST)
4. Componentele termo-electro-hidraulice (CTH)

ST se compune din 2 panouri solare termice cu tuburi vidate, fiecare panou având câte 10 tuburi. Acestea folosesc tehnologia Heat Pipe. Un tub are 1800 mm lungime, diametrul este de 58 mm şi încălzeşte 10 l de apă cu max. 35 grade, într-o zi de vară, în care intensitatea radiaţiei solare este de 1000 W/mp. Sistemul este de tip presurizat şi se montează în exteriorul clădirii deservite.

SB conţine un modul de gazeificare şi un modul de ardere şi transfer termic. Modulul de gazeificare are o putere de aprox. 10 kWth şi utilizează biomasă diversă (peleţi, brichete, aşchii de lemn etc.). În cazul peleţilor, cantitatea de peleţi necesară încărcării modulului este de 2,6 kg. Alimentarea cu aer pentru gazeificare şi ardere se face forţat, cu ajutorul a două ventilatoare de mică putere.

SST este reprezentat de un boiler bivalent (cu două serpentine) cu capacitate de 120 l, care dispune şi de o rezistenţă electrică.

În categoria CTH intră elementele active (electropompe, supape etc.), împreună cu elementele pasive (racorduri, nipluri, conducte rigide sau flexibile, aparate de măsură).

UNIUNEA EUROPEANĂ

Instrumente Structurale 2014-2020

Programul Operaţional Sectorial „Creşterea Competitivităţii Economice"
- co-finanţat prin Fondul European de Dezvoltare Regională
„Investiţii pentru viitorul dumneavoastră"

Comunicat de presă

Bucureşti, 11.08.2021

FINALIZARE PROIECT - Axa E

INSTITUTUL NAŢIONAL DE CERCETARE-DEZVOLTARE PENTRU OPTOELECTRONICĂ - INOE 2000, cu sediul în localitatea Măgurele, Bucureşti-Ilfov, str. Atomiştilor, C.P. 077125 nr. 409, judeţul Ilfov, România, telefon 0214574522, fax 0314056397, anunță finalizarea, la data de 30.08.2021, a implementării proiectului "**CREAREA UNUI NUCLEU DE COMPETENŢĂ DE ÎNALT NIVEL ÎN DOMENIUL CREŞTERII EFICIENŢEI DE CONVERSIE A ENERGIILOR REGENERABILE ŞI A AUTONOMIEI ENERGETICE PRIN UTILIZAREA COMBINATĂ A RESURSELOR**", finanţat prin PROGRAMUL OPERAŢIONAL COMPETITIVITATE, în baza contractului de finanţare nr. 37/2016, ID: P_37_752, My SMIS 103396, încheiat cu INSTITUTUL NAŢIONAL DE CERCETARE-DEZVOLTARE PENTRU OPTOELECTRONICĂ-INOE 2000.

Valoarea totală a proiectului este de 5.735.282,21 lei, din care asistenţa financiară nerambursabilă este de 5.700.282,21 lei.

Proiectul s-a implementat la sediul filialei INOE 2000 – IHP, în localitatea Bucureşti, sector 4, str. Cuţitul de Argint nr. 14, C.P. 040558, pe o durată de 60 luni (incluzând perioada de suspendare de 3 luni).

Obiectivul proiectului a constat în crearea unui nucleu de competentă ştiinţifică şi tehnologică, de înalt nivel, în domeniul creşterii performanţelor de conversie pentru tipurile de energie regenerabilă care se găsesc în cantități importante pe teritoriul României (solară, biomasă, eoliană, hidro). Nucleul are ca obiectiv prioritar participarea la competiţiile naţionale, dar mai ales internaţionale în domeniu.

Beneficiar: INOE 2000-IHP

Potenţiali beneficiari ai rezultatelor proiectului: persoane publice sau private care vor utiliza sistemele combinate, persoane angajate în fabricarea, vânzarea, montarea, întreţinerea şi exploatarea produselor.

Rezultate realizate:

Proiectul a fost finalizat în proporție de 100%, indicatorii de realizare ai acestuia fiind: noi cercetători în entitatea care beneficiază de sprijin (ENI), publicaţii științifice rezultate din proiect, co-publicaţii științifice public-private, propuneri de proiecte depuse pentru Orizont 2020, cereri de brevet, rapoarte de încercare /testare, metodologii de testare, cărţi tehnice, referenţiale, studii tehnice, studii de fezabilitate, prototipuri realizate, documentatii complete de introducere în fabricație, proiecte tehnice ce pot fi dezvoltate, standuri realizate, modele experimentale realizate, modele demonstrative, workshop-uri pe teme de energie regenerabilă, modele la scară realizate si testate.

Proiect co-finanţat din Fondul European de Dezvoltare Regională prin Programul Operaţional Competitivitate 2014-2020.

Detalii suplimentare puteţi obţine de la:
Nume persoană contact: Dr. Ing. Cătălin DUMITRESCU
Funcţie: DIRECTOR INOE 2000 - IHP
Tel.: 0213363991, Fax: 0213373040, e-mail: dumitrescu.ihp@fluidas.ro

FLUIDAS

NATIONAL PROFESSIONAL ASSOCIATION OF HYDRAULICS AND PNEUMATICS IN ROMANIA

fluidas@fluidas.ro